ABSTRACT

MATHEMATICAL PROBLEMS ARISING IN INTERFACIAL ELECTROHYDRODYNAMICS

by
Dmitri Tseluiko

In this work we consider the nonlinear stability of thin films in the presence of electric fields. We study a perfectly conducting thin film flow down an inclined plane in the presence of an electric field which is uniform in its undisturbed state, and normal to the plate at infinity. In addition, the effect of normal electric fields on films lying above, or hanging from, horizontal substrates is considered. Systematic asymptotic expansions are used to derive fully nonlinear long wave model equations for the scaled interface motion and corresponding flow fields. For the case of an inclined plane, higher order terms are need to be retained to regularize the problem in the sense that the long wave approximation remains valid for long times. For the case of a horizontal plane the fully nonlinear evolution equation which is derived at the leading order, is asymptotically correct and no regularization procedure is required. In both physical situations, the effect of the electric field is to introduce a non-local term which arises from the potential region above the liquid film, and enters through the electric Maxwell stresses at the interface. This term is always linearly destabilizing and produces growth rates proportional to the cubic power of the wavenumber – surface tension is included and provides a short wavelength cut-off, that is, all sufficiently short waves are linearly stable.

For the case of film flow down an inclined plane, the fully nonlinear equation can produce singular solutions (for certain parameter values) after a finite time, even in the absence of an electric field. This difficulty is avoided at smaller amplitudes where the weakly nonlinear evolution is governed by an extension of the Kuramoto-Sivashinsky (KS) equation. Global existence and uniqueness results are proved, and refined estimates of the radius of the absorbing ball in L^2 are obtained in terms of the parameters of the

equations for a generalized class of modified KS equations. The established estimates are compared with numerical solutions of the equations which in turn suggest an optimal upper bound for the radius of the absorbing ball. A scaling argument is used to explain this, and a general conjecture is made based on extensive computations. We also carry out a complete study of the nonlinear behavior of competing physical mechanisms: long wave instability above a critical Reynolds number, short wave damping due to surface tension and intermediate growth due to the electric field. Through a combination of analysis and extensive numerical experiments, we elucidate parameter regimes that support non-uniform travelling waves, time-periodic travelling waves and complex nonlinear dynamics including chaotic interfacial oscillations. It is established that a sufficiently high electric field will drive the system to chaotic oscillations, even when the Reynolds number is smaller than the critical value below which the non-electrified problem is linearly stable. A particular case of this is Stokes flow, which is known to be stable for this class of problems (an analogous statement holds for horizontally supported films also). Our theoretical results indicate that such highly stable flows can be rendered unstable by using electric fields. This opens the way for possible heat and mass transfer applications which can benefit significantly from interfacial oscillations and interfacial turbulence.

For the case of a horizontal plane, a weakly nonlinear theory is not possible due to the absence of the shear flow generated by the gravitational force along the plate when the latter is inclined. We study the fully nonlinear equation, which in this case is asymptotically correct and is obtained at the leading order. The model equation describes both overlying and hanging films – in the former case gravity is stabilizing while in the latter it is destabilizing. The numerical and theoretical analysis of the fully nonlinear evolution is complicated by the fact that the coefficients of the highest order terms (surface tension in this instance) are nonlinear. We implement a fully implicit two level numerical scheme and perform numerical experiments. We also prove global boundedness of positive periodic smooth solutions, using an appropriate energy functional. This global boundedness result is seen

in all our numerical results. Through a combination of analysis and extensive numerical experiments we present evidence for global existence of positive smooth solutions. This means, in turn, that the film does not touch the wall in finite time but asymptotically at infinite time. Numerical solutions are presented to support such phenomena.

MATHEMATICAL PROBLEMS ARISING IN INTERFACIAL ELECTROHYDRODYNAMICS

by
Dmitri Tseluiko

A Dissertation
Submitted to the Faculty of
New Jersey Institute of Technology and
Rutgers, The State University of New Jersey – Newark
in Partial Fulfillment of the Requirements for the Degree of
Doctor of Philosophy in Mathematical Sciences

Department of Mathematical Sciences, NJIT
Department of Mathematics and Computer Science, Rutgers-Newark

May 2006

APPROVAL PAGE

MATHEMATICAL PROBLEMS ARISING IN INTERFACIAL ELECTROHYDRODYNAMICS

Dmitri Tseluiko

Demetrios T. Papageorgiou, Ph.D., Dissertation Advisor — Date
Professor, Department of Mathematical Sciences, NJIT

Nadine N. Aubry, Ph.D., Committee Member — Date
Distinguished Professor, Department of Mechanical Engineering, NJIT

Peter G. Petropoulos, Ph.D., Committee Member — Date
Associate Professor, Department of Mathematical Sciences, NJIT

Michael S. Siegel, Ph.D., Committee Member — Date
Professor, Department of Mathematical Sciences, NJIT

Jean-Marc Vanden-Broeck, Ph.D., Committee Member — Date
Professor, School of Mathematics, University of East Anglia

BIOGRAPHICAL SKETCH

Author: Dmitri Tseluiko

Degree: Doctor of Philosophy

Date: May 2006

Undergraduate and Graduate Education:

- Doctor of Philosophy in Mathematical Sciences,
  New Jersey Institute of Technology, Newark, NJ, 2006
- Master of Science in Applied Mathematics,
  New Jersey Institute of Technology, Newark, NJ, 2004
- Master of Science in Pure Mathematics,
  University of Tartu, Tartu, Estonia, 2001
- Bachelor of Science in Pure Mathematics,
  University of Tartu, Tartu, Estonia, 1999

Major: Applied Mathematics

To my parents.

ACKNOWLEDGMENT

I would like to express my sincere gratitude and appreciation to my advisor, professor Demetrius Papageorgiou, who introduced me to this problem. This dissertation would not have been possible without his expert guidance and support.

I would like to thank professors Nadine Aubry, Peter Petropoulos, Michael Siegel, and Jean-Marc Vanden-Broeck for agreeing to be my committee members and for their valuable advice and help. Special thanks are due to professors Michael Booty, Vladislav Goldberg, Lou Kondic, Robert Miura, Cyrill Muratov, Yiorgos-Sokratis Smyrlis. I am grateful to professor Maido Rahula, my former advisor at the University of Tartu, for his moral and academic support.

The author is grateful to the Department of Mathematical Sciences at New Jersey Institute of Technology for providing financial support for this research.

I would also like to thank present and former graduate students at the Department of Mathematical Sciences for their friendship, help and support, in particular Lyudmyla Barannyk, Oleksandr Dybenko, Muhammad Hameed, Valeriy Lukyanov, Yuriy Mileyko, Oleg Petrenko, Filippo Posta, Tetyana Segin, Tsezar Seman, Xing Li Wang, Ivan Zorych.

The author deeply appreciates the encouragement, help and moral support from his friends Oleksii Mostovyi, Andrei Titov, Duca Bjelica. Special thanks are due to Veronica Shelekhova, Maria and Aleksandr Stepanyuk. Thanks to anyone who I maybe missing.

And finally, grateful thanks and deep appreciation to my parents and my sister for their support, encouragement and love through all these years.

TABLE OF CONTENTS

TABLE OF CONTENTS
(Continued)

Chapter Page

LIST OF TABLES

Table **Page**

LIST OF FIGURES

LIST OF FIGURES
(Continued)

Figure **Page**

LIST OF FIGURES
(Continued)

Figure **Page**

CHAPTER 1

INTRODUCTION

We consider several mathematical problems arising in interfacial electrohydrodynamics. Electrohydrodynamics deals with the fluid motion when an electric field is applied. It can be considered both as a branch of fluid dynamics which is involved with the effects of applied electric fields, and as a branch of electrodynamics which is involved with the effects of moving media on electric fields. Applications of electrohydrodynamics include spraying, ink jet printing, mixing and emulsification, coalescence, boiling, enhancement of heat and mass transfer, fluidized bed stabilization, pumping, and polymer dispersion.

Perhaps the earliest known electrohydrodynamic experiments were done by William Gilbert in the seventeenth century. He described the formation of a conical shape upon bringing a charged rod above a sessile drop, see Taylor [115]. Until the 1960s most work focused on problems including perfect conductors or perfect dielectrics as the liquids. Other branches of electrohydrodynamics include problems which deal with poorly conducting liquids (leaky dielectrics) and electrolytes, see Allan & Mason [5], Russel et al. [99], Saville [102].

In the present work we study the evolution of thin liquid films on inclined and horizontal planes when electric fields act on them. Thin films have received a lot of attention since the experiments of Kapitza & Kapitza [64] (also Binny [16]). They arise in a variety of physical and technological applications including cooling systems and coating processes for example, as well as in biological applications, for example in fusion of lipid bilayers or biological membranes. In cooling applications, for instance, it has been observed that heat or mass transfer can be increased by an order of magnitude if there are waves present on the liquid film – Bontozoglou [18], Dukler [35], Nagasaki et al. [83], Serifi et al. [105], Sisoev et al. [107], Yoshimura et al. [127].

The initial linear stage of the instability on falling films was considered by Benjamin [10] and Yih [126] who showed that the flow becomes unstable to long waves above a critical Reynolds number that depends on the angle of inclination (for vertical inclinations the critical Reynolds number is zero); the waves travel with a speed which is twice the unperturbed flow speed at the interface. Periodic, two-dimensional nonlinear waves emerge whose structure depends on the forcing frequency that produces them (see Alekseenko et al. [4], Liu et al. [78]), and in general these are susceptible to three dimensional instabilities and ensuing spatiotemporal complexity – Chang et al. [23], Johnson et al. [60], Joo & Davis [62], Liu & Gollub [76]. It is observed that the long time behavior of the flow is dominated by solitary wave pulses and the interactions between them, and hence a fundamental understanding of their existence and dynamics, in different physical situations, is of importance. Experiments confirming the central role of solitary wave structures have been carried out by Argyriadi et al. [6], Liu & Gollub [77], Vlachogiannis & Bontozoglou [121].

Direct numerical simulations of the falling film problem on flat substrates have been carried out by several investigators including Argyriadi et al. [6], Gao et al. [42], Gu et al. [49], Kunugi & Kino [69], Malamataris et al. [80], Salamon et al. [100]; calculations and experiments over wavy walls can be found in Malamataris & Bontozoglou [79] and Vlachogiannis & Bontozoglou [122], respectively. The computations of Malamataris et al. [80] evaluate the spatial linear stability stage of the dynamics and consider in detail the velocity profiles beneath solitary waves with the finding that a strong non-parabolicity emerges in front of the main humps along with a small region of backflow. The dynamics is quite delicate and it is useful, therefore, to obtain reduced systems that can be studied in detail both numerically and analytically.

At Reynolds numbers not too far from critical, then, it is feasible to develop a long wave nonlinear theory as in Alekseenko et al. [4], Benney [11], Gjevik [43], for example, giving rise to the so-called "Benney" evolution equation. Even though this

equation contains different physical mechanisms and is potentially capable of describing the nonlinear dynamics, it lacks a global existence theory for its solutions. Evidence of this can be found in numerical experiments by Joo et al. [63], Pumir et al. [97], Rosenau & Oron [98]. On the other hand, it has been used to successfully describe experimental observations of three dimensional fingering instabilities in falling films – see Diez & Kondic [30], Diez & Kondic [31], Kondic & Diez [68]. Reviews of falling film flows and in particular their nonlinear analysis via long wave models at small and moderately large Reynolds numbers, can be found in Chang [22] and Chang & Demekhin [24].

Weakly nonlinear analysis of the Benney equation leads to the Kuramoto-Sivashinsky (KS) equation, which deserves a special mention. This equation arises in a variety of physical problems and is one of the simplest one-dimensional evolution equations which exhibit complex dynamics. Applications include falling film flows (Benney [11], Hooper & Grimshaw [55], Shlang & Sivashinsky [106], Sivashinsky & Michelson [110]), core-annular flows (Coward et al. [28], Papageorgiou et al. [90]) flame-front instabilities and reaction diffusion combustion dynamics (Sivashinsky [108], Sivashinsky [109]), chemical physics for propagation of concentration waves (Kuramoto [70], Kuramoto & Tsuzuki [71], Kuramoto & Tsuzuki [72]), and plasma physics (Cohen et al. [25]). The rescaled KS equation on 2π-periodic intervals contains a single parameter $\nu = (\pi/L)^2$ (here L is half of the interval on which the equation is considered) which is inversely proportional to the square of the length of the system. In scaled variables, the equation takes the following form:

$$u_t + uu_x + u_{xx} + \nu u_{xxxx} = 0, \quad (x,\, t) \in \mathbb{R} \times \mathbb{R}_+, \tag{1.1}$$
$$u(x,\, t) = u(x + 2\pi,\, t).$$

The equation was extensively studied computationally (Frisch et al. [41], Greene & Kim [46], Hyman & Nicolaenko [56], Hyman et al. [57], Kevrekidis et al. [65], Papageorgiou & Smyrlis [92], Sivashinsky & Michelson [110], Smyrlis & Papageorgiou [112], Smyrlis &

Papageorgiou [113]) as well as analytically (Collet et al. [26], Collet et al. [27], Goodman [45], Ilyashenko [58], Jolly et al. [61]). It is established that the KS equation produces complicated dynamics in both space and time, and when the parameter ν is small enough the solutions become chaotic. A computational verification of a period-doubling route to chaos according to the Feigenbaum scenario along with calculation of the two universal constants, can be found in Papageorgiou & Smyrlis [92], Smyrlis & Papageorgiou [112], Smyrlis & Papageorgiou [113]. The analyticity properties of the solutions of the Kuramoto-Sivashinsky equation were studied by Collet et al. [26]. They showed that the solutions are analytic in a strip around the real axis, and gave a bound for the width of this strip. They also provided several stronger results regarding the analyticity of the solutions based on a series of numerical experiments.

The possibility of controlling the film flow using a vertical electric field has been suggested by Bankoff et al. [7], Bankoff et al. [8], Griffing et al. [48], Kim et al. [66], Kim et al. [67] in their consideration of the electrostatic liquid film radiator. The idea is to utilize the reduction of pressure induced by the electric Maxwell stresses at the liquid/air interface, to reduce or stop leakage of fluid out of punctures on the outer casing of cooling equipment which is exposed to cosmic particle impacts in space applications. The theoretical study of Kim et al. [66] is two-dimensional (so the holes are slits) and considers a perfect dielectric liquid and a finite length electrode placed relatively close to the grounded infinite plane substrate. An evolution equation is derived which is similar to the Benney equation but contains an additional local term due to the electric field (surface tension is not included); an analogous analysis is performed for higher Reynolds numbers using the von Karman-Pohlhausen parabolic profile approximation to obtain closure – see Chang & Demekhin [24]. Numerical solutions show reasonable agreement with direct Navier-Stokes simulations and indicate the feasibility of attaining sufficiently negative pressures in the vicinity of the electrode that can arrest leakage. The linear stability is also considered for perfectly conducting fluids and it is found that the presence of a vertical

electric field reduces the critical Reynolds number below which the flow is stable. A comparison between experiment and lubrication theory (for a finite length electrode) is made in Griffing et al. [48] and agreement is reasonable. A striking experimental demonstration of the instability due to a vertical field in the absence of a shear flow can be found in Dong et al. [33], where the field induces the formation and protrusion of liquid columns of one liquid into a second immiscible liquid with different electrical properties. Even though the observed phenomenon is three-dimensional, a fundamental understanding of two-dimensional nonlinear interfacial electrohydrodynamics is a suitable starting point and is one of the aims of the present work. The presence of shear (see the experiments of Bankoff et al. [7] and Griffing et al. [48]) is found to nonlinearly saturate the interfacial amplitudes and this is also established by our theoretical study of the modified KS equation. An interesting analogue of shear stabilization is that of the nonlinear saturation of capillary instability in core-annular flows – see for example Papageorgiou et al. [90].

Recently, Gonzalez & Castellanos [44] considered a perfectly conducting liquid film on an inclined plane with the upper electrode placed far from the grounded substrate. A Benney type equation is written down which contains a nonlocal contribution due to the electric field above the liquid layer and the fact that the second electrode is at infinity. The form of such nonlocal terms has been derived formally in related horizontal electric field problems by Papageorgiou & Vanden-Broeck [93], Papageorgiou & Vanden-Broeck [94], Tilley et al. [117]. The weakly nonlinear version of this equation is a KS equation with an additional linear term due to the electric field that induces a linear growth which is worse than the negative diffusion but is still dominated by the fourth order damping. The scaled version of the equation is (see Chapter 3 for details):

$$u_t + uu_x \pm u_{xx} + \nu u_{xxxx} + \mu \mathcal{H}[u_{xxx}] = 0, \quad (x,\, t) \in \mathbb{R} \times \mathbb{R}_+, \tag{1.2}$$

$$u(x,\, t) = u(x + 2\pi,\, t),$$

where $\mathcal{H}$ is the Hilbert transform operator, $\mu > 0$ measures the electric field intensity and the $\pm$ sign is taken for Reynolds numbers above and below critical, respectively.

At sufficiently small Reynolds numbers, Gonzalez & Castellanos [44] identify a critical electric field strength above which a mode with non-zero wavenumber first becomes un-stable. They in turn use a Ginzburg-Landau weakly nonlinear expansion to establish a supercritical bifurcation. The behavior of the flow at arbitrary electric field values was not studied and is undertaken in a systematic way in the present work. It is important to also emphasize that if the Reynolds number is sufficiently large (so that the non-electrified problem is linearly unstable to long waves), the weakly nonlinear theory of Gonzalez & Castellanos [44] is not possible and the problem must be addressed numerically. We address the modified KS equation numerically (at Reynolds numbers above and below critical) as well as analytically. The dynamics is quite different depending on the Reynolds number, but in all cases the system evolves to mostly chaotic dynamics as the length of the system is increased. We also observe numerically that the solutions remain bounded and exhibit a complex behavior including chaotic oscillations as in the case of the usual KS equation. Analytical results of global existence, uniqueness and uniform boundedness of the solutions were obtained by Duan & Ervin [34], who also obtain a bound for the radius of the absorbing ball.

We also study analytically a generalization of the modified KS equations with the extension of the nonlocal operator that enables a parametric study of the increasing instability. Results of global existence and uniqueness of the solutions are proved (based on the general theory of initial value problems for abstract nonlinear evolutionary equations, see Henry [52] or Sell & You [104]). Also, we prove the existence of the absorbing ball in the L^2-norm and we also obtain new estimates for its radius, which improve those of Duan & Ervin [34]. The analytical estimates are also compared with the results of extensive numerical experiments which in turn guide us to conjecture an optimal bound for the attractor which we can explain using scaling arguments.

The basic idea in obtaining the estimate of the radius of the absorbing ball in L^2-norm is the use of the method of Liapunov. We find a functional F with the property that there is a constant F_*, such that if u is a solution of the modified KS equation and $F[u] \geq F_*$ then $\frac{dF[u]}{dt} \leq 0$. This implies (with careful analysis) that $\limsup_{t\to\infty} F[u]$ is bounded. The functional F should be chosen such that the inequality $F[u] \leq F_*$ holds if and only if $\|u\|_2 \leq C_1$ for some constant C_1. Then we get boundedness of $\limsup_{t\to\infty} \|u\|_2$ as well.

The approach of Nicolaenko et al. [86] was to consider the following functional

$$F[u] = \|u - \varphi\|_2^2, \tag{1.3}$$

where $\varphi(x)$ is a well chosen gauge function. This approach works well for odd periodic solutions of the usual Kuramoto-Sivashinsky equation. For general solutions (not necessarily odd), the idea of Collet et al. [27] was to consider a generalization of the comparison function φ. Namely, they considered the following Liapunov function:

$$F[u] = \|u(x, t) - \varphi_a(x)\|_2^2, \tag{1.4}$$

where $\varphi_a(x) = \varphi(x + a)$, and $a = a(t)$ is a suitably chosen translation function. We used Goodman's choice for $a(t)$ (see Goodman [45]), namely $a(t)$ is chosen such that

$$\|u(x, t) - \varphi(x + a(t))\|_2^2 = \inf_{\psi\in S} \|u(x, t) - \psi(x)\|_2^2, \tag{1.5}$$

for all $t > 0$. Here S is the following translation invariant set of functions:

$$S = \{\psi | \exists a, \text{ s.t. } \psi(x) \equiv \varphi(x + a)\}. \tag{1.6}$$

This is equivalent to saying that

$$F[u] = \text{dist}^2(u, S). \tag{1.7}$$

In the present work we also consider the related problem of a perfectly conducting liquid film on a horizontal plane with the upper electrode placed far from the grounded

substrate. A long wave theory leads to a nonlocal nonlinear evolutionary equation at leading order, which by a modification of the sign of the gravitational parameter also describes thin liquid films wetting the underside of flat plates when a normal electric field is applied appropriately. A similar equation for the nonelectrical case was derived by Ehrhard & Davis [38], who studied spreading of viscous drops on smooth horizontal surfaces which are uniformly heated or cooled. (In the isothermal case, with the no-slip boundary conditions their equation coincides with the equation derived here when there is no electric field.) The same "nonelectrical" equation was also obtained and studied numerically in Yiantsios & Higgins [124] who considered the behavior of a viscous fluid film bounded below by a wall and above by a second heavier immiscible fluid. For the case when the ratio of the viscosities $m = \mu_1/\mu_2$ is $\mathcal{O}(1)$, they obtained the same evolution equation for the interface. In Ehrhard [37], using the model of Ehrhard & Davis [38], the author considered the quasi-steady evolution of a viscous drop hanging on the earth-faced side of a smooth horizontal plate, which is either uniformly heated or cooled. Also, other similar equations arising in the modelling of thin liquid films have been derived and studied in Bertozzi [12], Dussan [36], Greenspan [47], Haley & Miksis [50], Hocking [54], Myers [82], Oron et al. [88]. For clarity, we include the equation derived in Chapter 5 below. If $u(x,\, t)$ denotes the scaled interfacial position, then the equation takes the form

$$u_t + \frac{1}{3}\left[u^3\left(\frac{1}{C}u_{xxx} - Gu_x + 2W_e\mathcal{H}[u_{xx}]\right)\right]_x = 0, \quad (x,\, t) \in \mathbb{R} \times \mathbb{R}_+, \tag{1.8}$$

$$u(x,\, t) = u(x + 2L,\, t),.$$

where $C > 0$, $W_e > 0$ and G can be positive or negative. The sign of the gravitational parameter G depends on whether the film is resting above or wetting the underside of a horizontal flat plate, respectively. In the absence of an electric field the film is linearly stable or unstable depending on whether $G > 0$ or $G < 0$, respectively, as is expected on physical grounds. The addition of an electric field can always make the film unstable irrespective of the sign of G.

A weakly nonlinear theory is not possible in this situation and we are confined to the study of the fully nonlinear equation (the physical reason for this is the absence of an underlying shear flow). Even though the electric field term is always destabilizing, we succeeded in proving that positive smooth solutions on a periodic interval $[-L,\ L]$ do not blowup and are uniformly bounded for all time in the H^1-norm (if they exist). The approach is based on the construction of an appropriate energy functional $\mathcal{E}[h]$ having the steady state solutions as extrema. Our analysis extends that of Bertozzi & Pugh [14] to nonlocal equations. Let us also note that Hocherman & Rosenau [53] considered a generalized class of long wave thin film equations (when the coefficients in front of the derivatives have more general form, e.g., are polynomials of higher or lower degree of unknown function). They were interested in identifying when such equations admit solutions that blow up in finite time, and they made a conjecture regarding when the solutions blow up or are globally stable. The possibility of finite time blow-up was also recently studied in Bertozzi & Pugh [14], Bertozzi & Pugh [15], and Witelski et al. [123] based on both rigorous analysis and numerical computations.

For the equation derived here it can also be established analytically that the spatial integral of positive solutions is bounded on each time interval. This could be used to show the global existence of the positive smooth solutions (i.e., that the film does not touch the wall in finite time) if we had proven the boundedness of the H^2-norm of the solutions on each time interval (this has not been done yet and is a topic of future research).

In order to obtain the quantitative characteristics of the solutions, we have implemented a fully implicit two level numerical scheme for this class of equations. We used the ideas introduced in Bertozzi & Pugh [13], Diez et al. [32]. The equation is solved on a uniform spatial grid, and the spatial derivatives are discretized using central differences. Our numerical experiments suggest boundedness of the H^2-norm of the solutions, which, as was noticed above, also implies that the film does not touch the wall in finite time (though it is likely that it happens in infinite time). The numerical scheme can also be used

to provide numerical "proofs" of conjectures (in the manner of Bertozzi & Pugh [14]) on finite/infinite time singularities, or the global existence and the boundedness of the solutions of generalized electrified horizontal thin film equations.

The structure of the present work is as follows: In Chapter 2 we consider the governing equations of electrohydrodynamics. In Chapter 3 we first formulate the mathematical problem and the nonlinear interfacial boundary conditions for the problem of an electrified thin film flow down an inclined plane; we then develop a formal asymptotic solution valid for long waves and point out some associated difficulties for fully nonlinear waves. A weakly nonlinear analysis of the fully nonlinear system is shown to lead to the modified KS equation. Next we present detailed numerical solutions and construct a fairly complete picture of the competing nonlinear dynamics (for Reynolds numbers above and below critical); some analytical results are also provided. At the end of this chapter we present our conclusions. In Chapter 4 we present analytical results for the modified KS equations. First we compile some relevant general results regarding existence and uniqueness of the solutions for Cauchy problems for nonlinear evolutionary equations on Banach spaces, which are used to prove global existence and uniqueness of the solutions of the modified KS equations in H^1. First, we prove local existence following the approach of Duan and Ervin [34] (see also Henry [52]) and then establish global results by proving uniform boundedness of the solutions in H^1 on each time interval. To establish uniform boundedness of the solutions in H^1 we first prove uniform boundedness in L^2, which is done by a modification of the method of Collet et al. [27]. After proving global existence this also provides the existence of the absorbing ball in L^2 as well as estimates for its radius. We also compare the analytical estimate with values obtained from numerical computations. In Chapter 5 we consider electrified liquid films on a horizontal plane. First we formulate the mathematical problem and derive the long wave evolution equation for the interface. Then we discuss the numerical schemes for this equation and present detailed numerical solutions. Rigorous analytical results are also established. Finally, we provide some conclusions.

CHAPTER 2

GOVERNING EQUATIONS OF ELECTROHYDRODYNAMICS

In this chapter we consider the governing equations of electrohydrodynamics. First, we present Maxwell's equations and the charge conservation law and explain how these can be simplified to the so-called electroquasistatic equations under certain assumptions. Next, we present the equations that govern the motion of a fluid, and finally the boundary conditions are considered. For more a detailed description of the governing equations and boundary conditions of electrohydrodynamics see Castellanos [20], Castellanos & Gonzalez [21], Saville [103].

2.1 Electrical Equations

The basic laws governing the behavior of electromagnetic fields are given by the well-known Maxwell's equations, see Jackson [59], Landau & Lifshitz [74], Panofsky & Phillips [89]. The differential form of these equations in the MKS system of units is

$$\nabla \cdot \boldsymbol{D} = q, \tag{2.1}$$

$$\nabla \times \boldsymbol{E} = -\frac{\partial \boldsymbol{B}}{\partial t}, \tag{2.2}$$

$$\nabla \cdot \boldsymbol{B} = 0, \tag{2.3}$$

$$\nabla \times \boldsymbol{H} = \boldsymbol{J} + \frac{\partial \boldsymbol{D}}{\partial t}. \tag{2.4}$$

Here $\boldsymbol{E}$ and $\boldsymbol{B}$ are the electric and magnetic fields, $\boldsymbol{D}$ is the electric displacement vector, $\boldsymbol{H}$ is the magnetic field intensity, q is the volume charge density, and $\boldsymbol{J}$ is the current density. The above equations represent Gauss's law, Faraday's law, the solenoidal nature of the magnetic field, and the Ampère-Maxwell equation, respectively.

Another equation relating the volume charge density q and the current density $\boldsymbol{J}$ is the charge conservation law

$$\frac{\partial q}{\partial t} + \nabla \cdot \boldsymbol{J} = 0. \tag{2.5}$$

This conservation law essentially states that the rate of decrease of the charge density inside a small control volume, is equal to the rate at which charge flows out by crossing the bounding surface of the volume. Use of the divergence theorem enables the physical law to be written in the form (2.5).

The electric displacement vector is defined by

$$\boldsymbol{D} = \varepsilon_0 \boldsymbol{E} + \boldsymbol{P}, \tag{2.6}$$

where $\varepsilon_0 = 10^7/4\pi c^2 \approx 8.8542 \times 10^{-12}\mathrm{F} \cdot \mathrm{m}^{-1}$ is the permittivity of free space (here $c \approx 2.9979 \times 10^8 \mathrm{m} \cdot \mathrm{s}^{-1}$ is the speed of light in free space), and $\boldsymbol{P}$ is the polarization vector (the dipole moment per unit volume). In most cases the polarization vector is proportional to the electric field and can be written in terms of the electric susceptibility χ_e as follows:

$$\boldsymbol{P} = \varepsilon_0 \chi_e \boldsymbol{E}. \tag{2.7}$$

The displacement vector becomes, therefore,

$$\boldsymbol{D} = \varepsilon_0 \kappa_e \boldsymbol{E}, \tag{2.8}$$

where $\kappa_e = 1 + \chi_e$ is called the dielectric constant. The constant $\varepsilon = \varepsilon_0 \kappa_e$ is called the electric permittivity.

The magnetic field intensity $\boldsymbol{H}$ is defined by

$$\boldsymbol{H} = \frac{1}{\mu_0}\boldsymbol{B} - \boldsymbol{M}, \tag{2.9}$$

where $\mu_0 = 4\pi \times 10^{-7}\mathrm{Wb} \cdot \mathrm{A}^{-1} \cdot \mathrm{m}^{-1} \approx 1.2566 \times 10^{-6}\mathrm{Wb} \cdot \mathrm{A}^{-1} \cdot \mathrm{m}^{-1}$ is the permeability of free space, and $\boldsymbol{M}$ is the magnetization vector (the magnetic moment per unit volume).

In most cases the magnetization is proportional to the magnetic field intensity, enabling us to write

$$\boldsymbol{M} = \chi_m \boldsymbol{H}, \tag{2.10}$$

where χ_m is called the magnetic susceptibility. So, we get

$$\boldsymbol{B} = \mu_0(1 + \chi_m)\boldsymbol{H} = \mu_0 \kappa_m \boldsymbol{H} = \mu \boldsymbol{H}, \tag{2.11}$$

where $\kappa_m = 1 + \chi_m$ is called the relative permeability of the medium, and $\mu = \mu_0 \kappa_m$ is called its absolute permeability.

For the sake of simplicity, it will be assumed that the electric permittivity ε and the magnetic permeability μ are constant (this is the case in the problems of interest here). We will also assume that the electroquasistatic assumption is satisfied (see Plonsey [96], for instance). This condition can be written as $|kL| \ll 1$, where L is the characteristic unit of length and $|1/k|$ is the spatial wavelength of an infinite, parallel, electromagnetic plane wave of angular velocity ω (the temporal frequency of interest) travelling in the material. Consequently, a physical interpretation of this assumption is that the ratio of the length of the structure to the spatial wavelength is small.

Under the previous assumptions Maxwell's equations (2.1)-(2.4) can be reduced to the following system of equations:

$$\nabla \cdot \boldsymbol{E} = \frac{1}{\varepsilon} q, \tag{2.12}$$

$$\nabla \times \boldsymbol{E} = \boldsymbol{0}, \tag{2.13}$$

$$\nabla \cdot \boldsymbol{B} = 0, \tag{2.14}$$

$$\frac{1}{\mu} \nabla \times \boldsymbol{B} = \boldsymbol{J}. \tag{2.15}$$

Under the electroquasistatic assumption, therefore, Maxwell's equations can be written as a separate set of equations (2.12), (2.13) for the electric field and equations (2.14), (2.15) for the magnetic field. Since we are not interested in finding the magnetic field we will

consider the electric equations only. Besides, when the external magnetic field is absent, magnetic effects can be ignored completely, see Saville [103].

To relate the distribution of current to the electric field, an equation is required which connects the current and the electric field at any particular point. Typically this equation is given by

$$\boldsymbol{J} = mq\boldsymbol{E} + q\boldsymbol{u} - D\nabla q, \tag{2.16}$$

where m is the mobility of the charge carriers, D is the coefficient of the molecular diffusion, and $\boldsymbol{u}$ is the flow velocity (in the given liquid or gas). In most cases $D \ll m$, at ambient temperature, and unless the electric field is of order D/m, diffusion may be neglected, i.e.,

$$\boldsymbol{J} = \varsigma\boldsymbol{E} + q\boldsymbol{u}, \tag{2.17}$$

where $\varsigma = mq$ is called the electrical conductivity.

In electrohydrodynamics, then, the electric equations reduce to

$$\nabla \cdot \boldsymbol{E} = \frac{1}{\varepsilon}q, \quad \nabla \times \boldsymbol{E} = \boldsymbol{0}, \quad \frac{\partial q}{\partial t} + \nabla \cdot \boldsymbol{J} = 0. \tag{2.18}$$

Note that since the electric field is irrotational ($\nabla \times \boldsymbol{E} = \boldsymbol{0}$), it can be written as the gradient of some scalar field. Therefore the electric equations (2.18) can also be written in the following form:

$$\nabla^2 V = -\frac{1}{\varepsilon}q, \quad \boldsymbol{E} = -\nabla V, \quad \frac{\partial q}{\partial t} + \nabla \cdot \boldsymbol{J} = 0, \tag{2.19}$$

where V is the voltage potential, and $\boldsymbol{J}$ is given by (2.17).

Finally, we consider the motion of charges in the given fluid governed by the charge conservation law (2.5). We will present an argument that shows that if charges are initially present in the fluid and there are no current sources, then the charge density will decay to zero in a short time scale. This is the phenomenon of charge relaxation. The initially

imposed charge will move onto the interface (see later for a discussion of interfacial conditions). If the electrical conductivity is constant, equation (2.5) together with (2.17) imply

$$\frac{\partial q}{\partial t} = -\nabla \cdot (\varsigma \boldsymbol{E} + q\boldsymbol{u}) = -\varsigma \nabla \cdot \boldsymbol{E} - \nabla q \cdot \boldsymbol{u} - q\nabla \cdot \boldsymbol{u}. \tag{2.20}$$

Using equations (2.12) and the continuity equation (2.23) of hydrodynamics discussed in the next section, we get

$$\frac{\partial q}{\partial t} = -\frac{\varsigma}{\varepsilon} q - \nabla q \cdot \boldsymbol{u}. \tag{2.21}$$

For a medium at rest (i.e., $\boldsymbol{u} = 0$) the charge relaxes exponentially, the solution can be written as $q = q_0 e^{-t/\tau}$, where $\tau = \varepsilon/\varsigma$ is the charge relaxation time constant. The relaxation time can be estimated by using typical values for the conductivity and $\varepsilon \approx 8.85 \times 10^{-12}\text{F} \cdot \text{m}^{-1}$. Considering liquids such as Castor oil, for example, we have $\varsigma \approx 3.54 \times 10^{-11}\text{Siemens} \cdot \text{m}^{-1}$ (see Burcham & Saville [19]). This gives the estimate $\tau \approx 0.25\text{s}$. In applications relevant to the present study, the relaxation time scales can be significantly smaller; as pointed out by Craster & Matar [29], a typical range of values in the related problem of electrically induced pattern formation is $10^{-11}\text{Siemens} \cdot \text{m}^{-1} \leq \varsigma \leq 10^{-3}\text{Siemens} \cdot \text{m}^{-1}$. This in turn leads to relaxation time scales in the range $10^{-8}\text{s} \lesssim \tau \lesssim 1\text{s}$. Since the hydrodynamic scales are much longer than these, it is consistent to ignore time derivatives in the Maxwell equations in the present problem.

2.2 Hydrodynamical Equations

The equations governing a viscous incompressible fluid flow are the Navier-Stokes equations (which follow from conservation of momentum) and the mass conservation equation, see Acheson [3], Batchelor [9], Landau & Lifshitz [73]. Let us consider a Newtonian fluid of density ρ and dynamic viscosity μ. Let $\boldsymbol{u} = \boldsymbol{u}(\boldsymbol{x}, t)$ be the velocity field in the fluid which describes the velocity $\boldsymbol{u}$ of a particle at any point $\boldsymbol{x}$ at any time t.

The mass conservation law in differential form is

$$\frac{D\rho}{Dt} + \rho\nabla \cdot \boldsymbol{u} = 0, \tag{2.22}$$

where $\frac{D}{Dt} = \frac{\partial}{\partial t} + \boldsymbol{u} \cdot \nabla$ is the material derivative. In many cases, including the present class of problems, the fluids are incompressible, i.e., $\rho = \text{const}$. Then, the mass conservation equation (2.22) reduces to

$$\nabla \cdot \boldsymbol{u} = 0. \tag{2.23}$$

The Navier-Stokes equations in vector form can be written as

$$\rho\frac{D\boldsymbol{u}}{Dt} = \nabla \cdot \boldsymbol{T} + \rho\boldsymbol{g}, \tag{2.24}$$

where $\boldsymbol{g}$ is the gravitational acceleration, and $\boldsymbol{T}$ is the stress tensor. Generally, in electrohydrodynamics the stress tensor has two parts, the mechanical stress tensor $\boldsymbol{T}^{\text{mech}}$ and the Maxwell stress tensor $\boldsymbol{T}^{\text{elec}}$ which appears due to the presence of the electric field, see Castellanos [20], Jackson [59], Panofsky & Phillips [89], Saville [103], i.e.,

$$\boldsymbol{T} = \boldsymbol{T}^{\text{mech}} + \boldsymbol{T}^{\text{elec}}. \tag{2.25}$$

For an incompressible Newtonian fluid

$$\boldsymbol{T}^{\text{mech}} = -p\boldsymbol{I} + \mu\big(\nabla\boldsymbol{u} + (\nabla\boldsymbol{u})^T\big), \tag{2.26}$$

while the Maxwell stress tensor is given by

$$\boldsymbol{T}^{\text{elec}} = \varepsilon\boldsymbol{E}\boldsymbol{E} - \frac{1}{2}\varepsilon(1-a)|\boldsymbol{E}|^2\boldsymbol{I}, \tag{2.27}$$

where $\boldsymbol{I}$ is the unit tensor, p is the pressure, ε is the permittivity, and $a = (\rho/\varepsilon)(d\varepsilon/d\rho)$ is the electrostriction coefficient. In our case the permittivity is assumed to be constant, so $a = 0$. (In general there is also a magnetic part in the Maxwell stress tensor, but since

magnetic effects are ignored we consider the electric part only.) We also note that both for the case of perfect electric conductors and perfect dielectrics of constant permittivity, the divergence of the Maxwell stress is zero, see for example Pease & Russel [95]. So the Maxwell stress can be ignored completely in the Navier-Stokes equations and appears only in the stress jump condition at the interface (see the next section).

In Cartesian coordinates (x_i) ($i = 1, 2$ in two-dimensions or $i = 1, 2, 3$ in three-dimensions) we can write

$$T_{ij}^{\text{mech}} = -p\delta_{ij} + \mu\left(\frac{\partial u_i}{\partial x_j} + \frac{\partial u_j}{\partial x_i}\right), \tag{2.28}$$

and

$$T_{ij}^{\text{elec}} = \varepsilon\left(E_i E_j - \frac{1}{2}|\boldsymbol{E}|^2\delta_{ij}\right). \tag{2.29}$$

Here (u_i) are the components of the velocity field $\boldsymbol{u}$, and (E_i) are the components of the electric field $\boldsymbol{E}$.

2.3 Boundary and Jump Conditions

First, we consider the conditions at a fluid-solid boundary. The impermeability of the solid implies continuity of the normal component of the velocity across the boundary. Also, experimental observations reveal continuity of the tangential component of the velocity. This condition is known as the no-slip boundary condition. Hence, at the solid interface

$$\boldsymbol{u} = \boldsymbol{u}_s, \tag{2.30}$$

where $\boldsymbol{u}$ and $\boldsymbol{u}_s$ are the velocities of the fluid and the solid at the boundary.

Next, we consider the conditions at the interface. Let S be the interface between two fluids (or between a fluid and a hydrodynamically passive region, e.g., air). Let us denote the corresponding regions by Region I and Region II. The condition that reflects the fact that a particle on the surface remains on it during the course of evolution, is called the

kinematic condition. If $F(\boldsymbol{x}, t) = 0$ is the equation of the interface, then this condition can be written as

$$\frac{DF}{Dt} = 0 \quad \text{for } \boldsymbol{x} \in S. \tag{2.31}$$

(More rigorously we should write $\lim_{\boldsymbol{x} \to S} \frac{DF}{Dt} = 0$, and if both regions are occupied with fluids we get two conditions – the first condition when $\boldsymbol{x} \to S$ from points in Region I, and the second condition when $\boldsymbol{x} \to S$ from points in Region II.) Using $\frac{D}{Dt} = \frac{\partial}{\partial t} + \boldsymbol{u} \cdot \nabla$, we can write

$$\frac{\partial F}{\partial t} + \boldsymbol{u} \cdot \nabla F = 0 \quad \text{for } \boldsymbol{x} \in S. \tag{2.32}$$

For an illustrative example, let us consider the two dimensional case. Let (x_1, x_2) be the Cartesian coordinates and (u_1, u_2) be the components of the velocity. If the equation of the interface is given by $x_2 = h(x_1, t)$ (i.e., $F(x_1, x_2, t) = x_2 - h(x_1, t)$) then the kinematic condition can be written as

$$u_2 = \frac{\partial h}{\partial t} + u_1 \frac{\partial h}{\partial x_1} \quad \text{on } x_2 = h(x_1, t). \tag{2.33}$$

Note that when both regions are occupied by fluids, the kinematic condition also implies the continuity of the normal component of the velocity.

Another condition follows from the equilibria of forces at the interface. It states that the difference between the values of the stress on two surface elements parallel to the boundary and immediately on either side of it, is a normal force due wholly to surface tension. Let σ be the constant surface tension coefficient, $\boldsymbol{n}$ be the unit normal vector pointing out of Region I. Then this condition can be written as

$$[\boldsymbol{T} \cdot \boldsymbol{n}]_{\mathrm{II}}^{\mathrm{I}} = \sigma \kappa \boldsymbol{n}, \tag{2.34}$$

Here $\boldsymbol{T}$ is the stress tensor defined by (2.25), (2.26), (2.27), and $\kappa = -\nabla \cdot \boldsymbol{n}$ (in two dimensions κ is the curvature of the curve representing the interface, in three dimensions

κ is the doubled mean curvature of the surface representing the interface). We use the notation $[*]^{\mathrm{I}}_{\mathrm{II}} = (*)^{\mathrm{I}} - (*)^{\mathrm{II}}$ for the jump in quantities between Regions I and II.

In two dimensions (2.34) can be written as

$$[\boldsymbol{t} \cdot \boldsymbol{T} \cdot \boldsymbol{n}]^{\mathrm{I}}_{\mathrm{II}} = 0, \tag{2.35}$$

$$[\boldsymbol{n} \cdot \boldsymbol{T} \cdot \boldsymbol{n}]^{\mathrm{I}}_{\mathrm{II}} = \sigma\kappa, \tag{2.36}$$

where $\boldsymbol{t}$ is the unit tangent vector to the interface. In Cartesian coordinates $(x_1,\, x_2)$ we get

$$\boldsymbol{n} = \frac{1}{\sqrt{1 + h_{x_1}^2}}(-h_{x_1},\, 1), \quad \boldsymbol{t} = \frac{1}{\sqrt{1 + h_{x_1}^2}}(1,\, h_{x_1}), \tag{2.37}$$

and the curvature κ of the interface $x_2 = h(x_1,\, t)$ is given by

$$\kappa = \frac{h_{x_1 x_1}}{(1 + h_{x_1}^2)^{3/2}}. \tag{2.38}$$

Now we consider the jump conditions at the interface satisfied by the electric field. First, the tangential components of the electric field must be continuous:

$$[\boldsymbol{n} \times \boldsymbol{E}]^{\mathrm{I}}_{\mathrm{II}} = 0, \tag{2.39}$$

or equivalently the potential V must be continuous at the interface

$$[V]^{\mathrm{I}}_{\mathrm{II}} = 0. \tag{2.40}$$

Another condition is for the jump of normal components of the electric displacement:

$$[\boldsymbol{n} \cdot (\varepsilon \boldsymbol{E})]^{\mathrm{I}}_{\mathrm{II}} = -q_s, \tag{2.41}$$

where q_s is the surface charge density. This condition arises by application of Gauss's law over a control volume that contains an element of the interface and whose upper and lower faces are locally parallel to the interface and lie in regions I and II, respectively (such a

volume element is known as a "pillbox"). Using the fact that q is non-zero on the interface alone and applying the divergence theorem to the pillbox, gives the desired result.

Finally, the surface charge conservation law is (see Castellanos [20], Castellanos & Gonzalez [21])

$$\frac{\partial q_s}{\partial t'} - \kappa u_n q_s + \nabla_s \cdot \boldsymbol{K}_s - \boldsymbol{n} \cdot [\boldsymbol{J}]_{\mathrm{II}}^{\mathrm{I}} + u_n [q]_{\mathrm{II}}^{\mathrm{I}} = 0, \tag{2.42}$$

where q_s is the surface charge density, $u_n = \boldsymbol{u} \cdot \boldsymbol{n}$ is the normal velocity, $\boldsymbol{K}_s$ is the surface current density. The primed time derivative means the derivative when we follow the surface along a direction normal to itself, $\frac{\partial}{\partial t'} = \frac{\partial}{\partial t} + u_n \boldsymbol{n} \cdot \nabla$, and the operator ∇_s is the surface gradient operator. The surface current density can be written in the form

$$\boldsymbol{K}_s = \lambda_s q_s \boldsymbol{E}_s + \varsigma_s \boldsymbol{E}_s + q_s \boldsymbol{u}_s - D_s \nabla q_s, \tag{2.43}$$

where λ_s is the surface mobility, ς_s is the surface conductivity and D_s is surface diffusion coefficient. In addition $\boldsymbol{E}_s$ and $\boldsymbol{u}_s$ denote the electric field and fluid velocity tangential to the interface as measured by an observer in a fixed laboratory frame. The charge conservation law (2.42) has been given in its most general form and various simplifications can be made in different modelling situations. For example, if λ_s, ς_s, $D_s \ll 1$, that is surface mobility, conductivity and diffusion coefficients are small with respect to other effects such as convection and stretching of the interface, then $\boldsymbol{K}_s = q_s \boldsymbol{u}_s$, to leading order, a version that has appeared in the literature (see for example Craster & Matar [29], Papageorgiou & Petropoulos [91]). In addition, if equation (2.42) is considered at times $t \gg \tau$, then the charge densities in the bulk regions are zero and the last source term in the equation can be dropped. In the problems studied here the fluid in Region I is a perfect conductor and hence $\varsigma \gg 1$. In such problems any charge that may be present on the interface can be determined by use of Gauss's law (2.41) after the voltage is found. In the problems considered here such calculations for the charge can be carried out *a posteriori* as explained above.

CHAPTER 3

TWO-DIMENSIONAL FLUID FLOW DOWN AN INCLINED PLANE UNDER NORMAL ELECTRIC FIELD

3.1 Physical Model

We investigate a two-dimensional fluid flow down an inclined plane when an electric field acts on it. We consider the isothermal case. The physical model of a two-dimensional flow is depicted in Figure 3.1. A Newtonian liquid of constant density ρ and viscosity μ,

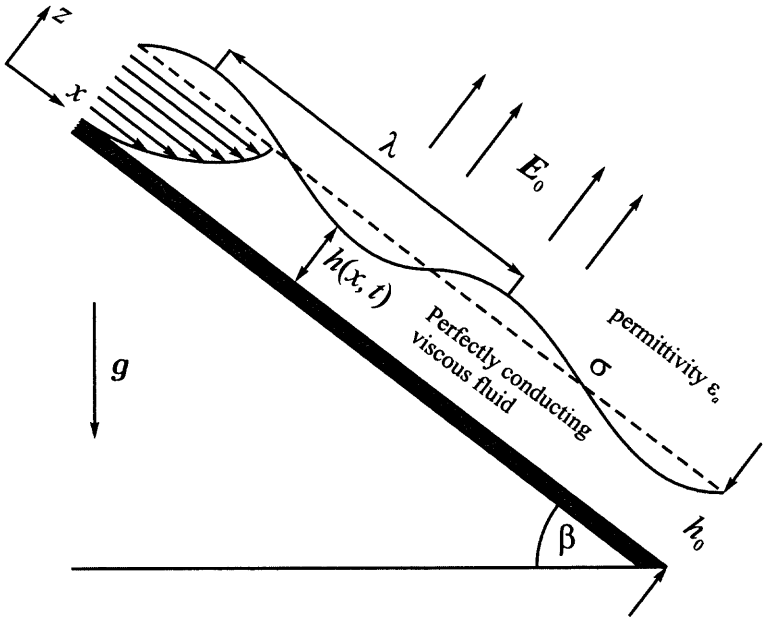

Figure 3.1 Schematics of the problem.

flows under gravity along an infinitely long flat plate which is inclined at an angle β to the horizontal. A coordinate system (x, z) is adopted with x measuring distance down and along the plate and z distance perpendicular to it (see Figure 3.1). The film thickness is $z = h(x, t)$ and its unperturbed value is h_0. The surface tension coefficient between the liquid and the surrounding medium is σ and the gravitational acceleration in denoted by $\boldsymbol{g}$. The plate is taken to be an infinite electrode which, without loss of generality, is held at

zero voltage potential, i.e., the electrode is grounded. Far from the plate the electric field $\boldsymbol{E}_0$ is uniform and normal to the plate. The surrounding medium is assumed to be a perfect dielectric with permittivity ε_a, and the corresponding voltage potential in it is denoted by V. In this study the liquid is assumed to be perfectly conducting implying that the potential on the deformed liquid interface is zero (the electric field in the liquid is also zero). Along with the usual viscous stresses at the free surface, the electric field causes additional Maxwell stresses which can affect flow stability and the ensuing dynamics. Physically, this occurs by a reduction in pressure just beneath the interface due to the field and we wish to study systematically this effect on the nonlinear dynamics of the falling film. More details of the mathematical model are presented next.

3.2 Governing Equations

Let the velocity field in the $(x,\, z)$ coordinate system be $\boldsymbol{u} = (u,\, v)$. In what follows we denote the liquid layer by Region I and the surrounding medium by Region II:

$$\text{Region I} = \{(x,\, z) |\, 0 < z < h(x,\, t)\}, \tag{3.1}$$

$$\text{Region II} = \{(x,\, z) |\, z > h(x,\, t)\}. \tag{3.2}$$

The governing equations in Region I are the mass conservation equation (2.23) and the momentum equations (2.24). There is no electric field in Region I since in our case the fluid is a perfect electric conductor. Therefore the stress tensor $\boldsymbol{T}$ has only the mechanical part $\boldsymbol{T}^{\text{mech}}$. Using the component form of $\boldsymbol{T}^{\text{mech}}$ given by (2.28) with $i,\, j = 1,\, 2$, and $x_1 = x$, $x_2 = z$, $u_1 = u$, $u_2 = v$, we obtain the component form of the equations:

$$u_t + uu_x + vu_z = -\frac{p_x}{\rho} + \nu(u_{xx} + u_{zz}) + g\sin\beta, \tag{3.3}$$

$$v_t + uv_x + vv_z = -\frac{p_z}{\rho} + \nu(v_{xx} + v_{zz}) - g\cos\beta, \tag{3.4}$$

$$u_x + v_z = 0. \tag{3.5}$$

We note that since the liquid is a perfect electric conductor the electric field is zero in Region I. Hence we consider equations (2.19) only in Region II. Also, in Region II there are no free charges, i.e., $q = 0$ and $\boldsymbol{J} = 0$. So, in Region II the electric field can be written as the gradient of a potential function V, $\boldsymbol{E} = -\nabla V$, and the potential V satisfies the Laplace equation:

$$\nabla^2 V = 0, \tag{3.6}$$

or in the component form:

$$V_{xx} + V_{zz} = 0. \tag{3.7}$$

The boundary conditions are those of no slip at the wall,

$$u|_{z=0} = 0, \quad v|_{z=0} = 0, \tag{3.8}$$

and a uniform field condition at infinity,

$$V_x \to 0,\ V_z \to -E_0 \quad \text{as } z \to \infty. \tag{3.9}$$

At the interface $z = h(x,\ t)$ we must satisfy a kinematic condition, the zero (or constant) potential condition and balance of normal and tangential stresses. The out pointing unit normal and unit tangent vectors at any point on $z = h(x,\ t)$ are given by $\boldsymbol{n} = (-h_x,\ 1)/(1+h_x^2)^{1/2}$ and $\boldsymbol{t} = (1,\ h_x)/(1 + h_x^2)^{1/2}$. The kinematic condition is

$$v = h_t + uh_x, \tag{3.10}$$

and noting that $\nabla V \cdot \boldsymbol{t} = 0$ is equivalent to a constant potential on the interface, we obtain

$$V = 0 \quad \Rightarrow \quad V_x + h_x V_z = 0 \quad \text{on} \quad z = h(x,\ t). \tag{3.11}$$

The components of the stress tensors in Region I are

$$T_{ij}^{\mathrm{I}} = -p\delta_{ij} + \mu\left(\frac{\partial u_i}{\partial x_j} + \frac{\partial u_j}{\partial x_i}\right), \tag{3.12}$$

and in Region II

$$T_{ij}^{\mathrm{II}} = -p_{\mathrm{atm}}\delta_{ij} + \varepsilon_a\left(E_iE_j - \frac{1}{2}|\boldsymbol{E}|^2\delta_{ij}\right), \tag{3.13}$$

where p_{atm} is the constant atmospheric pressure. Here, and everywhere in this chapter, we assume that $i, j = 1, 2$, $x_1 = x$, $x_2 = z$, $u_1 = u$, $u_2 = v$, and (E_1, E_2) are the components of the electric field. Note that the stresses in Region I do not have an electric part due to the absence of a field, while those in Region II do not have a viscous part since the outer phase is assumed to be hydrodynamically passive. In general, both viscous and electrical stresses are present (for perfect dielectrics see Savettaseranee et al. [101], for example). The Maxwell stresses do not contribute to the tangential stress balance unless there is a finite conductivity in either of the two phases as in the leaky dielectric model (see for example Papageorgiou & Petropoulos [91]). This can be verified directly for the present problem by using condition (3.11) in (2.35); if in addition we use $u_x = -v_z$ from the continuity equation, the boundary condition (2.35) becomes

$$(1 - h_x^2)(u_z + v_x) + 4h_xv_z = 0 \quad \text{on} \quad z = h(x, t). \tag{3.14}$$

Using a similar procedure and the identity $u_z + v_x = -\frac{4h_xv_z}{1-h_x^2}$, which follows from (3.14) above, yields the following normal stress boundary condition

$$p_{\mathrm{atm}} - p - \frac{\varepsilon_a}{2}(1 + h_x^2)V_z^2 + 2\mu\frac{1 + h_x^2}{1 - h_x^2}v_z = \frac{\sigma h_{xx}}{(1 + h_x^2)^{3/2}} \quad \text{on} \quad z = h(x, t). \tag{3.15}$$

This completes the statement of the problem which, when supplemented with initial conditions, constitutes a formidable nonlinear free boundary problem. We will proceed asymptotically and seek nonlinear evolution equations valid for long waves. Before doing this it is useful to identify an exact (albeit unstable) solution and an appropriate nondimensionalization.

An exact solution exists which has $h(x, t) = h_0$ with h_0 being a positive constant. This is analogous to the Nusselt solution for the non-electric case (see Benjamin [10],

Nusselt [87]) and is given by

$$\bar{u} = \frac{g \sin\beta}{2\nu}(2h_0 z - z^2), \tag{3.16}$$

$$\bar{v} = 0, \tag{3.17}$$

$$\bar{p} = p_{\text{atm}} - \frac{\varepsilon_a E_0^2}{2} - \rho g(z - h_0)\cos\beta, \tag{3.18}$$

$$\overline{V} = E_0(h_0 - z). \tag{3.19}$$

We see that the steady velocity profile is parabolic in z, while the electric potential varies linearly with z.

3.3 Dimensionless Equations

To nondimensionalize the equations distances are scaled by the unperturbed depth h_0, velocities by the base velocity at the interface $u_0\big|_{z=h_0} \equiv U_0 = \frac{gh_0^2 \sin\beta}{2\nu}$, the time scale is chosen to be $\frac{h_0}{U_0} = \frac{2\nu}{gh_0 \sin\beta}$, pressure is scaled by ρU_0^2, and the unit for the voltage potential is taken from the change in the basic potential, which is $E_0 h_0$. Introducing the following nondimensional variables,

$$x^* = \frac{1}{h_0}x, \quad z^* = \frac{1}{h_0}z, \quad t^* = \frac{U_0}{h_0}t, \tag{3.20}$$

$$u^* = \frac{1}{U_0}u, \quad v^* = \frac{1}{U_0}v, \quad p^* = \frac{1}{\rho U_0^2}p, \quad V^* = \frac{1}{E_0 h_0}V, \quad h^* = \frac{1}{h_0}h, \tag{3.21}$$

substituting into equations (3.3)-(3.7) and the boundary conditions (3.10), (3.11), (3.14) and (3.15) and dropping the stars, provides the following nondimensional equations and boundary conditions: In Region I the Navier-Stokes equations become

$$u_t + uu_x + vu_z = -p_x + \frac{1}{R}(u_{xx} + u_{zz}) + \frac{2}{R}, \tag{3.22}$$

$$v_t + uv_x + vv_z = -p_z + \frac{1}{R}(v_{xx} + v_{zz}) - \frac{2}{R}\cot\beta, \tag{3.23}$$

$$u_x + v_z = 0, \tag{3.24}$$

and in Region II we have the Laplace equation for the electric potential:

$$V_{xx} + V_{zz} = 0. \tag{3.25}$$

No slip holds at the wall, $u|_{z=0} = 0$, $v|_{z=0} = 0$ and at infinity we have

$$V_x \to 0,\ V_z \to -1 \quad \text{as} \quad z \to \infty. \tag{3.26}$$

At the interface $z = h(x,\ t)$ we have:

$$V = 0, \tag{3.27}$$

$$v = h_t + uh_x, \tag{3.28}$$

$$(1 - h_x^2)(u_z + v_x) + 4h_x v_z = 0, \tag{3.29}$$

$$-\frac{W_e}{2}(1 + h_x^2)V_z^2 + \frac{1 + h_x^2}{1 - h_x^2}v_z + \frac{R}{2}(\bar{p}_{\text{atm}} - p) = \frac{h_{xx}}{2C(1 + h_x^2)^{3/2}}, \tag{3.30}$$

where $\bar{p}_{\text{atm}} = p_{\text{atm}}/(\rho U_0^2)$ is the nondimensional constant pressure in Region II. The other dimensionless parameters are a Reynolds number R (measuring the ratio of inertial to viscous forces), a Capillary number C (measuring the ratio of viscous to capillary forces) and an electric Weber number W_e (measuring the ratio of electrical to gravitational forces), and are given by

$$R = \frac{U_0 h_0}{\nu} = \frac{g h_0^3 \sin\beta}{2\nu^2}, \quad C = \frac{U_0 \mu}{\sigma} = \frac{\rho g h_0^2 \sin\beta}{2\sigma}, \quad W_e = \frac{\varepsilon_a E_0^2}{\rho g h_0 \sin\beta}. \tag{3.31}$$

The exact solutions (3.16)-(3.19) are nondimensionalized analogously. In what follows we write all dependent variables as the undisturbed dimensionless solution plus an arbitrary disturbance. Thus, we introduce new unknowns $\tilde{u}$, $\tilde{v}$, $\tilde{p}$, $\widetilde{V}$:

$$u = \bar{u} + \tilde{u}, \tag{3.32}$$

$$v = \bar{v} + \tilde{v}, \tag{3.33}$$

$$p = \bar{p} + \tilde{p}, \tag{3.34}$$

$$V = \overline{V}_0 + \widetilde{V}, \tag{3.35}$$

and drop tildes in the field equations and boundary conditions (note that we use bars to denote corresponding dimensionless base solutions). For brevity, we only give the transformed boundary conditions at the interface $z = h(x, t)$:

$$V = h - 1, \tag{3.36}$$

$$v = h_t + (h(2 - h) + u)\, h_x, \tag{3.37}$$

$$(1 - h_x^2)\,(2(1 - h) + u_z + v_x) + 4h_x v_z = 0, \tag{3.38}$$

$$-\frac{W_e}{2}\left[(1 - V_z)^2(1 + h_x^2) - 1\right] + \frac{1 + h_x^2}{1 - h_x^2}v_z - \cot\beta(1 - h) - \frac{R}{2}p = \frac{h_{xx}}{2C(1 + h_x^2)^{3/2}}. \tag{3.39}$$

3.4 Derivation of the Long Wave Evolution Equations

Assume that typical interfacial deformation wavelengths λ are long compared to the undisturbed thickness h_0, i.e., $\delta = \frac{h_0}{\lambda} \ll 1$. This condition can also be formulated as $\left|\frac{\partial h}{\partial x}\right| \ll 1$. Since lengths have been scaled with h_0, there is a separation of length scales in the liquid layer (Region I) and we introduce the following appropriate change of variables:

$$x = \frac{1}{\delta}\xi, \quad z = z, \quad t = \frac{1}{\delta}\tau, \quad v = \delta w. \tag{3.40}$$

The boundary conditions at the interface ($z = h(\xi, t)$) become:

$$w = h_\tau + (\bar{u} + u)h_\xi, \tag{3.41}$$

$$(1 - \delta^2 h_\xi^2)\left(\frac{d\bar{u}}{dz} + u_z + \delta^2 w_\xi\right) + 4\delta^2 h_\xi w_z = 0, \tag{3.42}$$

$$-\frac{W_e}{2}\left[(1 - V_z)^2(1 + \delta^2 h_\xi^2) - 1\right] + \delta\frac{1 + \delta^2 h_\xi^2}{1 - \delta^2 h_\xi^2}w_z - \cot\beta(1 - h) - \frac{R}{2}p = \frac{\delta^2 h_{\xi\xi}}{2C(1 + \delta^2 h_\xi^2)^{3/2}}. \tag{3.43}$$

Boundary condition (3.43) contains a nonlocal contribution since V satisfies the Laplace equation in the potential region above the fluid layer – see Figure 3.2. Before proceeding

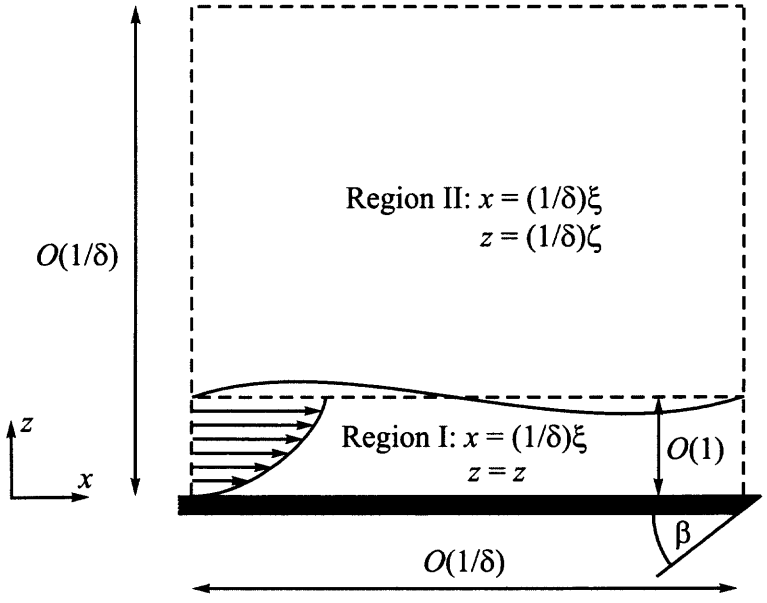

Figure 3.2 Rescaling of x and z in Regions I and II.

with an asymptotic solution in Region I we calculate the nonlocal contribution in (3.43) in terms of $h(\xi, t)$. To achieve this, we introduce the following independent variables in Region II:

$$x = \frac{1}{\delta}\xi, \quad z = \frac{1}{\delta}\zeta, \quad t = \frac{1}{\delta}\tau. \tag{3.44}$$

The perturbation voltage potential satisfies

$$V_{\xi\xi} + V_{\zeta\zeta} = 0, \tag{3.45}$$

$$V_\xi \to 0, \; V_\zeta \to 0 \quad \text{as} \quad \zeta \to \infty. \tag{3.46}$$

The boundary condition at the interface is

$$V|_{\zeta=\delta h} = h(\xi, \tau) - 1 \quad \Rightarrow \quad V|_{\zeta\approx 0} = h(\xi, \tau) - 1, \tag{3.47}$$

keeping the leading term in δ.

To solve this problem we note that $f(\chi) = V_\xi - iV_\zeta$ is an analytic function of the complex variable $\chi = \xi + i\zeta$. Next we apply Cauchy's theorem (see for example Ablowitz

& Fokas [2], Markushevich [81]) to $f(\chi)$ on a rectangular contour bounding Region II, see Figure 3.3; the upper part of the contour is located at $\zeta = D$ and the vertical parts are placed at $\xi = \pm L$, for some D, $L > 0$ (periodicity in ξ can be achieved also – see later). As $D \to \infty$ the contribution to the integral along the line $\zeta = D$ vanishes (see (3.46)) as

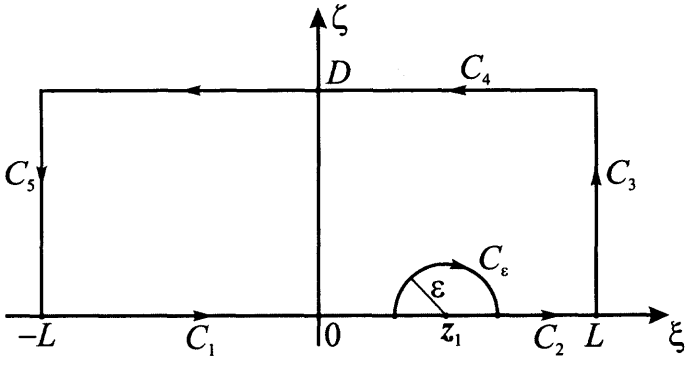

Figure 3.3 Contour of integration C.

does the contribution along the vertical parts as $L \to \infty$ (in the periodic case the vertical contributions vanish due to the direction of the contour integration). As $\zeta \to 0$ the contour integration gives

$$V_\xi(\xi,0) - iV_\zeta(\xi,0) = -\frac{1}{i\pi} PV \int_{-\infty}^{\infty} \frac{V_\xi(\xi',0) - iV_\zeta(\xi',0)}{\xi - \xi'} d\xi', \tag{3.48}$$

where PV denotes the principal value of the integral. Taking the imaginary part of equation (3.48) and differentiating (3.47) with respect to ξ to obtain $V_\xi(\xi,0) = h_\xi$, gives

$$V_\zeta(\xi,0) = -\mathcal{H}[h_\xi], \tag{3.49}$$

where $\mathcal{H}$ is the Hilbert transform operator defined by:

$$\mathcal{H}[g](\xi) = \frac{1}{\pi} PV \int_{-\infty}^{\infty} \frac{g(\xi')}{\xi - \xi'} d\xi'. \tag{3.50}$$

Some properties of the Hilbert transform are given in Appendix A.

With the nonlocal contribution of the electric field known, and noting that V_z transforms to δV_ζ in terms of outer variables, boundary condition (3.43) becomes

$$-\delta W_e \mathcal{H}[h_\xi] + \delta w_z - \cot\beta(1-h) - \frac{R}{2}p + \mathcal{O}(\delta^2) = \frac{\delta^2 h_{\xi\xi}}{2C(1+\delta^2 h_\xi^2)^{3/2}} \quad (\text{on } z=h). \tag{3.51}$$

In order to retain the effect of surface tension and the electric field in the leading order dynamics, we take the canonical scalings

$$C = \delta^2 \overline{C}, \quad W_e = \frac{\overline{W}_e}{\delta}, \tag{3.52}$$

where $\overline{C}$ and $\overline{W}_e$ are order one constants. This leads to

$$p|_{z=h} = \frac{2}{R}\Big[-\overline{W}_e \mathcal{H}[h_\xi] - \cot\beta(1-h) - \frac{1}{2\overline{C}} h_{\xi\xi}\Big]. \tag{3.53}$$

In Region I the appropriate asymptotic expansions are

$$u = u_0 + \delta u_1 + \delta^2 u_2 + \cdots, \qquad w = w_0 + \delta w_1 + \delta^2 w_2 + \cdots, \tag{3.54}$$

$$p = p_0 + \delta p_1 + \delta^2 p_2 + \cdots, \qquad h = H_0 + \delta H_1 + \delta^2 H_2 + \cdots. \tag{3.55}$$

In what follows the Reynolds number R is assumed to be of order one (for long wave analyses at large R the reader is referred to the monograph of Chang & Demekhin [24] and numerous historical references therein). At the leading order we find:

$$u_0 = 2(H_0 - 1)z, \tag{3.56}$$

$$w_0 = -z^2 H_{0\xi}, \tag{3.57}$$

$$p_0 = \frac{2}{R}\Big[-\overline{W}_e \mathcal{H}[H_{0\xi}] + (H_0 - 1)\cot\beta - \frac{1}{2\overline{C}} H_{0\xi\xi}\Big], \tag{3.58}$$

$$H_{0\tau} + 2H_0^2 H_{0\xi} = 0. \tag{3.59}$$

The last equation represents mass conservation and is also found in the non-electrical case – Benney [11], Lin [75], Nakaya [84]. In general, the solution of this equation has infinite

slope singularities after a finite time and the long wave asymptotic expansion breaks down near the singularity; the usual way to proceed is to regularize the dynamics by incorporating high order effects. We also note that for the case of weakly nonlinear evolution considered later, $H_0 \equiv 1$ satisfies (3.59) exactly and there is no need of composite solutions that contain both order one and order δ terms. Proceeding to the next order we find the following equation for H_1:

$$H_{1\tau} + H_0^2 H_{1\xi} + 2H_0 H_{0\xi} H_1 + u_1|_{z=H_0} H_{0\xi} - w_1|_{z=H_0} = 0, \tag{3.60}$$

where

$$u_1|_{z=H_0} = -\frac{R}{2} H_0^2 p_{0\xi} + \frac{5}{6} R H_0^5 H_{0\xi} + 2H_0 H_1, \tag{3.61}$$

$$w_1|_{z=H_0} = \frac{R}{3} H_0^3 p_{0\xi\xi} + \frac{R}{2} H_0^2 H_{0\xi} p_{0\xi} - \frac{71}{30} R H_0^5 H_{0\xi}^2 - \frac{8}{15} R H_0^6 H_{0\xi\xi} - H_0^2 H_{1\xi}, \tag{3.62}$$

$$p_0 = \frac{2}{R}\left[-\overline{W}_e \mathcal{H}[H_{0\xi}] + (H_0 - 1)\cot\beta - \frac{1}{2\overline{C}} H_{0\xi\xi}\right]. \tag{3.63}$$

Using these expressions in (3.60) casts the latter into the more compact form:

$$H_{1\tau} + \left[2H_0^2 H_1 - \frac{R}{3} H_0^3 p_{0\xi} + \frac{8}{15} R H_0^6 H_{0\xi}\right]_\xi = 0. \tag{3.64}$$

A regularized equation for the new dependent variable $H = H_0 + \delta H_1$ can now be sought by adding δ times equation (3.60) to equation (3.59). It is essential to show, however, that the resulting evolution equation for $H(\xi, \tau)$ is correct to order δ^2 to ensure asymptotic consistency. This calculation is provided in Appendix B. The resulting regularized equation is given by

$$H_\tau + \left[\frac{2}{3} H^3 + \delta\left(\frac{8}{15} R H^6 - \frac{2}{3}\cot\beta H^3\right) H_\xi + \frac{\delta}{3\overline{C}} H^3 H_{\xi\xi\xi} + \frac{2\delta}{3}\overline{W}_e H^3 \mathcal{H}[H_{\xi\xi}]\right]_\xi = 0. \tag{3.65}$$

This equation was derived by Gonzalez & Castellanos [44] using an intuitive approach rather than formal asymptotics. It is an electrostatically modified version of the nonlinear interfacial models of Lin [75], Nakaya [84] and the extensive analytical and numerical

study of Pumir et al. [97]. The latter study is particularly interesting because it shows that equation (3.65) with $\overline{W}_e = 0$ supports solitary as well as heteroclinic travelling waves. In addition, numerical solutions of the initial value problem provide strong evidence that solutions may not exist for all time and for all values of the parameters. One such calculation corresponds to our parameters $R = 13, \cot\beta = 5, \overline{C} = 1/2000$, and is found to blow up in a finite time, t_s say; a self-similar structure is postulated in the form

$$H \sim (t_s - t)^{-1/9} G(\xi/(t_s - t)^{1/6}),$$

where G is a scaling function that was not calculated. In addition to the evidence that global existence of solutions is unlikely, we see from equations (3.59) and (3.64) that in general $H_{0\xi}$ and higher derivatives become infinite in finite time and this also holds for H_1 and its derivatives. In fact if $H_\xi = H_{0\xi} + \delta H_{1\xi}$, for example, is to remain bounded (as is the case for most parameter values) then H_1 and higher terms become unbounded in finite time. As shown in Appendix B the neglected order δ^2 terms that lead to (3.65) contain H_1 and these will become as large as the retained terms even when H remains smooth. We must proceed iteratively, then, writing $H = \sum_{j=0}^{n} \delta^j H_j$, $n = 2, 3, \ldots$, and showing that an evolution equation is obtained which is correct to $\mathcal{O}(\delta^{n+1})$, for each n. This calculation has not been carried out for $n \geq 3$. In the light of these difficulties, then, we construct rational asymptotic solutions that do not have a δ-dependence. This is achieved by looking for weakly nonlinear corrections to $H_0 = 1$ which solves (3.59) exactly – see also Sivashinsky & Shlang [111] for the related problem of film flow down a vertical column when the column radius is asymptotically large compared to the film thickness. It is also important to note that when the plate is horizontal, $\beta = 0$, a fully nonlinear long wave evolution equation which is independent of δ, appears at leading order – see Oron et al. [88]. This case is analyzed in a separate chapter (see Chapter 5).

3.4.1 Weakly Nonlinear Evolution

We seek a consistent asymptotic evolution of long waves by imposing $H_0(\xi, \tau) \equiv 1$. We write $H = 1 + \alpha(\delta)\eta$ where $\alpha(\delta) = o(\delta^{1/2})$ and $\eta = \mathcal{O}(1)$. Substituting into (3.65) we obtain, correct to order δ,

$$\eta_\tau + 2\eta_\xi + 4\alpha\eta\eta_\xi - \frac{2D}{3}\delta\eta_{\xi\xi} + \frac{\delta}{3\overline{C}}\eta_{\xi\xi\xi\xi} + \frac{2\overline{W}_e}{3}\delta\mathcal{H}[\eta_{\xi\xi\xi}] = 0, \tag{3.66}$$

where $D = \cot\beta - \frac{4}{5}R$. The advective term $2\eta_\xi$ is removed by a Galilean transformation and a canonical equation arises from (3.66) when the following change of variables is used:

$$\xi - 2\tau = \frac{1}{(2\overline{C}|D|)^{1/2}}x, \quad \delta\tau = \frac{3}{4\overline{C}D^2}t, \quad \eta = \frac{\delta}{6\alpha}(2\overline{C}|D|^3)^{1/2}u, \tag{3.67}$$

to obtain

$$u_t + uu_x \pm u_{xx} + u_{xxxx} + \gamma\mathcal{H}[u_{xxx}] = 0. \tag{3.68}$$

Note that u from now on represents the scaled interfacial amplitude and is unrelated to previous dependent variables; $\gamma = 2\overline{W}_e\overline{C}/|D|^{1/2}$ is a positive constant and the plus sign in front of u_{xx} is taken if D is negative while the minus sign is taken if D is positive. As a weakly nonlinear approximation of (3.65) equation (3.68) is valid for $u = o(\delta^{-1/2})$. When the electric field is absent, i.e., $W_e = 0$, and $D < 0$, the canonical equation is the Kuramoto-Sivashinsky (KS) equation (see Pumir et al. [97] and Introduction):

$$u_t + uu_x + u_{xx} + u_{xxxx} = 0. \tag{3.69}$$

3.4.2 Linear Stability

Linearizing (3.68) about $u = 0$ gives $u_t \pm u_{xx} + u_{xxxx} + \gamma\mathcal{H}[u_{xxx}] = 0$ which has normal mode solutions proportional to $\exp(ikx + st)$ if the dispersion relation

$$s(k) = -k^4 + \gamma|k|^3 \pm k^2, \tag{3.70}$$

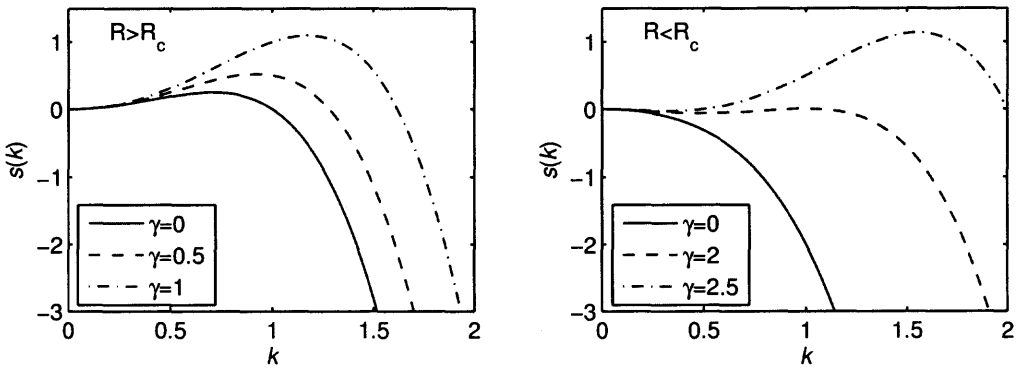

Figure 3.4 Changes in the dispersion relation due to the electric field. The left panel corresponds to the flow above the critical Reynolds number, the right panel – below the critical Reynolds number.

is satisfied. This dispersion relation was also given by Gonzalez & Castellanos [44] in an unscaled form. The case with the positive sign corresponds to $D < 0$ ($R > R_c = \frac{5\cot\beta}{4}$) and gives a band of unstable modes for $0 < k < \frac{\gamma+\sqrt{\gamma^2+4}}{2}$. As γ increases the size of the band as well as the corresponding maximum growth rate, increase. Representative results are shown in Figure 3.4.

If $D > 0$ ($R < R_c$) we obtain the negative sign in (3.70), and as pointed out in Gonzalez & Castellanos [44] there are two sub-cases: (i) $\gamma \leq 2$ where all modes are stable, i.e., $s(k) \leq 0$ for all k, and, (ii) $\gamma > 2$ where there appears a band of unstable waves extending from $k = \frac{\gamma-\sqrt{\gamma^2-4}}{2}$ to $k = \frac{\gamma+\sqrt{\gamma^2-4}}{2}$. Typical results are shown in Figure 3.4.

In both cases the electric field is destabilizing. The weakly nonlinear stability in the vicinity of $\gamma = 2$ was carried out by Gonzalez & Castellanos [44] where a Ginzburg-Landau equation admitting supercritical states was derived. The present work has very little overlap with that study since we are interested in the dynamics well-beyond critical in Case II; we also study Case I which is not amenable to a similar weakly nonlinear theory.

3.5 Spatio-temporal Dynamics: Regular and Chaotic Solutions

Linear theory predicts that sufficiently long waves are unstable and that the electric field increases the instability band to include relatively shorter waves. For the KS equation it is established (numerically and analytically) that nonlinearity acts to saturate the instability (negative diffusion and fourth derivative damping) to produce a host of rich dynamical behavior: steady states, Hopf bifurcations to time periodic solutions, period doubling cascades to chaos according to the Feigenbaum scenario, chaotic attractors with coexisting stable multi-modal fixed points, etc. The electric field enhances the instability and the objective of this section is a systematic mapping of its effect on the dynamics as compared to those known for the KS equation. Note also that Case II above, is not the KS equation when $\gamma = 0$, and in what follows we present evidence that chaotic states emerge in this case also if γ is sufficiently large. This suggests that the electric field can be used to produce interfacial turbulence at small or zero Reynolds numbers where all disturbances would otherwise be damped. We are not aware of any controlled experiments that have observed such behavior, and the present calculations could be useful in suggesting such studies.

Consider (3.68) on a finite interval $[-L, L]$ with periodic boundary conditions; L measures the size of the system and controls the number of unstable modes present (in the context of the KS equation). We can normalize equation (3.68) to 2π-periodic domains using the rescaling

$$\bar{t} = (\pi/L)^2 t, \quad \bar{x} = (\pi/L)x, \quad \bar{u} = (L/\pi)u, \tag{3.71}$$

which (on dropping the bars) casts the equation into

$$u_t + uu_x \pm u_{xx} + \nu u_{xxxx} + \mu \mathcal{H}[u]_{xxx} = 0, \tag{3.72}$$

where $\nu = (\pi/L)^2$ and $\mu = (\pi/L)\gamma$. Periodic initial conditions are also prescribed (see later).

We used two different numerical methods. The first method implements a linear propagator so that the linear part of the operator is done exactly in Fourier space and the stiffness is removed (see for example Trefethen [118]). For example if hats denote Fourier transforms, and $\hat{U} = e^{-s(k)t}\hat{u}$, the equation becomes

$$\hat{U}_t + \frac{i}{2}e^{-s(k)t}k\widehat{u^2} = 0 \tag{3.73}$$

where $s(k)$ is the spectrum from linear theory (see above). Using a pseudo-spectral representation of derivatives, equation (3.73) becomes an ordinary differential equation (ODE) for $\hat{U}$ (for each k), and is solved with a fourth order Runge-Kutta method.

The second method is a Fourier-Galerkin one. Let $\hat{u}_k(t)$ be the Fourier coefficients of $u(x,\, t)$, i.e.,

$$u(x,\, t) = \sum_{k=-\infty}^{\infty} \hat{u}_k(t)e^{ikx}. \tag{3.74}$$

Equation (3.72) is equivalent to the following infinite dimensional system of ODEs

$$\frac{d\hat{u}_k(t)}{dt} = (-\nu k^4 + \mu|k|^3 \pm k^2)\hat{u}_k(t) - \frac{i}{2}k \sum_{k_1+k_2=k} \hat{u}_{k_1}(t)\hat{u}_{k_2}(t). \tag{3.75}$$

These equations were integrated using the Matlab integrator `ode23tb` for stiff differential equations with variable step size to ensure stability and accuracy. The modes $\hat{u}_k$ are only computed for $|k| < K_{\max}$, all other $\hat{u}_k$ being set to 0, with $K_{\max}$ chosen so that the neglected modes have magnitudes less than 10^{-15}. The value of $K_{\max}$ depends on μ and ν and in most of the computations described here it has a value of 30 or less.

The initial condition used is

$$u_0(x) = \frac{1}{10}\sum_{k=1}^{10}\big(\alpha_k \cos(kx) + \beta_k \sin(kx)\big), \tag{3.76}$$

where the coefficients α_k, β_k, $k = 1,\, 2,\, \ldots,\, 10$, are chosen randomly in the interval $[0,\, 1]$. The methods were implemented and tested for a very large number of the values of the parameters ν and μ. For the first method, for example, the space discretization ranged from

128 to 512 modes and the time step was taken to be 10^{-3} or smaller with typical maximum integration times of 100-1000 time units. A variety of diagnostics are used to determine the form of the solution – these include the tracking of the maxima and minima of the L^2 norm of the solution, return maps using these, and Fourier transforms of large time series data. Such diagnostics have been used successfully in the past for different problems – see Smyrlis & Papageorgiou [112], Smyrlis & Papageorgiou [113], Hall & Papageorgiou [51], Blyth et al. [17]. Typically, for each set of the parameters we track the time evolution of the profile, its energy (L^2-norm) and its Fourier modes. The evolution of the energy was used to classify various attractors. For example, for steady or steady-state-travelling waves the energy reaches a constant value at large times, and for periodic attractors the energy is a periodic function of time. For chaotic solutions the energy becomes highly oscillatory and information is extracted by numerically constructing return maps and studying their geometry – e.g., self-similar folding behavior is strong evidence of a chaotic attractor – see references above.

3.5.1 Numerical Results, Case I: Modified Kuramoto-Sivashinsky Equation

All our numerical results indicate that the solutions remain bounded as t becomes large. A proof of such a result is available for the KS equation (see Introduction) and this has been extended to the modified KS equation recently (Duan & Ervin [34], Tseluiko & Papageorgiou [120]). In what follows we provide a quantitative description of the different attractors as ν and μ vary (decreasing ν corresponds to an increased length of the system and increasing μ corresponds to an increased applied voltage difference).

It was also observed numerically that as the coefficient μ of the integral term goes to zero, the solutions of the modified KS equation converge in L^2 to the corresponding solutions of the usual KS equation, i.e., the results confirm that for given t,

$$\|S_\mu(t)u_0 - S(t)u_0\|_2 \to 0 \quad \text{as} \quad \mu \to 0, \tag{3.77}$$

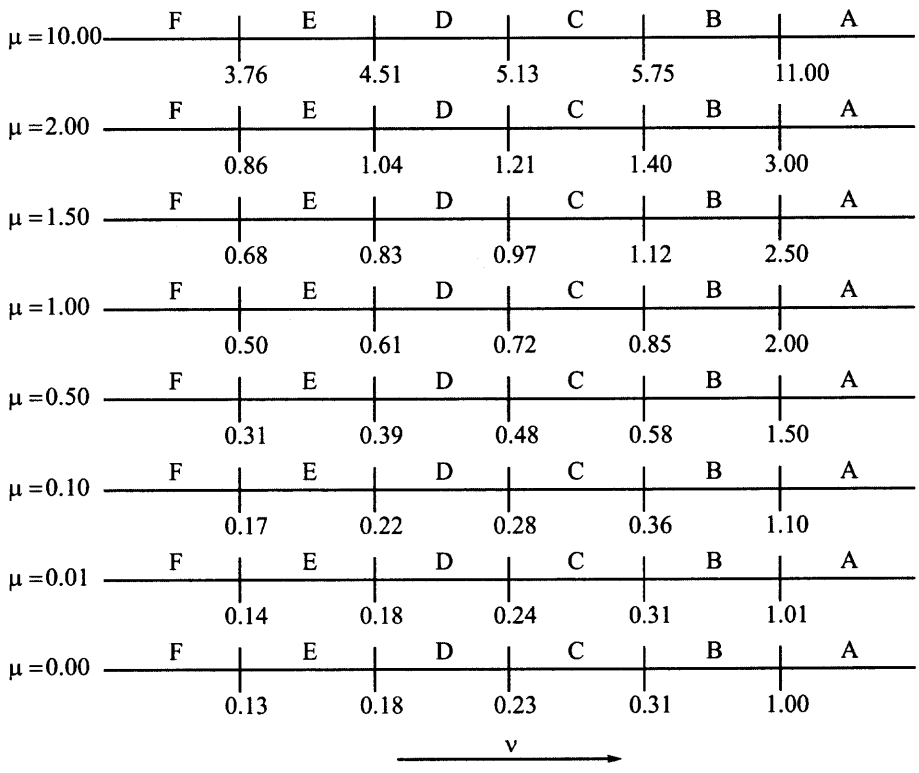

Figure 3.5 Schematic of the various attractors.

where $S_\mu(t)$ and $S(t)$ are the solution operators (semigroups) for the modified KS equation and the usual KS equation, respectively. At $\mu = 0$ we recover the results obtained for the usual KS equation; this also confirms the accuracy of the numerical simulations.

In Figure 3.5 we depict a summary of the results for different values of μ as ν decreases. The two parameter phase space is quite large and we confine our results to an overall description of the dynamical features rather than a detailed study of individual attractors. The letters A-F are used to identify windows of the parameter ν for various attractors for fixed but moderate values of μ. As μ increases the qualitative dynamics

is unaltered but the windows A-F widen in ν. The boundaries in the $\nu - \mu$ plane that separate the attractors A-F are shown in Figure 3.6, from which it is seen that all follow linear laws (for μ sufficiently large) with slopes larger than or equal to one. The right-most boundary separating attractors A and B has been established analytically but we do not have an explanation for the linear behavior of the other boundaries at present. We note that the lines "fan" out and do not cross. A brief description of the different attractors along with sample numerical results is given next.

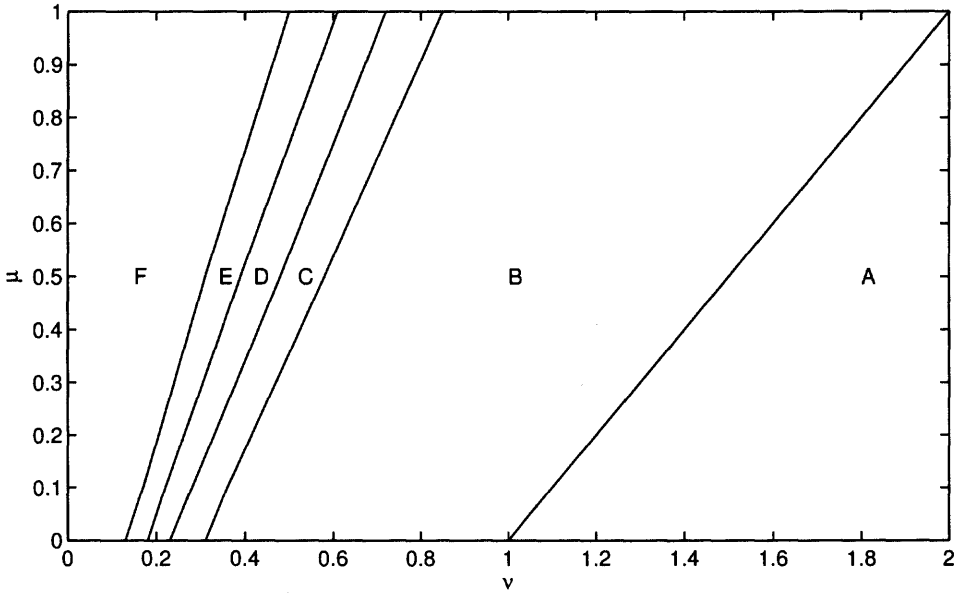

Figure 3.6 The boundaries between attractors in the $\nu - \mu$ plane. Case I.

In the attractor labelled A, the solutions decay to zero as time increases and a trivial steady state is achieved (note that the initial condition has zero spatial mean). This result can be proved analytically for any μ, using the Poincaré inequality (see Temam [116]):

$$\int_{-\pi}^{\pi} g^2 dx \leq \int_{-\pi}^{\pi} g_x^2 dx, \tag{3.78}$$

for periodic functions of period 2π. In fact we can prove the following: If $\nu > 1 + \mu$ then the solutions of (3.72) converge to zero (in L^2_{per}) as t goes to infinity. (Here L^2_{per} is the

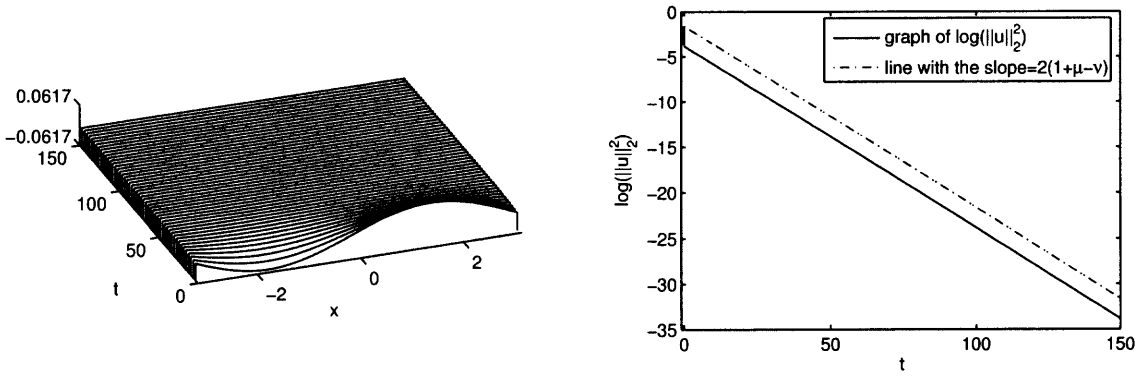

Figure 3.7 Window A, $\mu = 0.5$, $\nu = 1.6$. The left panel shows the evolution of the profile and the right panel shows the semi-log plot of the evolution of the energy, verifying the decay predicted by the theoretical estimate (3.84).

subspace of $L^2(-\pi, \pi)$ consisting of periodic functions with period 2π.) To prove this, we multiply equation (3.72) by u, integrate from $-\pi$ to π with respect to x and use periodicity to obtain

$$\frac{1}{2}\frac{d}{dt}\int_{-\pi}^{\pi} u^2 dx = \int_{-\pi}^{\pi} u_x^2 dx - \nu \int_{-\pi}^{\pi} u_{xx}^2 dx + \mu \int_{-\pi}^{\pi} u_x \mathcal{H}[u]_{xx} dx \tag{3.79}$$

Using the Cauchy-Schwarz inequality and the properties of the Hilbert transform, we can estimate

$$\begin{aligned}\int_{-\pi}^{\pi} u_x \mathcal{H}[u]_{xx} dx &\leq \frac{1}{2}\int_{-\pi}^{\pi} u_x^2 dx + \frac{1}{2}\int_{-\pi}^{\pi} \mathcal{H}[u]_{xx}^2 dx \\ &= \frac{1}{2}\int_{-\pi}^{\pi} u_x^2 dx + \frac{1}{2}\int_{-\pi}^{\pi} \mathcal{H}[u_{xx}]^2 dx, \\ &= \frac{1}{2}\int_{-\pi}^{\pi} u_x^2 dx + \frac{1}{2}\int_{-\pi}^{\pi} u_{xx}^2 dx. \end{aligned} \tag{3.80}$$

Using this in (3.79) along with inequality (3.78) for $g = u_x$, gives

$$\frac{1}{2}\frac{d}{dt}\int_{-\pi}^{\pi} u^2 dx \leq (1 + \mu - \nu)\int_{-\pi}^{\pi} u_{xx}^2 dx. \tag{3.81}$$

The Poincaré inequality (3.78) also implies

$$\int_{-\pi}^{\pi} u_{xx}^2 dx \geq \int_{-\pi}^{\pi} u^2 dx. \tag{3.82}$$

Hence, for $\nu > 1 + \mu$ we have

$$\frac{1}{2}\frac{d}{dt}\int_{-\pi}^{\pi} u^2 dx \leq (1 + \mu - \nu)\int_{-\pi}^{\pi} u^2 dx. \tag{3.83}$$

Therefore there exists a nonnegative constant C such that

$$\int_{-\pi}^{\pi} u^2 dx \leq Ce^{2(1+\mu-\nu)t}. \tag{3.84}$$

This implies that $\|u\|_2 \to 0$ as $t \to \infty$, as required. This fact is fully reflected in the results of Figure 3.5 and hence serves as an additional check on the numerical work. A sample run which quantifies the rate of decay, is given in Figure 3.7 for $\mu = 0.5$, $\nu = 1.6$; it is verified numerically, therefore, that the decay is exponential with a rate given by the estimate (3.84).

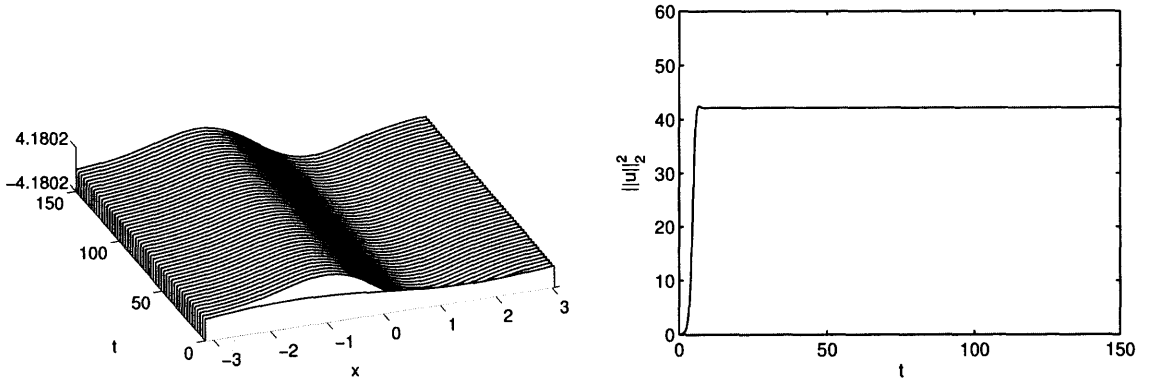

Figure 3.8 Window B: Unimodal steady state for $\mu = 0.5$, $\nu = 0.7$. The left panel shows the evolution of the profile and the right panel shows the evolution of the energy.

For $\nu < 1 + \mu$ the trivial solution bifurcates to provide a branch of unimodal (2π-periodic) steady states – window B in Figure 3.5. These are globally attracting and are stable (the latter observation is based on our time-dependent numerical procedure). Figure 3.8 depicts the evolution of the profile and the corresponding energy for $\nu = 0.7$, $\mu = 0.5$. The solution reaches its steady state in about 10 time units and the long integration to 150 time units provides strong evidence of stability. The size of the windows of attractor B

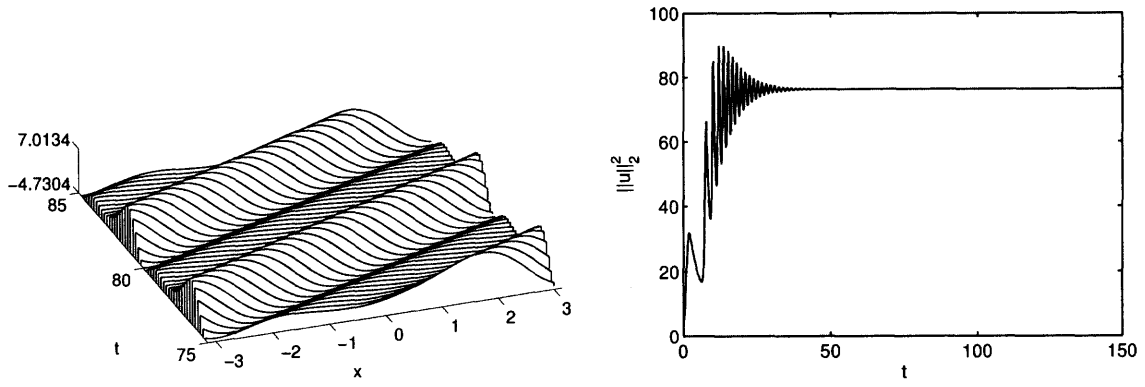

Figure 3.9 Window C: Unimodal steady state travelling wave for $\mu = 0.5$, $\nu = 0.5$. The left panel shows the evolution of the profile and the right panel shows the evolution of the energy.

increase as μ increases but at the same time the lower boundary of attractor B shifts to larger values of ν. For example when $\mu = 0$ the lower boundary of B is at $\nu \approx 0.31$ while for $\mu = 0.5$ the corresponding value is $\nu \approx 0.5$. This behavior persists for higher values of μ and for different attractors as is seen in Figure 3.5. Physically, the implication is that as the voltage potential difference is increased, more complicated dynamics emerge as compared to the KS equation.

As ν decreases further, solutions in attractor B loose stability through a Hopf bifurcation to travelling wave states. These nonlinear travelling waves are unimodal (i.e., they have spatial periods of 2π). For fixed μ the speed of the travelling waves increases monotonically as ν is decreased. Typical results from this window are shown in Figure 3.9 for $\mu = 0.5$, $\nu = 0.5$. It is observed from the evolution of the energy that the initial transient stages of the solution are oscillatory in time, indicating the presence of a time-periodic attractor in the vicinity of these values of the parameters. These transient oscillations become longer lived as ν is decreased (for all μ discussed here), and indeed another Hopf bifurcation takes place this time producing temporally homoclinic bursts. It is found that the solution between bursts is a bimodal fixed point (i.e., the shortest spatial period is π – alternatively, all the energy is carried by the even Fourier modes). The bursts are identical

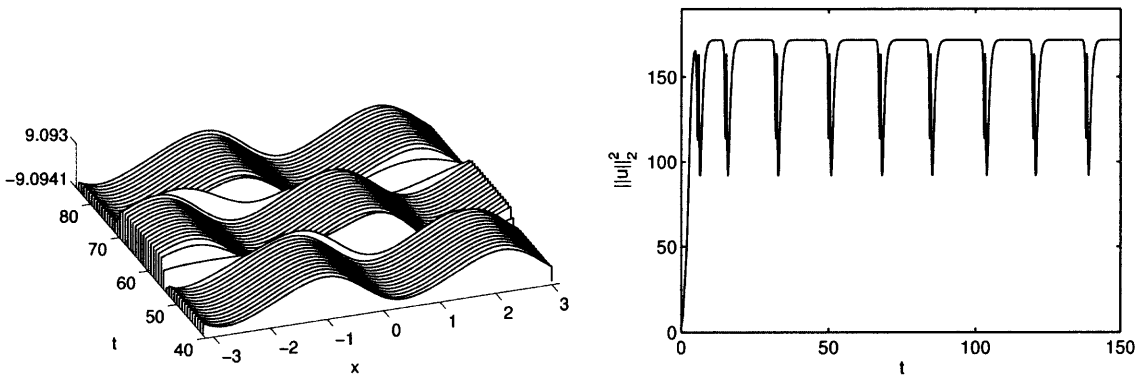

Figure 3.10 Window D: Periodic homoclinic bursts for $\mu = 0.5$, $\nu = 0.45$. The left panel shows the evolution of the profile and the right panel shows the evolution of the energy.

(this has been checked by studying the phase plane of the energy, for example) but the time between bursts is not constant and so the solution is not strictly time periodic – this is also true for the KS equation, Smyrlis & Papageorgiou [113]. The minimum time between bursts (after transients disappear) increases as ν is decreased for a fixed value of μ. Typical results are shown in Figure 3.10 which depicts the profile evolution and the corresponding energy evolution for $\mu = 0.5$, $\nu = 0.45$.

Further decrease of ν leads to a new bimodal fixed point attractor denoted by E in Figure 3.5. This attractor emerges from attractor D as the period of oscillation of the homoclinic bursts becomes increasingly larger. We have checked the stability of these fixed point solutions by integrating to very large times. Typical results are depicted in Figure 3.11 for $\mu = 0.5$, $\nu = 0.35$.

In the initial stages of window F, the bimodal steady states loose stability and a Hopf bifurcation to time periodic solutions takes place. As ν decreases the period increases monotonically until a period doubling takes place. Sample results are given in Figure 3.12 which depicts the profile evolution and the corresponding energy evolution for $\mu = 0.5$ and $\nu = 0.298$. The period has undergone several period doublings and its current value is approximately 0.8. This pattern of subharmonic bifurcations follows the Feigenbaum

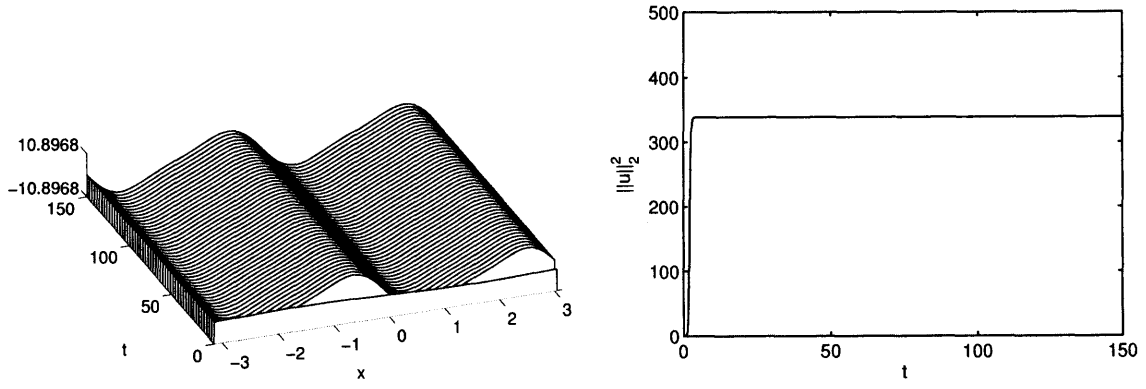

Figure 3.11 Window E: Bimodal steady state for $\mu = 0.5$, $\nu = 0.35$. The left panel shows the evolution of the profile and the right panel shows the evolution of the energy.

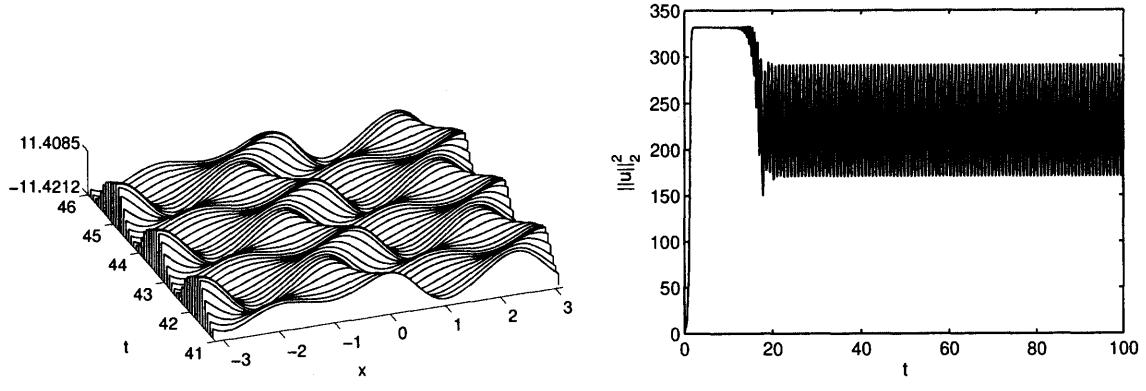

Figure 3.12 Window F: Time periodic attractor for $\mu = 0.5$, $\nu = 0.298$. The left panel shows the evolution of the profile and the right panel shows the evolution of the energy.

scenario in much the same way as for the non-electric case (see for example Papageorgiou & Smyrlis [92], Smyrlis & Papageorgiou [112], Smyrlis & Papageorgiou [113]). We have not carried out an exhaustive study to estimate the Feigenbaum universal constants as was done in the papers above, but have confirmed the trend and the geometric contraction of time-periodic windows of increasingly larger periods. Just beyond the accumulation point (in ν for fixed μ), the solutions get attracted to chaotic homoclinic bursts which are spaced apart at roughly equal time intervals, the profile between bursts being bimodal. Representative solutions are given in Figure 3.13 for $\mu = 0.5$ and $\nu = 0.29$. In this case

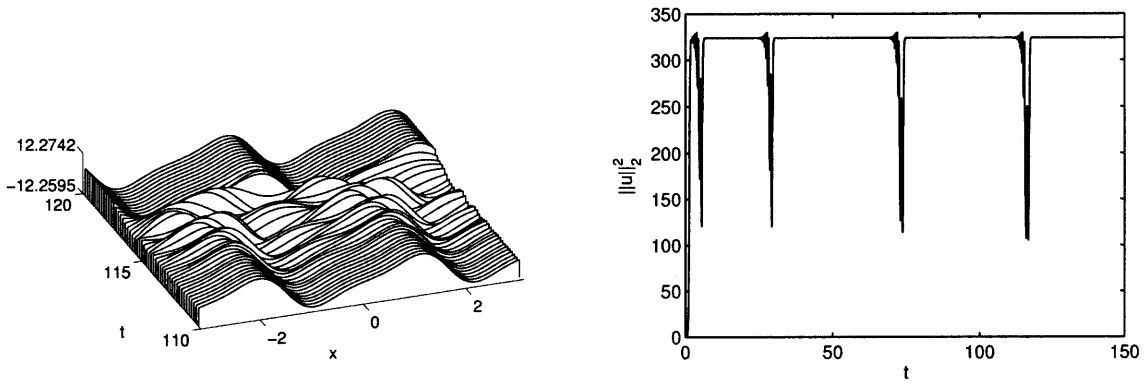

Figure 3.13 Window F: Chaotic homoclinic bursts for $\mu = 0.5$, $\nu = 0.29$. The left panel shows the evolution of the profile and the right panel shows the evolution of the energy.

the time between chaotic bursts is approximately 44 time units. As ν decreases further the dynamics becomes more complicated and we have computed solutions in small windows supporting multimodal fixed points, for example. The strongest attractors appear to be chaotic, however, in line with the dynamics of the KS equation. Such features are illustrated in Figure 3.14 which contains computations for $\mu = 0.5$ and $\nu = 0.1$ (the value of ν is substantially below the accumulation point that heralds the beginning of the first chaotic attractor). The solution is a pentamodal fixed point (the spatial period is $2\pi/5$ and only the Fourier modes which are multiples of 5 appear in the spectrum) and the trough to crest distance is relatively large, approximately equal to 95 units. Such waves have been observed in KS calculations also – see Frisch et al. [41], Smyrlis & Papageorgiou [113]. We note also that the transient to the steady state is about 20 time units and appears to be chaotic, but fixed point solutions are more attracting in this particular region of the phase space (this statement is based on the fact that our initial conditions are chosen randomly). Finally, in Figure 3.15 we reduce the value of ν to 0.05 and the emerging solution is chaotic for the duration of the run which is 100 time units.

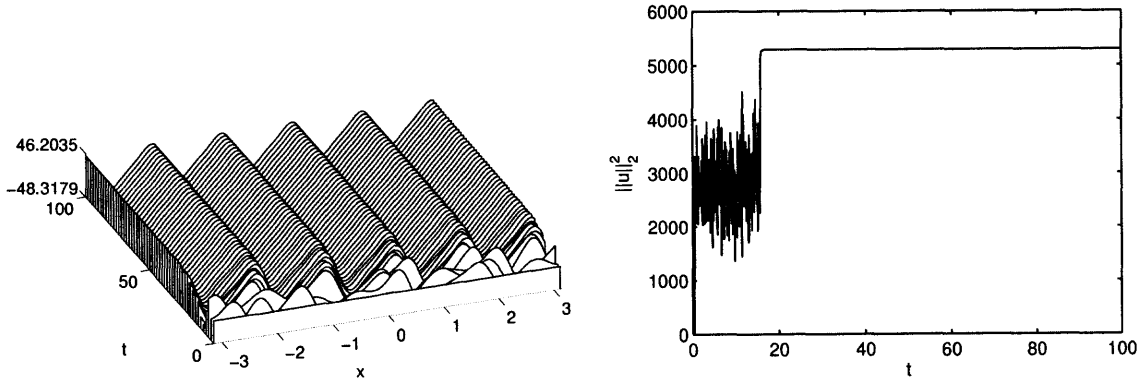

Figure 3.14 Window F: Multimodal steady attractor for $\mu = 0.5$, $\nu = 0.1$. The left panel shows the evolution of the profile and the right panel shows the evolution of the energy.

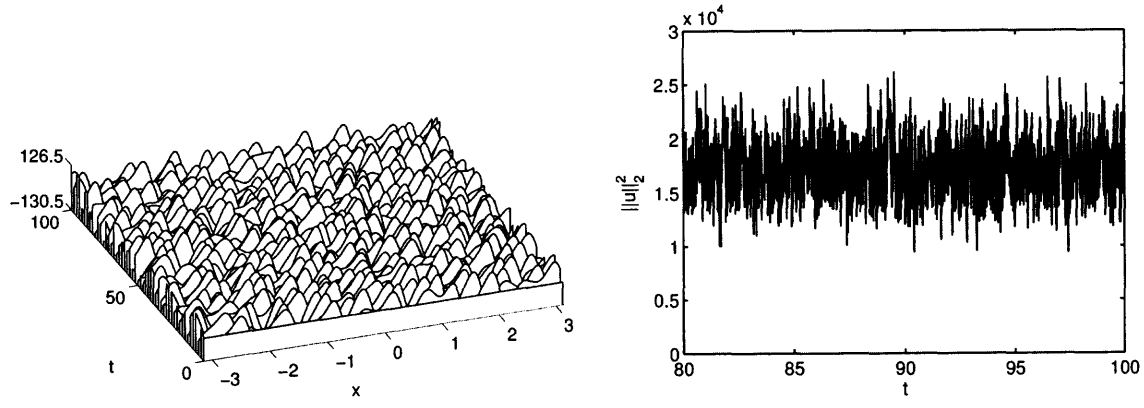

Figure 3.15 Window F: Chaotic oscillations for $\mu = 0.5$, $\nu = 0.05$. The left panel shows the evolution of the profile and the right panel shows the evolution of the energy.

3.5.2 Numerical Results, Case II: Damped Modified Kuramoto-Sivashinsky Equation

In this case the minus sign is picked in the canonical equation (3.72) and if $\mu \leq 2\sqrt{\nu}$ the growth rate is non-positive and all waves are stable. A necessary condition for instability is $\mu^2 > 4\nu$ in which case all waves in the interval (k_-, k_+) are unstable where

$$k_\pm = \frac{\mu \pm \sqrt{\mu^2 - 4\nu}}{2\nu}. \tag{3.85}$$

Clearly, if μ is fixed and ν is sufficiently large, all modes are stable. In fact, modifying the analysis of Section 3.5.1 we can prove that $\|u\|_2 \to 0$ as $t \to \infty$ as long as

$$\nu > \mu - 1. \tag{3.86}$$

The main difference is the minus sign in the first term on the right hand side of (3.79) and the expression of the bound in terms of $\|u_x\|_2$ first rather than $\|u_{xx}\|_2$. It has been established numerically that the bound (3.86) is sharp as long as $\mu > 2$, that is trivial solutions are guaranteed at large times in this case. When $\mu < 2$, the analysis is modified by introducing the Poincaré inequality for multimodal solutions. This is guided by numerical solutions as well as linear theory for the finite periodic domains of interest here, as we describe next.

Consider the countably infinite set of points (μ, ν) where the modes $k = 1, 2, \ldots$ first become unstable (note that we are restricted to integer k due to the particular choice of periodic boundary conditions). These must lie on the curve $\mu = 2\sqrt{\nu}$ (see above), and must satisfy

$$k_- = k_+ = m, \quad m = 1, 2, \ldots. \tag{3.87}$$

Solving we obtain

$$\nu = \frac{1}{m^2}, \quad \mu = \frac{2}{m}, \quad m = 1, 2, \ldots, \tag{3.88}$$

which shows that if we fix $\mu = \frac{2}{m}$ and increase ν above $1/m^2$, a trivial solution emerges at large times. To get a sharp stability boundary we need to consider values of ν and μ away from these neutral points. For example if $k = m$ is to be unstable, then we require it to be contained in the interval (k_-, k_+), that is

$$k_- < m, \quad k_+ > m \quad \Rightarrow \quad \mu > m\nu + \frac{1}{m}. \tag{3.89}$$

The boundary of these regions is seen to be the tangent curve to $\mu = 2\sqrt{\nu}$ at each of the neutral monochromatic modes (3.88) for each $m = 1, 2, \ldots$. The stability boundary is therefore a polygonal curve made up of the segments $\mu = m\nu + 1/m$ so that the curve with the smallest μ is kept. The points of intersection of two such curves at successive values m and $m + 1$, say, indicate points (ν, μ) where the modes $k = m$ and $k = m + 1$ are neutral simultaneously. These intersections are given by

$$\mu = \frac{2m+1}{m(m+1)}, \quad \nu = \frac{1}{m(m+1)}, \quad m = 1, 2, \ldots. \tag{3.90}$$

Note also that the $m = 1$ line becomes the sharp first bifurcation boundary $\mu = \nu + 1$ that holds for $\mu > 2$ analyzed earlier. In Figure 3.16 we show the first three segments of this boundary – higher elements become increasingly difficult to distinguish from the parabolic curve due to the geometric clustering of the higher neutral points as m increases.

Bifurcations in the neighborhood of the circles produce m-modal non-uniform steady states of period $2\pi/m$ as m increases (that is as $\mu, \nu \to 0$). For large ν trivial solutions emerge when (3.86) is satisfied. In general the bifurcated solutions near this curve are unimodal steady states since the $k = 1$ mode becomes active first. The bifurcation near the points (3.90) marked by squares in Figure 3.16 produces unimodal behavior due to the nonlinear interaction of modes which differ by unit wavenumber. These stability results provide some explanations for the the results of numerical experiments described next.

We have carried out extensive numerical experiments and the results are collected in Figure 3.17. As described above, the limit $\mu, \nu \to 0$ deserves separate attention since we

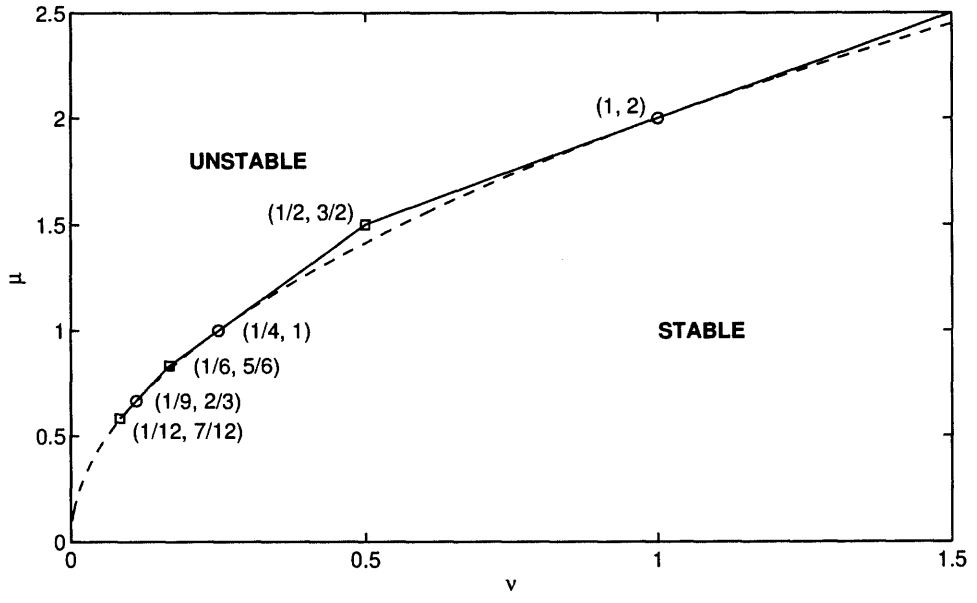

Figure 3.16 The first bifurcation boundary in the $\nu - \mu$ plane. The first three segments of the boundary are shown. Circles (from top to bottom) denote points where the modes $k = 1, 2, 3$ are neutral, respectively. Squares (from top to bottom) are points where the modes $k = 1, 2$, $k = 2, 3$ and $k = 4, 5$ are neutral.

expect a host of interesting dynamical behavior such as multimodal attractors and resonant wave interactions. We do not pursue this limit further in the present work, but note the run having $\mu = 1$ in Figure 3.17. This run is chosen to correspond with the dynamics originating from the bifurcation point denoted by an open circle at $(1/4, 1)$ in Figure 3.16. The run fixes $\mu = 1$ and decreases ν below 0.25. As discussed above, a bimodal steady state is expected since a wave with $k = 2$ is marginally stable at $(1/4, 1)$. The numerical results show that a supercritical bifurcation takes place and a bimodal steady state is supported in the region $0.227 \leq \nu < 0.25$, indicated by the letter E. Just below $\nu = 0.227$ the dynamics become complicated with chaotic solutions emerging as labelled by the attractor F on the Figure. Two other values, $\mu = 0.8$ and 1.4 fall within this "small" μ, ν region. For $\mu = 0.8$ a non-trivial steady state bifurcates at $\nu = (0.8 - 1/3)/3 \approx 0.1556$ (this comes from the segment defined by (3.89) for $m = 3$ – see also Figure 3.16). The neutral

wavenumber has $k = 3$ but the long time dynamics computed here indicate attractor F behavior. One explanation for this is that due to the geometric contraction of the segments comprising the polygonal stability boundary, it is increasingly difficult to find attractors which are supported on windows of diminishing size. A bifurcation analysis of this limit is the subject of future work. Similar reasoning can be applied to the other numerical example that has $\mu = 1.4$. The bifurcation is now through a $k = 2$ neutral mode and the sequence of computed windows begins with periodic homoclinic bursts, to bimodal steady states to dynamics in attractor F.

The other results in Figure 3.16 are at values of $\mu \geq 2$, and they all have similar bifurcation paths, namely the sequence of attractors $A \rightarrow B \rightarrow C \rightarrow D \rightarrow E \rightarrow F$, in much the same way as was discovered for Case I earlier. These cases lie outside the small μ, ν bifurcation scenario given above and all bifurcations are unimodal with $k = 1$ being the neutral mode. In addition, subwindow lengths increase as μ increases, the behavior being linear and similar to that depicted in Figure 3.6. Ultimately, however, our numerical results indicate that for any μ, the dynamics gets attracted to chaotic states if ν is sufficiently small. This happens at small electric fields also and generic dynamical phenomena are observed.

3.6 Summary and Further Discussion

We have derived and used long wave model equations to study the behavior of falling films when a normal electric field is present. Through a combination of analysis and computations, we have established the spatio-temporal interfacial dynamics when the amplitudes are small but a nonlinearity is present. This has been done by considering solutions of a modified KS equation, the modification being a non-local term due to the electric field. There are two canonical evolution equations, one valid for Reynolds numbers above critical value, $R > \frac{5}{4}\cot\beta$, and one below critical; both canonical equations depend on two parameters: $\nu = (\pi/L)^2 > 0$, where L is the length of the system, and $\mu =$

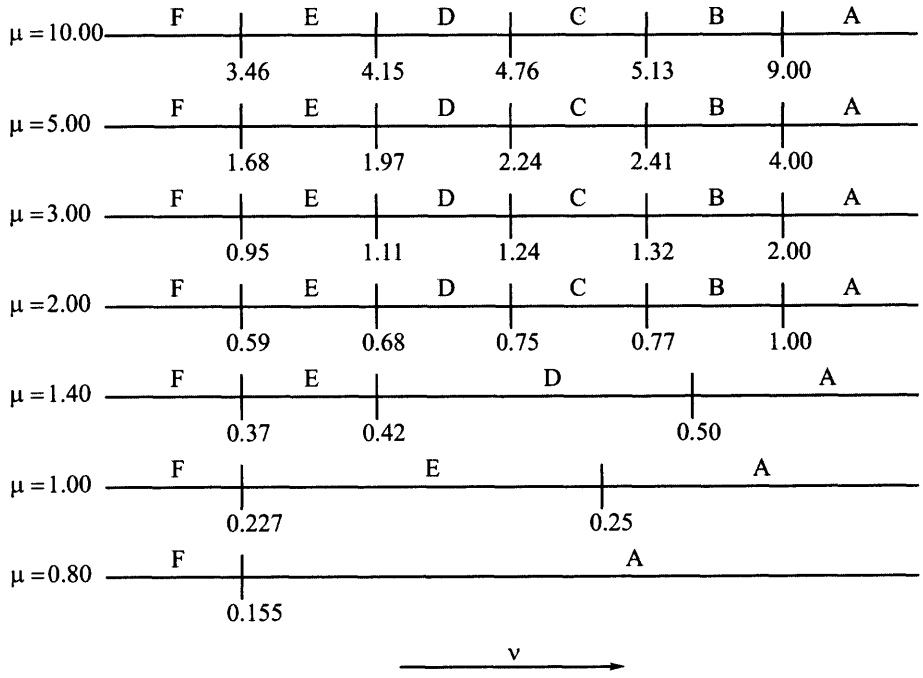

A Solution decays to zero
B Unimodal steady state
C Unimodal steady state traveling wave
D Periodic homoclinic bursts
E Bimodal steady state
F Complicated dynamics including windows of time periodic attractors with period doubling, multimodal steady state attractors, homoclinic bursts, and chaotic oscillations

Figure 3.17 Schematic of the attractors for Case II.

$2\nu^{1/2}\overline{W}_e\overline{C}/|\cot\beta - \frac{4}{5}R|^{1/2} \geq 0$, which is proportional to the reduced electric Weber number $\overline{W}_e$ (this in turn is proportional to the square of the applied electric field, see (3.31)). In the absence of an electric field, the evolution equation above critical Reynolds numbers is the KS equation which has a band of linearly unstable waves for all values of $\nu < 1$. Below critical, however, there are no linearly unstable waves and instability is possible only if μ is sufficiently large. We have established numerically, that as long as a uniform constant interface is linearly unstable, then the large time dynamics depends on the value of ν: trivial states emerge if $\nu > \mu + 1$ or $\nu > \mu - 1$ for flows above/below critical, respectively; as ν is decreased, different attractors are found supporting non-uniform steady state solutions, time-periodic solutions and chaotic solutions if ν is sufficiently small. It is interesting to note that our results predict that interfacial chaos can be achieved at zero Reynolds numbers also, when fluid inertia is completely absent – the electric field provides the energy input for this phenomenon.

Finally, we consider some physical systems where such dynamics can be expected. In particular, we consider the experimental work of Griffing et al. [48] introduced in Chapter 1. In those experiments the fluid is a Convoil 20 with the following properties: $\rho = 890\ kg/m^3$, $\nu = 1.425 \times 10^{-4}\ m^2/s$, $\sigma = 3.32 \times 10^{-2}\ N/m$ and a relative permittivity $\epsilon_f = 2.13$. We note that the theory developed here is for perfectly conducting fluids, that is $\epsilon_f = \infty$ – as pointed out by Griffing et al. [48], however, the perfect conductor approximation retains a lot of the fluid-field coupling features observed in the experiments. The experiments were performed for inclines with angles $80^o < \beta < 90^o$ and Reynolds numbers in the range $0 < R < 0.375$ (we are using our definition of the Reynolds number as defined in (3.31) and note that this differs from that used by Griffing et al. [48] by a factor of $3/2$). Using the smallest angle reported, we estimate the critical Reynolds number to be $R_c = \frac{5}{4}\cot\beta \approx 0.22$, approximately, hence the experiments cover both Cases I and II that we analyzed above. Even though a direct comparison of profiles is not possible (the experiments use a finite electrode at a finite distance), we can use the operating and

physical parameters to evaluate the asymptotic approximations leading to the evolution equations. The available experiments are for electrodes of length $L = 0.0237\ m$ and voltage differences of $V_0 = 25\ kV$; the permittivity of free space is $\epsilon_a = 8.85 \times 10^{-12}\ F/m$. In Table 1 we collect data from the experiments and use it to estimate the capillary number C and the electric Weber number, W_e, and in turn their scaled versions $\overline{C} = C/\delta^2$ and $\overline{W}_e = \delta W_e$. The theory leading to the modified KS equation takes $\overline{C}$ and $\overline{W}_e$ to be of

Table 3.1 Experimental Results from Griffing et al. [48] and Calculation of the Parameters $\overline{C}$ and $\overline{W}_e$ Used in the Asymptotic Derivation of the Long Wave Model

R	$h_0\ (m)$	$U_0 = \frac{\nu R}{h_0}$	$\delta = \frac{h_0}{L}$	$C = \frac{U_0 \rho \nu}{\sigma}$	$W_e = \frac{\epsilon_a V_0^2}{\rho g L^2 h_0 \sin\beta}$	$\overline{C}$	$\overline{W}_e$
0.105	7.6×10^{-4}	0.0197	0.032	0.075	1.346×10^3	73.3	43.1
0.18	9.1×10^{-4}	0.0282	0.038	0.108	1.125×10^3	74.8	42.8
0.24	1×10^{-3}	0.0342	0.042	0.1305	1.023×10^3	74.0	43.0
0.27	1.04×10^{-3}	0.0370	0.044	0.141	9.84×10^2	72.8	43.3

order one and they are eventually scaled out of the problem to achieve a canonical evolution equation. This is reasonable in view of the qualitative agreement seen between lubrication theory and experiments in Griffing et al. [48] where the analogous $\overline{C}$, for example, is of order 10^4. An additional feature of the measured experimental profiles, is that their amplitudes are less than 1% of the undisturbed film thickness, implying that a weakly nonlinear analysis is a useful limit to analyze. In addition a comparison between numerical solutions of long wave model and experimentally observed profiles found good agreement.

CHAPTER 4

A GLOBAL ATTRACTING SET FOR NONLOCAL KURAMOTO-SIVASHINSKY EQUATIONS

In the previous chapter we presented results from extensive numerical computations for the modified Kuramoto-Sivashinsky (MKS) and the damped modified Kuramoto-Sivashinsky (DMKS) equations. As was pointed out, the presence of the electric field enhances the instability – the spectrum contains a "negative diffusion" term which is $\mathcal{O}(|k|k^2)$ and is worse than the usual $\mathcal{O}(k^2)$ negative diffusion present in the KS equation. The new term is still overcome by the fourth derivative stabilization at sufficiently short waves. It is well known that the KS equation can be described by low modal dynamics and possesses a globally attracting set that attracts the large time trajectories. Proofs are available for the global existence of solutions (see Nicolaenko & Scheurer [85], Tadmor [114]), for the estimates of the dimension of the attracting set (see Collet et al. [27], Il'yashenko [58], Jolly et al. [61]) as well as analyticity results (see Collet et al. [26]). The present study allows an interesting modification of these theories due to the additional growth supplied by the electric field. In fact we will study a generalization of the physical system presented in the previous chapter, where the nonlocal term has a growing spectrum proportional to $|k|^p$, where $p \in [3, 4)$. As the limit $p \to 4^-$ is approached, the problem becomes ill-posed. Our aim is to provide rigorous estimates for the dimension of the attractor as p varies ($p = 3$ then gives the problem of Chapter 3). We do this for parity and non-parity solutions.

We consider, then, the following generalization of equations (3.72):

$$u_t + uu_x \pm u_{xx} + \nu u_{xxxx} - \mu(\mathcal{H} \circ \partial_x)^p[u] = 0, \tag{4.1}$$

on a 2π-periodic interval with $\nu > 0$, $\mu \geq 0$. Here $p \in [3, 4)$ (for $p = 3$ equations (3.72) and (4.1) are identical), and the operator $(\mathcal{H} \circ \partial_x)^p$ is defined by its symbol in Fourier space,

namely $\mathcal{F}[(\mathcal{H} \circ \partial_x)^p] = |k|^p$ – see properties in Appendix A. We call the equation with the plus sign in front of u_{xx} the Modified Kuramoto-Sivashinsky (MKS) Equation, and the equation with the minus sing in front of u_{xx} – the Damped Modified Kuramoto-Sivashinsky (DMKS) Equation.

Linear stability of (4.1) follows by writing $u = \epsilon \exp[ikx + \omega t]$ ($k \in \mathbb{Z}$), linearizing with respect to ϵ and using the properties in Appendix A, to obtain

$$\omega_+(k) = k^2 + \mu|k|^p - \nu k^4, \tag{4.2}$$

$$\omega_-(k) = -k^2 + \mu|k|^p - \nu k^4, \tag{4.3}$$

where ω_+ and ω_- correspond to the MKS and DMKS equations, respectively. The nonlocal term is always destabilizing and enhances the hydrodynamic instability (for MKS) and can make a hydrodynamically stable flow unstable (for DMKS) if μ is sufficiently large. The extension of the nonlocal operator as defined above, to the interval $p \in [3, 4)$, enables a parametric study of the increasing instability. We expressly exclude the case $p = 4$ because equation (4.1) becomes ill-posed when $\mu > \nu$ (it becomes a fourth derivative negative diffusion equation).

We prove global existence and uniqueness results and the existence of the absorbing ball in L^2. In all the results presented in the sequel the dependence on $p \in [3, 4)$ is explicit and the physical problem results (when $p = 3$) follow readily. In fact we derive estimates for the L^2-norm of the solution as a function of μ, ν and p.

Throughout this Chapter we denote by L^2_{per}, H^k_{per}, $k = 1, 2, \ldots$, the subspaces of the Sobolev spaces $L^2(-\pi, \pi)$, $H^k(-\pi, \pi)$ consisting of periodic functions with period 2π. We also use $\dot{L}^2_{\text{per}}$, $\dot{H}^k_{\text{per}}$ to denote the subspaces of L^2_{per}, H^k_{per} consisting of functions with zero mean, and use L^2_{odd}, H^k_{odd} to denote the subspaces of $\dot{L}^2_{\text{per}}$, $\dot{H}^k_{\text{per}}$ consisting of odd functions.

4.1 Existence and Uniqueness Theory for Nonlinear Cauchy Problems

In this section we review some basic results regarding existence and uniqueness theory of the solutions of nonlinear partial differential equations which are relevant to our problem. For more information see for example Henry [52] or Sell & You [104].

Consider the following Initial Value Problem for an abstract nonlinear evolutionary equation:

$$\partial_t u + Au = F(u, t), \quad \text{for } u(t_0) = u_0 \in W \text{ and } t \geq t_0 \geq 0, \tag{4.4}$$

on a Banach space W, where A is a sectorial operator (for the problems considered in this chapter it is enough to consider self-adjoint operators which are bounded below and have point spectrum, for more general definition of a sectorial operator see for instance Henry [52] or Sell & You [104]). We also assume that F maps some open subset $U \subset W^\alpha \times \mathbb{R}^+$ into W, for some $\alpha \in [0, 1)$, and that $F \in C_{\text{Lip};\theta}(U, W)$, where $C_{\text{Lip};\theta}(U, W)$ are those functions which are locally Lipschitz continuous in u and locally Hölder continuous in t on U, i.e., for each $(u_1, t_1) \in U$ there exists a neighborhood $V \subset U$ of (u_1, t_1) such that for any $(v_1, s_1) \in V$, $(v_2, s_2) \in V$,

$$\|F(v_1, s_1) - F(v_2, s_2)\| \leq L(\|v_1 - v_2\|_\alpha + |s_1 - s_2|^\theta), \tag{4.5}$$

for some constants $L > 0, \theta \in (0, 1]$. It is also assumed that for every bounded set $B \subset U$, the image $F(B)$ is bounded in W.

Let $\tau > 0$ and $I = [t_0, t_0 + \tau)$ be an interval in $\mathbb{R}^+$.

Definition 4.1.1 *A pair (u, I) is said to be a solution of (4.4) in the space W^α on I if $u : I \to W$ is (strongly) continuous, $u(t_0) = u_0$, and on $(t_0, t_0 + \tau)$ we have $(u(t), t) \in U$, $u(t) \in D(A)$ (where $D(A)$ is the domain of the operator A), the mapping $t \to F(u(t), t)$ is locally Hölder continuous, u is (strongly) differentiable, and u satisfies the equation*

$$\partial_t u(t) + Au(t) = F(u(t), t) \tag{4.6}$$

in W, at each $t \in (t_0,\, t_0 + \tau)$.

The following local existence and uniqueness result holds:

Theorem 4.1.2 *Let A be a sectorial operator, $\alpha \in [0,\, 1)$, $F \in C_{\mathrm{Lip};\theta}(U,\, W)$, where U is an open subset of $W^\alpha \times \mathbb{R}^+$. Then for every $(u_0,\, t_0) \in U$ the initial value problem (4.4) has a unique solution in W^α on some interval $I = [t_0,\, t_0 + \tau)$, for some $\tau > 0$.*

Let $(u_1,\, I_1)$ and $(u_2,\, I_2)$ be two solutions of (4.4), where $I_i = [t_0,\, t_0 + \tau_i)$, $i = 1,\, 2$, and $\tau_1 \leq \tau_2$. The uniqueness of solutions implies $u_1(t) = u_2(t)$ for $t \in I_1$. Hence $(u_2,\, I_2)$ is an extension of $(u_1,\, I_1)$. If $\tau_1 < \tau_2$ then $(u_2,\, I_2)$ is said to be a proper extension of $(u_1,\, I_1)$. A solution $(u,\, I)$ is said to be a maximally defined solution if it has no proper extensions.

Theorem 4.1.3 *Let A and F be as in Theorem 4.1.2 above. Then for every $(u_0,\, t_0) \in U$ the initial value problem (4.4) has a unique maximally defined solution $(u,\, I)$ of (4.4) in W^α, where $I = [t_0,\, T)$. Furthermore, either $T = \infty$, or there exists a sequence $t_n \to T^-$, $n = 1,\, 2,\, \ldots$, such that $(u(t_n),\, t_n) \to \partial U$ as $n \to \infty$. (If U is unbounded, the point at infinity is included in ∂U, e.g., if ∂U has only the point at infinity, then $\lim_{t \to T^-} \|u(t)\|_\alpha = \infty$.)*

4.2 Results for the MKS and DMKS Equations

In this section we study the behavior of the solutions of equations (4.1) with periodic boundary conditions. Note that the operator $\mathcal{H} \circ \partial_x$ is self adjoint, densely defined and bounded below in L^2_{per}. Hence it is sectorial, and the powers $(\mathcal{H} \circ \partial_x)^p$ can be considered which are linear operators.

We will consider solutions having a vanishing spatial integral. This assumption is correct due to the conservation of spatial integrals, as can be seen by integrating equation (4.1):

$$\frac{d}{dt} \int_{-\pi}^{\pi} u(x,\, t) dx = 0. \tag{4.7}$$

So, if initially the spatial integral is zero, it remains zero for all time.

First, we will show local existence and uniqueness of the solutions in $\dot{H}^1_{\text{per}}$ on some time interval $[0,\ T(u_0))$ using the results above (Theorem 4.1.2) and then we will show that if $T(u_0)$ is finite then the solutions are uniformly bounded for all time in $\dot{H}^1_{\text{per}}$, which by Theorem 4.1.3 also implies global existence.

An estimate for the upper bound of the L^2-norm of the solutions in terms of the parameters of the equation will also be obtained. This will be done using the method of Collet et al. [27] by considering first the problem for antisymmetric (odd) solutions, and then expanding the results for general (not necessarily odd) solutions.

4.2.1 Local Existence and Uniqueness

For equations (4.1) we fix the basic space to be the real Hilbert space $\dot{L}^2_{\text{per}}$. We define the operator $A_1 : \mathcal{D}(A_1) \to \dot{L}^2_{\text{per}}$ by

$$A_1\varphi = \nu\partial_x^4\varphi \pm \partial_x^2\varphi + a\varphi, \quad \text{for } \varphi \in \mathcal{D}(A_1), \tag{4.8}$$

where $\mathcal{D}(A_1) = \dot{H}^4_{\text{per}}$, and we also define the operator $A_2 : \mathcal{D}(A_2) \to \dot{L}^2_{\text{per}}$ by

$$A_2\varphi = -\mu(\mathcal{H} \circ \partial_x)^p[\varphi], \quad \text{for } \varphi \in \mathcal{D}(A_2), \tag{4.9}$$

where $\mathcal{D}(A_2) = \{\varphi \in \dot{L}^2_{\text{per}} : \sum_{k=-\infty}^{\infty} |k|^{2p}\varphi_k^2 < \infty\}$. (Here φ_k, $k = 0, \pm1, \pm2, \ldots$, are the Fourier coefficients of φ.) (Note that $\mathcal{D}(A_1) \subset \mathcal{D}(A_2)$.)

Let a be chosen such that the eigenvalues of A_1 are all positive, i.e.,

$$\nu k^4 \mp k^2 + a > 0, \quad \text{for all } k = 0, \pm1, \pm2, \ldots. \tag{4.10}$$

Then A_1 is a positive sectorial operator. By Theorem 1.4.2 in Henry [52] the operator $A_1^{-p/4}$ is a bounded linear operator. It is easy to see that the operator $A_2 \circ A_1^{-p/4}$ is also bounded. Hence, Corollary 1.45 of Henry [52] implies that $A = A_1 + A_2$ is a sectorial operator.

Equations (4.1) take the form

$$\partial_t u + Au = F(u), \quad \text{for } t > 0, \tag{4.11}$$

where the nonlinear operator $F : \dot{H}^1_{\text{per}} \to \dot{L}^2_{\text{per}}$ is defined by

$$F(\varphi) = -\varphi\varphi_x + a\varphi, \quad \text{for } \varphi \in \dot{H}^1_{\text{per}}. \tag{4.12}$$

It can be verified that $F \in C_{\text{Lip}}(\dot{H}^1_{\text{per}}, \dot{L}^2_{\text{per}})$. Therefore, by Theorem 4.1.2, for every $u_0 \in \dot{H}^1_{\text{per}}$ there exists a unique maximally defined solution in $\dot{H}^1_{\text{per}}$ on the interval $[0, T)$, where $0 < T = T(u_0)$.

It remains to prove that the solution is uniformly bounded in $\dot{H}^1_{\text{per}}$ on every finite time interval. Then, from theory in the previous section (Theorem 4.1.3) it follows that $T(u_0) = \infty$. In order to accomplish the proof, we first need to establish uniform boundedness of the solutions in $\dot{L}^2_{\text{per}}$. This is done next, for both odd-parity and non-parity solutions.

4.2.2 Uniform Boundedness of the Solutions in $\dot{L}^2_{\text{per}}$

In what follows we analyze the MKS equation (the plus sign is taken in equation (4.1)) and prove uniform boundedness of the solutions in the $\dot{L}^2_{\text{per}}$ and $\dot{H}^1_{\text{per}}$ norms, along with estimates for the radius of the absorbing ball. When the DMKS equation is considered, the results are similar and are briefly discussed in Section 4.5.

The Antisymmetric Case First we study the antisymmetric case, i.e., we consider the solutions in L^2_{odd}. It is noticed that if a solution of (4.1) is initially in L^2_{odd} then it remains in L^2_{odd} for all time.

Define the linear operator $\mathcal{L} = \mathcal{L}_{\mu,\nu}$:

$$\mathcal{L} : f \mapsto -f_{xx} - \nu f_{xxxx} + \mu(\mathcal{H} \circ \partial_x)^p[f]. \tag{4.13}$$

Then equation (4.1) can be written as

$$u_t = \mathcal{L}u - uu_x. \tag{4.14}$$

If we express u as $u(x, t) = v(x, t) + \varphi(x)$, where $\varphi \in L^2_{\text{odd}}$ is an appropriately chosen gauge function found in the sequel, then the equation becomes:

$$v_t = \mathcal{L}v + \mathcal{L}\varphi - vv_x - v\varphi' - \varphi v_x - \varphi\varphi'. \tag{4.15}$$

Multiplying the last equation by v and integrating over the interval $[-\pi, \pi]$ gives

$$\begin{aligned}\frac{1}{2}\frac{d}{dt}\int_{-\pi}^{\pi} v^2 dx = &\int_{-\pi}^{\pi} v\mathcal{L}v dx + \int_{-\pi}^{\pi} v\mathcal{L}\varphi dx - \int_{-\pi}^{\pi} v^2 v_x dx \\ &- \int_{-\pi}^{\pi} v^2\varphi' dx - \int_{-\pi}^{\pi} vv_x\varphi dx - \int_{-\pi}^{\pi} v\varphi\varphi' dx.\end{aligned} \tag{4.16}$$

Integrating by parts and using periodicity, yields,

$$\frac{1}{2}\frac{d}{dt}\int_{-\pi}^{\pi} v^2 dx = \int_{-\pi}^{\pi} v\mathcal{L}v dx + \int_{-\pi}^{\pi} v\mathcal{L}\varphi dx - \frac{1}{2}\int_{-\pi}^{\pi} v^2\varphi' dx - \int_{-\pi}^{\pi} v\varphi\varphi' dx. \tag{4.17}$$

Next, define a bilinear form

$$\begin{aligned}(f, g)_{\alpha\varphi} = &\nu\int_{-\pi}^{\pi} f_{xx}g_{xx}dx - \int_{-\pi}^{\pi} f_x g_x dx \\ &+ \mu\int_{-\pi}^{\pi} f_{xx}(\mathcal{H}\circ\partial_x)^{p-2}[g]dx + \alpha\int_{-\pi}^{\pi} fg\varphi' dx,\end{aligned} \tag{4.18}$$

which also can be written as

$$(f, g)_{\alpha\varphi} = -\int_{-\pi}^{\pi} f(\mathcal{L} - \alpha\varphi')g dx. \tag{4.19}$$

Then (4.17) takes the form

$$\frac{1}{2}\frac{d}{dt}\int_{-\pi}^{\pi} v^2 dx = -(v, v)_{\frac{1}{2}\varphi} - (v, \varphi)_{\varphi}. \tag{4.20}$$

The main idea now is to find an odd function φ such that the bilinear form (4.19) becomes positive definite and for large enough L^2-norm of v the right hand side of (4.20) becomes negative.

We define the following auxiliary quadratic forms:

$$R_{\alpha\varphi}(u) = (u,\, u)_{\alpha\varphi}, \tag{4.21}$$

$$Q(u) = \frac{\nu}{4}\int_{-\pi}^{\pi} u_{xx}^2 dx + \frac{\eta(\gamma)}{4\nu}\int_{-\pi}^{\pi} u^2 dx, \tag{4.22}$$

where $\gamma = \nu^{1-p/2}\mu$, and η is a function of γ, which is defined as follows:

$$\eta(\gamma) = \begin{cases} 1, & \text{if } \gamma \le 1, \\ \gamma^4, & \text{if } \gamma > 1. \end{cases} \tag{4.23}$$

Using (4.18) we can write

$$R_{\alpha\varphi}(u) = \nu\int_{-\pi}^{\pi} u_{xx}^2 dx - \int_{-\pi}^{\pi} u_x^2 dx + \mu\int_{-\pi}^{\pi} u_{xx}(\mathcal{H}\circ\partial_x)^{p-2}[u]dx + \alpha\int_{-\pi}^{\pi} u^2\varphi' dx. \tag{4.24}$$

Proposition 4.2.1 *There exists a function $\varphi \in H^2_{\text{odd}}$ such that for $\mu \ge 0$ and $\nu \in (0,\, \nu_0(\mu))$, and for all $v \in H^2_{\text{odd}}$ and all $\alpha \in [\alpha_0,\, 1]$*

$$R_{\alpha\varphi}(v) \ge Q(v), \tag{4.25}$$

$$R_{\alpha\varphi}(\varphi) \le C(\gamma,\, \nu). \tag{4.26}$$

(The upper bound $\nu_0(\mu)$ is the unique positive solution of $k_0(\mu, \nu) = 1$ where k_0 is the unique positive solution of $\omega_+(k_0) = 0$. Note that for $p = 3$ it follows that $\nu_0(\mu) = 1 + \mu$. If $\nu > \nu_0(\mu)$, it can be proved, using Poincaré inequalities, that $\|u\|_2$ decays to zero uniformly as t tends to infinity. Also, α_0 is some fixed number in $(0,\, 0.5)$ and $C(\gamma,\, \nu)$ is a function of γ and ν only, which will be determined later.)

Proof: We work with the Fourier series of v and φ'. Since v and φ are odd functions with respect to x, we get

$$v(x) = i\sum_{n\in\mathbb{Z}} v_n e^{inx}, \tag{4.27}$$

where v_n are all real, and $v_0 = 0$, $v_n = -v_{-n}$ for $n = 1, 2, \ldots$, and

$$\varphi'(x) = -\sum_{n\in\mathbb{Z}} \psi_n e^{inx}, \tag{4.28}$$

where $\psi_n \in \mathbb{R}$ for all $n \in \mathbb{Z}$, and $\psi_0 = 0$, $\psi_n = \psi_{-n}$ for $n = 1, 2, \ldots$.

Next we will find the expressions for $R_{\alpha\varphi}(v)$ and $Q(v)$ in terms of the coefficients v_n and ψ_n. First, note that

$$\begin{aligned}\frac{1}{2\pi}\int_{-\pi}^{\pi} v^2\varphi' dx &= \frac{1}{2\pi}\sum_{k,l,m}\int_{-\pi}^{\pi} v_k v_l \psi_m e^{i(k+l+m)x}dx \\ &= \sum_{k+l+m=0} v_k v_l \psi_m = \sum_{k,l} v_k v_l \psi_{-k-l} = \sum_{k,l} v_k v_l \psi_{|k+l|}.\end{aligned} \tag{4.29}$$

Using (4.24) we get

$$\begin{aligned}\frac{1}{2\pi}R_{\alpha\varphi}(v) &= \nu\sum_{n\in\mathbb{Z}} n^4 v_n^2 - \sum_{n\in\mathbb{Z}} n^2 v_n^2 - \mu\sum_{n\in\mathbb{Z}} |n|^p v_n^2 + \alpha\sum_{k,l} v_k v_l \psi_{|k+l|} \\ &= -2\sum_{n=1}^{\infty}\omega_+(n)v_n^2 + \alpha\sum_{k,l>0} v_k v_l(\psi_{|k+l|} + \psi_{|-k-l|} - \psi_{|k-l|} - \psi_{|-k+l|}) \\ &= -2\sum_{n=1}^{\infty}\omega_+(n)v_n^2 + 2\alpha\sum_{k,l>0} v_k v_l(\psi_{|k+l|} - \psi_{|k-l|}) \\ &= 2\sum_{n=1}^{\infty}(-\omega_+(n) + \alpha\psi_{2n})v_n^2 + 2\alpha\sum_{k,l>0\, k\neq l} v_k v_l(\psi_{|k+l|} - \psi_{|k-l|}) \\ &= 2\left[\sum_{n=1}^{\infty}(-\omega_+(n) + \alpha\psi_{2n})v_n^2 + 2\alpha\sum_{k>l>0} v_k v_l(\psi_{|k+l|} - \psi_{|k-l|})\right],\end{aligned} \tag{4.30}$$

where $\omega_+(n) = -\nu n^4 + \mu|n|^p + n^2$, as was defined above. Also,

$$\frac{1}{2\pi}Q(v) = \frac{1}{2}\sum_{n=1}^{\infty}\left(\nu n^4 + \frac{\eta(\gamma)}{\nu}\right)v_n^2. \tag{4.31}$$

To prove the first part of the proposition, we need

$$2\left[\sum_{n=1}^{\infty}(-\omega_+(n)+\alpha\psi_{2n})v_n^2+2\alpha\sum_{k>l>0}v_kv_l(\psi_{|k+l|}-\psi_{|k-l|})\right]$$
$$\geq\frac{1}{2}\sum_{n=1}^{\infty}\left(\nu n^4+\frac{\eta(\gamma)}{\nu}\right)v_n^2. \tag{4.32}$$

First, let $N(\gamma,\,\nu)$ be an integer, such that

$$-\omega_+(n)\geq\frac{1}{2}\left(\nu n^4+\frac{\eta(\gamma)}{\nu}\right)\quad\text{for } n>N. \tag{4.33}$$

The inequality we need to solve takes the form

$$\frac{\nu}{2}n^4-\mu n^p-n^2-\frac{\eta(\gamma)}{2\nu}\geq 0, \tag{4.34}$$

or

$$\frac{1}{2}x^4-\gamma x^p-x^2-\frac{\eta(\gamma)}{2}\geq 0, \tag{4.35}$$

where $\gamma=\nu^{1-p/2}\mu$ as was defined before, and also $x=\nu^{1/2}n$.

In the general case $3\leq p<4$, consideration of the large γ behavior of equation (4.35), yields $N=\mathcal{O}\big(\nu^{-1/2}\gamma^{1/(4-p)}\big)$. Note that as $p\to 4^-$, $N\to\infty$ and the analysis breaks down as expected. When $p=3$ it can be easily verified that inequality (4.35) holds for $x>2.2(\gamma+1)$, which implies $n>2.2\nu^{-1/2}(\gamma+1)$. Therefore, when $p=3$, we can take $N=\lceil 2.2\nu^{-1/2}(\gamma+1)\rceil$.

Next, let $B=B(\gamma,\,\nu)$ be determined as follows:

$$B=\min_{0\leq n\leq N}\left(\frac{\nu}{2}n^4-\mu n^p-n^2-\frac{\eta(\gamma)}{2\nu}\right)$$
$$=\frac{1}{\nu}\min_{0\leq x\leq\nu^{1/2}N}\left(\frac{1}{2}x^4-\gamma x^p-x^2-\frac{\eta(\gamma)}{2}\right). \tag{4.36}$$

For simplicity, we denote $\delta=\delta(\gamma)\equiv-\min_{0\leq x\leq\nu^{1/2}N}\big(\frac{1}{2}x^4-\gamma x^p-x^2-\frac{\eta(\gamma)}{2}\big)$.

Even though δ cannot be obtained in closed form for general p, its large γ behavior can be calculated asymptotically, yielding

$$\delta = \mathcal{O}\big(\gamma^{4/(4-p)}\big) \quad \text{as } \gamma \to \infty. \tag{4.37}$$

When $p = 3$, the exact expression $\delta = \frac{1+\eta(\gamma)}{2} + (72\gamma^2 + 27\gamma^4 + \gamma(9\gamma^2+16)^{3/2})/64$ follows, which in turn implies that

$$\delta = \mathcal{O}\big(\gamma^4\big) \quad \text{as } \gamma \to \infty. \tag{4.38}$$

We choose

$$\psi_{2n} = -\frac{1}{\alpha_0} B = \frac{\delta}{\alpha_0 \nu} \quad \text{for } n \le N. \tag{4.39}$$

The remaining coefficients ψ_k are chosen to be nonnegative and will be specified later. Now

$$-\omega_+(n) + \alpha\psi_{2n} \ge \frac{1}{2}\left(\nu n^4 + \frac{\eta(\gamma)}{\nu}\right), \tag{4.40}$$

for all $n = 1, 2, \ldots$, and $\alpha \in [\alpha_0, 1]$.

We define

$$\tau_n = \sqrt{\frac{1}{2}\left(\nu n^4 + \frac{\eta(\gamma)}{\nu}\right)}, \tag{4.41}$$

and set $w_n = \tau_n v_n$ for $n = 1, 2, \ldots$. Then,

$$\frac{1}{2\pi} R_{\alpha\varphi}(v) \ge 2\left[\sum_{n=1}^{\infty} w_n^2 + 2\alpha \sum_{k>l>0} w_k \frac{\psi_{|k+l|} - \psi_{|k-l|}}{\tau_k \tau_l} w_l\right] \equiv 2\big(w, (\mathbf{Id} + 2\alpha\mathbf{\Gamma})w\big). \tag{4.42}$$

Hence the first part of the proposition will be proved if we find appropriate coefficients ψ_k, such that

$$\big(w, (\mathbf{Id} + 2\alpha\mathbf{\Gamma})w\big) \ge \frac{1}{2}(w, w), \quad \text{for } \alpha \in [\alpha_0, 1]. \tag{4.43}$$

So, we need to get $(w,\, w) \geq -4\alpha(w,\, \Gamma w)$. The sufficient condition for this is that the Hilbert-Schmidt norm of $4\alpha\Gamma$ is less than 1, i.e.,

$$(4\alpha)^2\|\Gamma\|_{\mathrm{HS}}^2 \equiv 16\alpha^2 \sum_{k>l>0} \left| \frac{\psi_{|k+l|} - \psi_{|k-l|}}{\tau_k \tau_l} \right|^2 < 1, \tag{4.44}$$

for all $\alpha \in [\alpha_0,\, 1]$. So, it is enough to find coefficients ψ_k such that

$$\|\Gamma\|_{\mathrm{HS}}^2 \equiv \sum_{k>l>0} \left| \frac{\psi_{|k+l|} - \psi_{|k-l|}}{\tau_k \tau_l} \right|^2 < \frac{1}{16}. \tag{4.45}$$

On the other hand, however, we need to find the coefficients ψ_k such that $(\varphi,\, \varphi)_{\alpha\varphi}$ is minimized (this is needed in the estimates that come later). We can satisfy (4.45) by choosing ψ_k to be constant. But then the corresponding Fourier series does not converge and the norm of φ becomes infinite. Therefore, we choose ψ_k to be a nonnegative and non-increasing function of k, vanishing sufficiently fast as k goes to infinity. This can be done by taking

$$\psi_{2m} = \begin{cases} \frac{\delta}{\alpha_0 \nu}, & \text{if } 1 \leq |m| \leq M, \\ \frac{\delta}{\alpha_0 \nu} f\left(\frac{|m|}{M} - 1\right), & \text{if } |m| > M, \end{cases} \tag{4.46}$$

where M is an integer which will be chosen later (of course we should take $M \geq N$ to be consistent with (4.39)), and $f \in C^1[0,\, \infty]$ is a nonnegative non-increasing function satisfying the conditions $f(0) = 1$, $f'(0) = 0$, $\sup |f'| < 1$, and

$$\int_0^\infty (1 + k^2) f^2(k) dk < \infty. \tag{4.47}$$

A plot of the function $\varphi(x)$ is provided in Figure 4.1.

For $k > l$ we get $|\psi_{k+l} - \psi_{k-l}| = 0$ if $k + l \leq 2M$ and also if $k + l$ and $k - l$ are both odd numbers (i.e., if k and l are of a different parity).

Next, if k and l are of the same parity and $k + l > 2M$, we get:

- If $k - l \leq 2M$

$$|\psi_{k+l} - \psi_{k-l}| = \frac{\delta}{\alpha_0 \nu} \left| f\left(\frac{k+l}{2M} - 1\right) - 1 \right| = \frac{\delta}{\alpha_0 \nu} \left| f\left(\frac{k+l}{2M} - 1\right) - f(0) \right|. \tag{4.48}$$

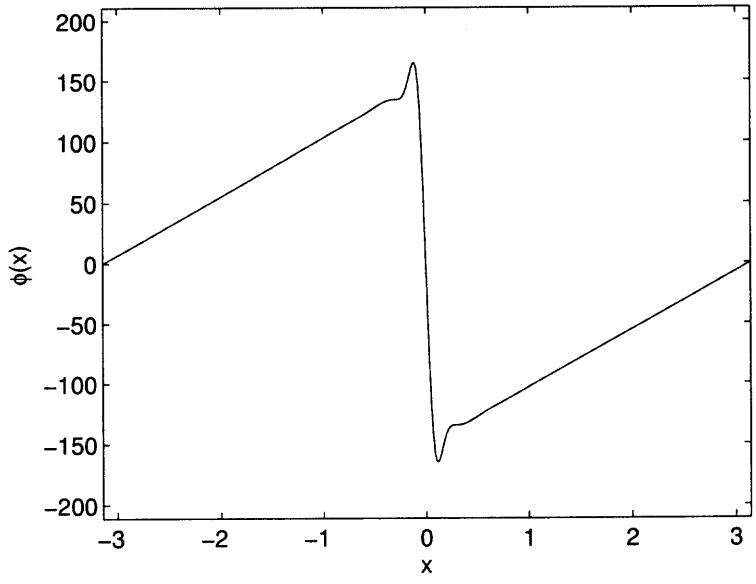

Figure 4.1 The graph of the gauge function $\varphi(x)$ for $\nu = 0.5$, $\mu = 1$, in physical space, when the function $f(k)$ in equation (4.46) is chosen as $f(k) = e^{-k^2}$.

Since $\sup |f'| < 1$ then by the mean value theorem we get

$$|\psi_{k+l} - \psi_{k-l}| \leq \frac{\delta}{\alpha_0 \nu}\left(\frac{k+l}{2M} - 1\right) = \frac{\delta}{\alpha_0 \nu}\left(\frac{k+l-2M}{2M}\right)$$
$$\leq \frac{\delta}{\alpha_0 \nu}\left(\frac{k+l-(k-l)}{2M}\right) = \frac{\delta}{\alpha_0 \nu}\frac{l}{M}. \tag{4.49}$$

- Similarly, if $k - l > 2M$

$$|\psi_{k+l} - \psi_{k-l}| = \frac{\delta}{\alpha_0 \nu}\left| f\left(\frac{k+l}{2M} - 1\right) - f\left(\frac{k-l}{2M} - 1\right)\right|$$
$$\leq \frac{\delta}{\alpha_0 \nu}\left[\left(\frac{k+l}{2M} - 1\right) - \left(\frac{k-l}{2M} - 1\right)\right] = \frac{\delta}{\alpha_0 \nu}\frac{l}{M}. \tag{4.50}$$

Hence, for all $k > l > 0$, $|\psi_{k+l} - \psi_{k-l}| = 0$ if $k + l \leq 2M$ or if k and l are of a different parity, and $|\psi_{k+l} - \psi_{k-l}| \leq \frac{\delta}{\alpha_0 \nu}\frac{l}{M}$ if $k + l > 2M$.

Hence, we get

$$\|\Gamma\|_{\mathrm{HS}}^2 = \sum_{l=1}^{M}\sum_{k=l+1}^{\infty}\left|\frac{\psi_{|k+l|} - \psi_{|k-l|}}{\tau_k \tau_l}\right|^2 + \sum_{l=M+1}^{\infty}\sum_{k=l+1}^{\infty}\left|\frac{\psi_{|k+l|} - \psi_{|k-l|}}{\tau_k \tau_l}\right|^2. \tag{4.51}$$

For the first term we obtain

$$\sum_{l=1}^{M}\sum_{k=l+1}^{\infty}\left|\frac{\psi_{|k+l|}-\psi_{|k-l|}}{\tau_k\tau_l}\right|^2=\left(\sum_{l=1}^{M}\sum_{k=l+1}^{2M-l}+\sum_{l=1}^{M}\sum_{k=2M-l+1}^{\infty}\right)\left|\frac{\psi_{|k+l|}-\psi_{|k-l|}}{\tau_k\tau_l}\right|^2$$
$$=0+\sum_{l=1}^{M}\sum_{k=2M-l+1}^{\infty}\left|\frac{\psi_{|k+l|}-\psi_{|k-l|}}{\tau_k\tau_l}\right|^2=\sum_{l=1}^{M}\sum_{k=2M-l+1}^{\infty}\left|\frac{\psi_{|k+l|}-\psi_{|k-l|}}{\tau_k\tau_l}\right|^2. \quad (4.52)$$

Hence,

$$\|\Gamma\|_{\mathrm{HS}}^2=\sum_{l=1}^{M}\sum_{k=2M-l+1}^{\infty}\left|\frac{\psi_{|k+l|}-\psi_{|k-l|}}{\tau_k\tau_l}\right|^2+\sum_{l=M+1}^{\infty}\sum_{k=l+1}^{\infty}\left|\frac{\psi_{|k+l|}-\psi_{|k-l|}}{\tau_k\tau_l}\right|^2$$
$$\le\sum_{l=1}^{M}\sum_{k=2M-l+1}^{\infty}\frac{\delta^2}{\alpha_0^2\nu^2}\frac{l^2}{M^2}\tau_k^{-2}\tau_l^{-2}+\sum_{l=M+1}^{\infty}\sum_{k=l+1}^{\infty}\frac{\delta^2}{\alpha_0^2\nu^2}\frac{l^2}{M^2}\tau_k^{-2}\tau_l^{-2}$$
$$=\frac{\delta^2}{\alpha_0^2\nu^2M^2}\sum_{l=1}^{M}l^2\tau_l^{-2}\sum_{k=2M-l+1}^{\infty}\tau_k^{-2}+\frac{\delta^2}{\alpha_0^2\nu^2M^2}\sum_{l=M+1}^{\infty}l^2\tau_l^{-2}\sum_{k=l+1}^{\infty}\tau_k^{-2}$$
$$\le\frac{\delta^2}{\alpha_0^2\nu^2M^2}\sum_{l=1}^{M}l^2\tau_l^{-2}\int_{2M-l}^{\infty}\tau_k^{-2}dk+\frac{\delta^2}{\alpha_0^2\nu^2M^2}\sum_{l=M+1}^{\infty}l^2\tau_l^{-2}\int_{l}^{\infty}\tau_k^{-2}dk. \quad (4.53)$$

Now,

$$\int_a^{\infty}\tau_k^{-2}dk=\int_a^{\infty}\frac{2}{\nu k^4+\eta(\gamma)/\nu}dk<\frac{2}{\nu}\int_a^{\infty}k^{-4}dk=\frac{2}{3}\nu^{-1}a^{-3}. \quad (4.54)$$

Thus,

$$\int_{2M-l}^{\infty}\tau_k^{-2}dk<\frac{2}{3}\nu^{-1}(2M-l)^{-3}\le\frac{2}{3}\nu^{-1}M^{-3}, \quad (4.55)$$

(the last step is true for $1\le l\le M$) and

$$\int_{l}^{\infty}\tau_k^{-2}dk<\frac{2}{3}\nu^{-1}l^{-3}. \quad (4.56)$$

Therefore,

$$\|\Gamma\|_{\mathrm{HS}}^2<\frac{2\delta^2}{3\alpha_0^2\nu^3}M^{-5}\sum_{l=1}^{M}l^2\tau_l^{-2}+\frac{2\delta^2}{3\alpha_0^2\nu^3}M^{-2}\sum_{l=M+1}^{\infty}l^{-1}\tau_l^{-2}$$
$$<\frac{2\delta^2}{3\alpha_0^2\nu^3}M^{-5}\int_0^{M}l^2\tau_l^{-2}dl+\frac{2\delta^2}{3\alpha_0^2\nu^3}M^{-2}\int_M^{\infty}l^{-1}\tau_l^{-2}dl$$

$$
\begin{aligned}
&= \frac{4\delta^2}{3\alpha_0^2\nu^3} M^{-5} \int_0^M \frac{l^2}{\nu l^4 + \eta(\gamma)/\nu} dl \\
&\quad + \frac{4\delta^2}{3\alpha_0^2\nu^3} M^{-2} \int_M^\infty \frac{1}{\nu l^5 + (\eta(\gamma)/\nu) l} dl. \qquad (4.57)
\end{aligned}
$$

Next we estimate the integrals in the last expression:

$$
\begin{aligned}
\int_0^M \frac{l^2}{\nu l^4 + \eta(\gamma)/\nu} dl &< \int_0^\infty \frac{\nu l^2}{\nu^2 l^4 + \eta(\gamma)} dl < \int_0^\infty \frac{1}{\sqrt{\nu^2 l^4 + \eta(\gamma)}} dl \\
&= \int_0^a \frac{1}{\sqrt{\nu^2 l^4 + \eta(\gamma)}} dl + \int_a^\infty \frac{1}{\sqrt{\nu^2 l^4 + \eta(\gamma)}} dl \\
&< \int_0^a \big(\eta(\gamma)\big)^{-1/2} dl + \int_a^\infty \frac{1}{\nu l^2} dl \\
&= a\big(\eta(\gamma)\big)^{-1/2} + (a\nu)^{-1}. \qquad (4.58)
\end{aligned}
$$

Taking $a = \nu^{-1/2}\big(\eta(\gamma)\big)^{1/4}$ gives

$$
\int_0^M \frac{l^2}{\nu l^4 + \eta(\gamma)/\nu} dl < 2\nu^{-1/2}\big(\eta(\gamma)\big)^{-1/4}. \qquad (4.59)
$$

Estimating the other integral yields

$$
\int_M^\infty \frac{1}{\nu l^5 + (\eta(\gamma)/\nu) l} dl < \int_M^\infty \frac{1}{\nu l^5} dl = \frac{1}{4}\nu^{-1} M^{-4}. \qquad (4.60)
$$

So,

$$
\|\mathbf{\Gamma}\|_{\mathrm{HS}}^2 < \frac{8\delta^2}{3\alpha_0^2}\nu^{-7/2}\big(\eta(\gamma)\big)^{-1/4} M^{-5} + \frac{\delta^2}{3\alpha_0^2}\nu^{-4} M^{-6}. \qquad (4.61)
$$

We choose $M \geq N$ such that the right hand side of the last inequality becomes less than $1/16$. This can be done since the right hand side of (4.61) is a positive function of M that decays to zero as $M \to \infty$. For "small" ν (that is $\nu \in (0, 1]$) if we take $M \geq \frac{5}{2}\alpha_0^{-2/5}\delta^{2/5}\eta(\gamma)^{-1/20}\nu^{-7/10}$, the condition $M \geq N$ is always satisfied. Hence, $M = \lceil \frac{5}{2}\alpha_0^{-2/5}\delta^{2/5}\eta(\gamma)^{-1/20}\nu^{-7/10} \rceil$; for large γ, therefore, it follows using (4.23) and (4.37), that

$$
M = \mathcal{O}\big(\gamma^{\frac{4+p}{5(4-p)}}\nu^{-7/10}\big). \qquad (4.62)
$$

When $p = 3$ we obtain $M = \mathcal{O}(\gamma^{7/5}\nu^{-7/10})$, a result that is used later.

Next we estimate the value $R_{\alpha\varphi}(\varphi)$. Using (4.24) we first note that $R_{\alpha\varphi}(\varphi) = R_0(\varphi)$, since the part which is dependent on α is equal to zero due to the periodicity of φ. Also, if

$$\varphi'(x) = -\sum_{n\in\mathbb{Z}} \psi_n e^{inx}, \tag{4.63}$$

then

$$\varphi(x) = i\sum_{n\in\mathbb{Z}} \frac{\psi_n}{n} e^{inx}. \tag{4.64}$$

Therefore,

$$\begin{aligned}
R_{\alpha\varphi}(\varphi) &= -4\pi\sum_{n=1}^{\infty}\omega_+(n)\left(\frac{\psi_n}{n}\right)^2 = -4\pi\sum_{k=1}^{\infty}\omega_+(2k)\left(\frac{\psi_{2k}}{2k}\right)^2 \\
&= 4\pi\sum_{k=1}^{\infty}\big(\nu(2k)^2 - \mu(2k)^{p-2} - 1\big)\psi_{2k}^2 < 4\pi\sum_{k=1}^{\infty} 4\nu k^2\psi_{2k}^2 \\
&= 4\pi\sum_{k=1}^{M} 4\nu k^2\psi_{2k}^2 + 4\pi\sum_{k=M+1}^{\infty} 4\nu k^2\psi_{2k}^2 \\
&= 16\pi\frac{\delta^2}{\alpha_0^2\nu}\sum_{k=1}^{M} k^2 + 16\pi\frac{\delta^2}{\alpha_0^2\nu}\sum_{k=M+1}^{\infty} k^2 f^2\left(\frac{k}{M} - 1\right) \\
&< 16\pi\frac{\delta^2}{\alpha_0^2\nu}M^3 + 16\pi\frac{\delta^2}{\alpha_0^2\nu}\int_M^{\infty} k^2 f^2\left(\frac{k}{M} - 1\right)dk.
\end{aligned} \tag{4.65}$$

Now, using the substitution $t = \frac{k}{M} - 1$ in the integral above, we get

$$\begin{aligned}
R_{\alpha\varphi}(\varphi) &< 16\pi\frac{\delta^2}{\alpha_0^2\nu}M^3 + 16\pi\frac{\delta^2}{\alpha_0^2\nu}M^3\int_0^{\infty}(t+1)^2 f^2(t)dt \\
&= 16\pi\frac{\delta^2}{\alpha_0^2\nu}M^3\left(1 + \int_0^{\infty}(t+1)^2 f^2(t)dt\right).
\end{aligned} \tag{4.66}$$

So, $R_{\alpha\varphi}(\varphi) < C(\gamma, \nu)$, where

$$C(\gamma, \nu) = 16\pi\frac{\delta^2}{\alpha_0^2\nu}M^3\left(1 + \int_0^{\infty}(t+1)^2 f^2(t)dt\right). \tag{4.67}$$

For large γ and small ν the value of $C(\gamma, \nu)$ is estimated using (4.37) and (4.62) to be

$$C(\gamma, \nu) = \mathcal{O}\big(\gamma^{\frac{52+3p}{5(4-p)}}\nu^{-31/10}\big). \tag{4.68}$$

Note that when $p = 3$, we get $C(\gamma, \nu) = \mathcal{O}\big(\gamma^{61/5}\nu^{-31/10}\big)$. ■

Now we are ready to prove uniform boundedness of the L^2-norm of the solutions of the MKS equation.

Theorem 4.2.2 *Let μ be any positive number and $\nu \in (0, \nu_0(\mu))$. If $u(x, t)$ is a solution of equation (4.1) such that $u(x, 0) = u_0(x) \in H^1_{\text{odd}}$, then there is a constant $K > 0$ (independent of μ, ν, u_0), and a constant $D > 0$ (independent of μ, u_0) such that*

$$\|u\|_2 \leq (\|u_0\|_2 + \|\varphi\|_2)\exp(-Dt) + K\sqrt{\frac{\nu}{\eta(\gamma)}C(\gamma, \nu)} + \|\varphi\|_2, \tag{4.69}$$

where φ is the function constructed in Proposition 4.2.1, and $C(\gamma, \nu)$ is given by (4.67).

Proof: Let φ be the function defined in Proposition 4.2.1. Then the bilinear form (4.19) is positive definite. Indeed, for any nonzero function w we get $(w, w)_{\alpha\varphi} = R_{\alpha\varphi}(w) \geq Q(w) > 0$. Then, applying first the Cauchy-Shwarz inequality and then Young's inequality (see Appendix C) to the second term in (4.20) we obtain

$$\begin{aligned}\frac{1}{2}\frac{d}{dt}\int_{-\pi}^{\pi} v^2 dx &= -(v, v)_{\frac{1}{2}\varphi} - (v, \varphi)_{\varphi} \\ &\leq -(v, v)_{\frac{1}{2}\varphi} + \frac{\varepsilon}{2}(v, v)_{\varphi} + \frac{1}{2\varepsilon}(\varphi, \varphi)_{\varphi},\end{aligned} \tag{4.70}$$

where ε is a positive number which will be chosen later. So,

$$\begin{aligned}\frac{1}{2}\frac{d}{dt}\int_{-\pi}^{\pi} v^2 dx &\leq \int_{-\pi}^{\pi} v\left(\mathcal{L} - \frac{1}{2}\varphi'\right)v dx - \frac{\varepsilon}{2}\int_{-\pi}^{\pi} v(\mathcal{L} - \varphi')v dx + \frac{1}{2\varepsilon}R_{\varphi}(\varphi) \\ &= \left(1 - \frac{\varepsilon}{2}\right)\int_{-\pi}^{\pi} v\left(\mathcal{L} - \frac{1-\varepsilon}{2-\varepsilon}\varphi'\right)v dx + \frac{1}{2\varepsilon}R_{\varphi}(\varphi) \\ &= -\left(1 - \frac{\varepsilon}{2}\right)R_{\frac{1-\varepsilon}{2-\varepsilon}\varphi}(v) + \frac{1}{2\varepsilon}R_{\varphi}(\varphi) \\ &\leq -\left(1 - \frac{\varepsilon}{2}\right)Q(v) + \frac{1}{2\varepsilon}R_{\varphi}(\varphi).\end{aligned} \tag{4.71}$$

The last step is true when $\frac{1-\varepsilon}{2-\varepsilon} \in [\alpha_0, 1]$, or $\varepsilon \leq \frac{1-2\alpha_0}{1-\alpha_0}$. Inequality (4.71) implies

$$\frac{d}{dt}\|v\|_2^2 \leq -\frac{\eta(\gamma)}{2\nu}\left(1 - \frac{\varepsilon}{2}\right)\|v\|_2^2 + \frac{1}{\varepsilon}C(\gamma, \nu). \tag{4.72}$$

The Gronwall inequality (see Temam [116], and also Appendix C) then implies:

$$\|v\|_2^2 \leq \|v_{t=0}\|_2^2 \exp\left[-\frac{\eta(\gamma)}{2\nu}\left(1-\frac{\varepsilon}{2}\right)t\right] + \frac{4\nu C(\gamma,\,\nu)}{\varepsilon(2-\varepsilon)\eta(\gamma)}. \tag{4.73}$$

Therefore

$$\|v\|_2 \leq \|v_{t=0}\|_2 \exp\left[-\frac{\eta(\gamma)}{4\nu}\left(1-\frac{\varepsilon}{2}\right)t\right] + \frac{2}{\sqrt{\varepsilon(2-\varepsilon)}}\sqrt{\frac{\nu}{\eta(\gamma)}C(\gamma,\,\nu)}. \tag{4.74}$$

Since $\|v\|_2 = \|u-\varphi\|_2 \geq \big|\|u\|_2 - \|\varphi\|_2\big|$ and $\|v_{t=0}\|_2 = \|u_0-\varphi\|_2 \leq \|u_0\|_2 + \|\varphi\|_2$, we get

$$\begin{aligned}\|u\|_2 \leq &(\|u_0\|_2 + \|\varphi\|_2)\exp\left[-\frac{\eta(\gamma)}{4\nu}\left(1-\frac{\varepsilon}{2}\right)t\right] \\ &+ \frac{2}{\sqrt{\varepsilon(2-\varepsilon)}}\sqrt{\frac{\nu}{\eta(\gamma)}C(\gamma,\,\nu)} + \|\varphi\|_2.\end{aligned} \tag{4.75}$$

Thus,

$$\|u\|_2 \leq (\|u_0\|_2 + \|\varphi\|_2)\exp(-Dt) + K\sqrt{\frac{\nu}{\eta(\gamma)}C(\gamma,\,\nu)} + \|\varphi\|_2, \tag{4.76}$$

where $D = \frac{\eta(\gamma)}{4\nu}\left(1-\frac{\varepsilon}{2}\right)$ and $K = \frac{2}{\sqrt{\varepsilon(2-\varepsilon)}}$.

We can chose ε to minimize the constant K. Since

$$\min_{0<\varepsilon\leq\frac{1-2\alpha_0}{1-\alpha_0}} \frac{1}{\sqrt{\varepsilon(2-\varepsilon)}} = \frac{1}{\sqrt{\varepsilon(2-\varepsilon)}}\bigg|_{\varepsilon=\frac{1-2\alpha_0}{1-\alpha_0}} = \frac{1-\alpha_0}{\sqrt{1-2\alpha_0}}, \tag{4.77}$$

we get a better estimate for K if $\varepsilon = \frac{1-2\alpha_0}{1-\alpha_0}$:

$$K = \frac{2(1-\alpha_0)}{\sqrt{1-2\alpha_0}}. \tag{4.78}$$

The constant α_0 can be chosen to minimize the righthand side of inequality (4.76) to get a better estimate. ■

Remark 1. We also have the following estimate for $\|\varphi\|_2$:

$$\begin{aligned}
\|\varphi\|_2^2 &= 4\pi \sum_{n=1}^{\infty} \left(\frac{\psi_n}{n}\right)^2 = 4\pi \sum_{k=1}^{\infty} \frac{\psi_{2k}^2}{4k^2} \\
&= \pi \sum_{k=1}^{M} \frac{\psi_{2k}^2}{k^2} + \pi \sum_{k=M+1}^{\infty} \frac{\psi_{2k}^2}{k^2} \\
&= \frac{\pi\delta^2}{\alpha_0^2\nu^2} \sum_{k=1}^{M} \frac{1}{k^2} + \frac{\pi\delta^2}{\alpha_0^2\nu^2} \sum_{k=M+1}^{\infty} \frac{1}{k^2} f^2\left(\frac{k}{M} - 1\right) \\
&< \frac{2\pi\delta^2}{\alpha_0^2\nu^2} + \frac{\pi\delta^2}{\alpha_0^2\nu^2} \int_M^{\infty} \frac{1}{k^2} f^2\left(\frac{k}{M} - 1\right) dk \\
&= \frac{2\pi\delta^2}{\alpha_0^2\nu^2} + \frac{\pi\delta^2}{\alpha_0^2\nu^2 M} \int_0^{\infty} \frac{f^2(t)}{(t+1)^2} dt \\
&\le \frac{\pi\delta^2}{\alpha_0^2\nu^2} \left(2 + \int_0^{\infty} \frac{f^2(t)}{(t+1)^2} dt\right) = \mathcal{O}\big(M^{-3} C(\gamma, \nu)\big).
\end{aligned} \tag{4.79}$$

Using the large γ and $0 < \nu \le 1$ result (4.62), we show that $\|\varphi\|_2 \ll \sqrt{\frac{\nu}{\eta(\gamma)} C(\gamma, \nu)}$. Thus, for the radius $\mathcal{R}$ of the absorbing ball in L^2_{odd} we get the following estimate:

$$\mathcal{R} = \mathcal{O}\left(\sqrt{\frac{\nu}{\eta(\gamma)} C(\gamma, \nu)}\right) = \mathcal{O}\big(\gamma^{\frac{23p-28}{10(4-p)}} \nu^{-21/20}\big), \tag{4.80}$$

which gives, for $p = 3$,

$$\mathcal{R} = \mathcal{O}\left(\sqrt{\frac{\nu}{\eta(\gamma)} C(\gamma, \nu)}\right) = \mathcal{O}\big(\gamma^{41/10} \nu^{-21/20}\big). \tag{4.81}$$

Note that estimate (4.81) pertains to the equation

$$u_t + uu_x + u_{xx} + \nu u_{xxxx} + \mu \mathcal{H}[u]_{xxx} = 0, \tag{4.82}$$

which arises from a rescaling of its $2L$-periodic version:

$$u_t + uu_x + u_{xx} + u_{xxxx} + \gamma \mathcal{H}[u]_{xxx} = 0. \tag{4.83}$$

The rescaling is (dropping the bars):

$$\bar{t} = \nu t, \quad \bar{x} = \nu^{1/2} x, \quad \bar{u} = \nu^{-1/2} u, \tag{4.84}$$

where $\nu = (\pi/L)^2$ and $\mu = (\pi/L)\gamma$ (see Chapter 3 and Tseluiko & Papageorgiou [119]).

In unscaled variables, therefore, the estimate for the radius of the absorbing ball takes the following form:

$$\widetilde{\mathcal{R}} = \nu^{1/4}\mathcal{R} = \mathcal{O}\big(\gamma^{41/10}\nu^{-4/5}\big) = \mathcal{O}\big(\gamma^{41/10}L^{8/5}\big), \tag{4.85}$$

which significantly improves the estimate $\mathcal{O}\big(\gamma^6 L^{5/2}\big)$ obtained by Duan & Ervin [34].

Remark 2. If $\mu = 0$ then $\gamma = 0$ and $\delta = 1$ which implies $\mathcal{R} = \mathcal{O}\big(\nu^{-21/10}\big)$. This value corresponds to the case of the usual Kuramoto-Sivashinsky equation:

$$u_t + uu_x + u_{xx} + \nu u_{xxxx} = 0. \tag{4.86}$$

In unscaled variables, therefore, the estimate for the radius of the absorbing ball in L^2_{odd} is $\mathcal{O}\big(\nu^{1/4}\nu^{-21/20}\big) = \mathcal{O}\big(\nu^{-4/5}\big) = \mathcal{O}(L^{8/5})$. This is the estimate which was obtained by Collet et al. [27] for the case of the usual Kuramoto-Sivashinsky equation.

Remark 3. It can be seen from the estimate (4.80) that in the general p case (recall that $3 \leq p < 4$), the estimated radius of the absorbing ball is an increasing function of p which blows up as $p \to 4^-$. This is expected due to the ill-posedness of the equation when $p = 4$.

The General Case For the general case, when solutions of (4.1) are not necessarily odd functions, the idea is to consider a generalization of the gauge function φ. We start by introducing the following Liapunov function:

$$F[u] = \operatorname{dist}^2(u, S) = \inf_{\psi \in S} \|u - \psi\|_2^2, \tag{4.87}$$

where S is the following translation-invariant set of functions:

$$S = \{\psi : \exists a, \text{ s.t. } \psi(x) \equiv \varphi(x + a)\}. \tag{4.88}$$

This is equivalent to saying that

$$F[u] = \|u(x, t) - \varphi_a(x)\|_2^2, \tag{4.89}$$

where $\varphi_a(x) = \varphi(x + a)$, and $a = a(t)$ is a suitably chosen translation function:

$$\|u(x, t) - \varphi(x + a(t))\|_2^2 = \inf_{\psi \in S} \|u(x, t) - \psi(x)\|_2^2, \tag{4.90}$$

for all $t > 0$. So, $a = a(t)$ must satisfy the optimality condition $dF/da|_{a=a(t)} = 0$, which can also be written as

$$\int_{-\pi}^{\pi} u\varphi_a' dx \Big|_{a=a(t)} = 0. \tag{4.91}$$

The function u is expressed as $u(x, t) = v(x, t) + \varphi_a(x)$. Equation (4.1) becomes

$$v_t + \varphi_a' a' = \mathcal{L}v + \mathcal{L}\varphi_a - vv_x - v\varphi_a' - \varphi_a v_x - \varphi_a\varphi_a'. \tag{4.92}$$

Multiplying the last equation by v and integrating over the interval $[-\pi, \pi]$ gives

$$\begin{aligned} \frac{1}{2}\frac{d}{dt}\int_{-\pi}^{\pi} v^2 dx + a' \int_{-\pi}^{\pi} v\varphi_a' dx = &\int_{-\pi}^{\pi} v\mathcal{L}v dx + \int_{-\pi}^{\pi} v\mathcal{L}\varphi_a dx \\ &- \int_{-\pi}^{\pi} v^2 v_x dx - \int_{-\pi}^{\pi} v^2\varphi_a' dx \\ &- \int_{-\pi}^{\pi} vv_x\varphi_a dx - \int_{-\pi}^{\pi} v\varphi_a\varphi_a' dx. \end{aligned} \tag{4.93}$$

This implies

$$\begin{aligned} \frac{1}{2}\frac{d}{dt}F[u] =& \frac{1}{2}\frac{d}{dt}\int_{-\pi}^{\pi} v^2 dx \\ =& \int_{-\pi}^{\pi} v\mathcal{L}v dx + \int_{-\pi}^{\pi} v\mathcal{L}\varphi_a dx - \frac{1}{2}\int_{-\pi}^{\pi} v^2\varphi_a' dx \\ &- \int_{-\pi}^{\pi} v\varphi_a\varphi_a' dx - a' \int_{-\pi}^{\pi} v\varphi_a' dx. \end{aligned} \tag{4.94}$$

Noting that the last term is zero due to our choice of a, and using the bilinear form (4.19), we can write this as

$$\frac{1}{2}\frac{d}{dt}F[u] = -(v, v)_{\frac{1}{2}\varphi_a} - (v, \varphi_a)_{\varphi_a}. \tag{4.95}$$

For a given t we can assume for simplicity that $a(t) = 0$ in (4.95) (since the right hand side of this equality is invariant under translations $a \to a +$ constant).

Next we want to get a result similar to Proposition 4.2.1 for the general case. Let w be any function in $\dot{H}^2_{\text{per}}$ and decompose it as follows:

$$w(x) = w(0) + \frac{1}{2}[w(x) + w(-x) - 2w(0)] + \frac{1}{2}[w(x) - w(-x)]. \tag{4.96}$$

So,

$$w(x) = w(0) + w_s(x) + w_a(x), \tag{4.97}$$

where $w_s(x) = \frac{1}{2}[w(x) + w(-x) - 2w(0)]$ is an even 2π-periodic function of x, and $w_a(x) = \frac{1}{2}[w(x) - w(-x)]$ is an odd 2π-periodic function of x. Besides, $w_s(0) = 0$.

Now, let us introduce the following operator:

$$\mathcal{T}[f](x) = \begin{cases} f(x), & \text{if } x \in [0, \pi], \\ -f(x), & \text{if } x \in [-\pi, 0). \end{cases} \tag{4.98}$$

For simplicity, let us reduce our consideration to half the interval, i.e., let us assume that all the functions are π-periodic. (We can perform this reduction without loss of generality, since it is always possible to transfer from L-periodic intervals to 2π-periodic domains and vice versa, without changing the form of the equation, see for example transformation (4.84). The only impact of such transformations on the equation is that the coefficients μ and ν are rescaled.) Then $\mathcal{T}[w_s]$ is an odd 2π-periodic function. Also, since $R_{\alpha\varphi_a}(w_s) = R_{\alpha\varphi_a}(\mathcal{T}[w_s])$ and $Q(w_s) = Q(\mathcal{T}[w_s])$ we get that Proposition 4.2.1 holds not only for w_a but for w_s too:

$$R_{\alpha\varphi_a}(w_a) \geq Q(w_a), \tag{4.99}$$

$$R_{\alpha\varphi_a}(w_s) \geq Q(w_s), \tag{4.100}$$

for all $\alpha \in [\alpha_0, 1]$. Next, it can be easily checked that

$$R_{\alpha\varphi_a}(w) = R_{\alpha\varphi_a}(w_a) + R_{\alpha\varphi_a}(w_s), \tag{4.101}$$

$$Q(w) = Q(w_a) + Q(w_s) - \frac{\pi}{2\nu}w^2(0), \tag{4.102}$$

for all $\alpha \in [\alpha_0, 1]$. Hence, (4.99) and (4.100) imply

$$R_{\alpha\varphi_a}(w) \geq Q(w) + \frac{\pi}{2\nu}w^2(0) \geq Q(w) \quad \text{for } \alpha \in [\alpha_0, 1]. \tag{4.103}$$

This means that with our choice of $a = a(t)$ Proposition 4.2.1 holds for the general case also.

After this point the proof of the nonlinear stability becomes the same as for the antisymmetric case. Thus the following result holds:

Theorem 4.2.3 *Let μ be any positive number and $\nu \in (0, \nu_0(\mu))$. If $u(x, t)$ is a solution of equation (4.1) such that $u(x, 0) = u_0(x) \in \dot{H}^1_{\text{per}}$, then there is a constant $K > 0$ (independent of μ, ν, u_0), and a constant $D > 0$ (independent of μ, u_0) such that*

$$\|u\|_2 \leq (\|u_0\|_2 + \|\varphi\|_2)\exp(-Dt) + K\sqrt{\frac{\nu}{\eta(\gamma)}C(\gamma, \nu)} + \|\varphi\|_2, \tag{4.104}$$

where φ is the function constructed in Proposition 4.2.1, and $C(\gamma, \nu)$ is given by (4.67).

(The constants D and K are the same as in Theorem 4.2.2.)

4.2.3 Uniform Boundedness of the Solutions in $\dot{H}^1_{\text{per}}$

To prove global existence of the solutions in $\dot{H}^1_{\text{per}}$ it is enough (according to Theorem 4.1.3) to prove uniform boundedness of the solutions in $\dot{H}^1_{\text{per}}$. This will be established by showing uniform boundedness of the L^2-norm of u_{xx}, which by Poincaré's inequality also implies boundedness of the L^2-norm of u_x.

Multiplying (4.1) by u_{xxxx} and integrating over $[-\pi, \pi]$ gives

$$\frac{1}{2}\frac{d}{dt}\|u_{xx}\|_2^2 + \nu\|u_{xxxx}\|_2^2 = - \int_{-\pi}^{\pi} u_{xx}u_{xxxx}dx - \int_{-\pi}^{\pi} uu_xu_{xxxx}dx + \mu\int_{-\pi}^{\pi} (\mathcal{H}\circ\partial_x)^p[u]u_{xxxx}dx. \tag{4.105}$$

Using Young's inequality, Agmon's inequality, the Nirenberg-Gagliardo inequalities and the interpolation inequalities (see Henry [52], Sell & You [104], Temam [116], and also Appendix C), the integrals on the right hand side of this expression can be estimated as follows:

$$-\int_{-\pi}^{\pi} u_{xx}u_{xxxx}dx \le \|u_{xx}\|_2\|u_{xxxx}\|_2 \le \varepsilon_1\|u_{xxxx}\|_2^2 + \frac{\varepsilon_1^{-1}}{4}\|u_{xx}\|_2^2, \tag{4.106}$$

$$\begin{aligned} -\int_{-\pi}^{\pi} uu_xu_{xxxx}dx &\le \|u\|_\infty\|u_x\|_2\|u_{xxxx}\|_2 \le \sqrt{2}\|u\|_2^{1/2}\|u_x\|_2^{3/2}\|u_{xxxx}\|_2 \\ &\le \sqrt{2\left[\|u_0\|_2 + 2\|\varphi\|_2 + K\sqrt{\frac{\nu}{\eta(\gamma)}C(\gamma,\nu)}\right]}\|u_x\|_2^{3/2}\|u_{xxxx}\|_2. \end{aligned} \tag{4.107}$$

Denoting for simplicity $\|u_0\|_2 + 2\|\varphi\|_2 + K\sqrt{\frac{\nu}{\eta(\gamma)}C(\gamma,\nu)}$ by C_1 gives

$$\begin{aligned} -\int_{-\pi}^{\pi} uu_xu_{xxxx}dx &\le \sqrt{2C_1}\|u_x\|_2^{3/2}\|u_{xxxx}\|_2 \\ &\le \sqrt{2C_1}\left(C_2\|u_{xx}\|_2^{1/2}\|u\|_2^{1/2}\right)^{3/2}\|u_{xxxx}\|_2 \\ &\le \sqrt{2}C_1^{5/4}C_2^{3/2}\|u_{xx}\|_2^{3/4}\|u_{xxxx}\|_2 \\ &\le \sqrt{2}C_1^{5/4}C_2^{3/2}(\varepsilon_2\|u_{xxxx}\|_2^2 + \frac{\varepsilon_2^{-1}}{4}\|u_{xx}\|_2^{3/2}) \\ &\le \sqrt{2}C_1^{5/4}C_2^{3/2}\left(\varepsilon_2\|u_{xxxx}\|_2^2 + \frac{\varepsilon_2^{-1}}{4}\|u_{xx}\|_2^{3/2}\right) \\ &\le \sqrt{2}C_1^{5/4}C_2^{3/2}\left(\varepsilon_2\|u_{xxxx}\|_2^2 + \frac{\varepsilon_2^{-1}}{4}\left[\frac{3}{4}\|u_{xx}\|_2^2 + \frac{1}{4}\right]\right). \end{aligned} \tag{4.108}$$

Denoting $A_1 = \sqrt{2}C_1^{5/4}C_2^{3/2}$, $A_2 = \frac{\sqrt{2}}{16}\varepsilon_2^{-1}C_1^{5/4}C_2^{3/2}$ gives

$$-\int_{-\pi}^{\pi} uu_xu_{xxxx}dx \le \varepsilon_2A_1\|u_{xxxx}\|_2^2 + 3A_2\|u_{xx}\|_2^2 + A_2. \tag{4.109}$$

Next,

$$\int_{-\pi}^{\pi}(\mathcal{H}\circ\partial_x)^p[u]u_{xxxx}dx \le \left\|(\mathcal{H}\circ\partial_x)^p[u]\right\|_2\|u_{xxxx}\|_2. \tag{4.110}$$

Also,

$$\begin{aligned}
\left\|(\mathcal{H}\circ\partial_x)^p[u]\right\|_2 =&\left\|(\mathcal{H}\circ\partial_x)^{p-3}\left[(\mathcal{H}\circ\partial_x)^3[u]\right]\right\|_2\\
\le&\left\|(\mathcal{H}\circ\partial_x)\left[(\mathcal{H}\circ\partial_x)^3[u]\right]\right\|_2^{(p-3)}\left\|(\mathcal{H}\circ\partial_x)^3[u]\right\|_2^{(4-p)}\\
=&\left\|(\mathcal{H}\circ\partial_x)^4[u]\right\|_2^{(p-3)}\left\|(\mathcal{H}\circ\partial_x)^3[u]\right\|_2^{(4-p)}\\
=&\left\|u_{xxxx}\right\|_2^{(p-3)}\left\|u_{xxx}\right\|_2^{(4-p)}\\
\le&(p-3)\varepsilon_3\|u_{xxxx}\|_2+(4-p)\varepsilon_3^{-\frac{p-3}{4-p}}\|u_{xxx}\|_2\\
\le&(p-3)\varepsilon_3\|u_{xxxx}\|_2+(4-p)\varepsilon_3^{-\frac{p-3}{4-p}}\left(C_4\|u_{xx}\|_2^{1/2}\|u_{xxxx}\|_2^{1/2}\right)\\
\le&(p-3)\varepsilon_3\|u_{xxxx}\|_2+\varepsilon_4\|u_{xxxx}\|_2\\
&+(4-p)^2C_4^2\varepsilon_3^{-\frac{2(p-3)}{4-p}}\frac{\varepsilon_4^{-1}}{4}\|u_{xx}\|_2\\
\le&[(p-3)\varepsilon_3+\varepsilon_4]\|u_{xxxx}\|_2\\
&+(4-p)^2C_4^2\varepsilon_3^{-\frac{2(p-3)}{4-p}}\frac{\varepsilon_4^{-1}}{4}\|u_{xx}\|_2.
\end{aligned}\tag{4.111}$$

Denoting $A_3=(4-p)^2C_4^2\varepsilon_3^{-\frac{2(p-3)}{4-p}}$ gives

$$\begin{aligned}
\int_{-\pi}^{\pi}(\mathcal{H}\circ\partial_x)^p[u]u_{xxxx}dx &\le [(p-3)\varepsilon_3+\varepsilon_4]\|u_{xxxx}\|_2^2+A_3\|u_{xx}\|_2\|u_{xxxx}\|_2\\
&\le [(p-3)\varepsilon_3+\varepsilon_4]\|u_{xxxx}\|_2^2+A_3\varepsilon_5\|u_{xxxx}\|_2^2+A_3\frac{\varepsilon_5^{-1}}{4}\|u_{xx}\|_2^2\\
&= [(p-3)\varepsilon_3+\varepsilon_4+A_3\varepsilon_5]\|u_{xxxx}\|_2^2+A_3\frac{\varepsilon_5^{-1}}{4}\|u_{xx}\|_2^2.
\end{aligned}\tag{4.112}$$

We finally obtain:

$$\begin{aligned}
\frac{1}{2}\frac{d}{dt}\|u_{xx}\|_2^2+\nu\|u_{xxxx}\|_2^2 \le&[\varepsilon_1+\varepsilon_2A_1+\mu(\varepsilon_3(p-3)+\varepsilon_4+\varepsilon_5A_3)]\|u_{xxxx}\|_2^2\\
&+\left[\frac{\varepsilon_1^{-1}}{4}+3A_2+\mu A_3\frac{\varepsilon_5^{-1}}{4}\right]\|u_{xx}\|_2^2+A_2.
\end{aligned}\tag{4.113}$$

Choosing $\varepsilon_1, \varepsilon_2, \varepsilon_3, \varepsilon_4, \varepsilon_5$ to be sufficiently small and denoting for simplicity $A_4 = \frac{\varepsilon_1^{-1}}{4} + 3A_2 + \mu A_3 \frac{\varepsilon_5^{-1}}{4}$ gives:

$$\frac{1}{2}\frac{d}{dt}\|u_{xx}\|_2^2 \leq A_4\|u_{xx}\|_2^2 + A_2. \tag{4.114}$$

Applying the uniform Gronwall inequality (see Temam [116], and also Appendix C) implies that $\|u_{xx}\|$ is bounded on the time interval $[0, T(u_0))$ if $T(u_0)$ is finite. This also implies boundedness of $\|u_x\|_2$. Theorem 4.1.3 then gives $T(u_0) = \infty$. Therefore the following result holds:

Theorem 4.2.4 *For every $u_0 \in \dot{H}^1_{\text{per}}$ there exists a unique globally defined solution of equation (4.1).*

Now, having global existence of the solutions of (4.1), Theorem 4.2.3 implies existence of an absorbing ball in $\dot{L}^2_{\text{per}}$ and the following estimate for the radius of this absorbing ball:

Corollary 4.2.5 *Let μ be any positive number and $\nu \in (0, \nu_0(\mu))$. If $u(x, t)$ is a solution of equation (4.1) such that $u(x, 0) = u_0(x) \in \dot{H}^1_{\text{per}}$, then there is a constant K (independent of μ, ν, u_0), such that*

$$\limsup_{t\to\infty} \|u\|_2 \leq K\sqrt{\frac{\nu}{\eta(\gamma)}C(\gamma, \nu)} + \|\varphi\|_2. \tag{4.115}$$

(Here K, $C(\gamma, \nu)$, φ are the same as in Theorem 4.2.2.)

4.3 Numerical Evaluation of the Analytical Results

The MKS equation (4.1) was solved numerically with periodic boundary conditions using a modification (when $p \neq 3$) of the methods used in Tseluiko & Papageorgiou [119]. Our main objective is to compare the analytical bound (4.122) for the radius of the absorbing ball in the space $\dot{L}^2_{\text{per}}$, with the "exact" numerically computed value $\|u\|_2$. A comparison at large values of γ (equivalently large $\mu = \nu^{1/2}\gamma$) for fixed ν , is particularly amenable due to the simple algebraic nature of the estimate in this limit (see (4.80)) – the large

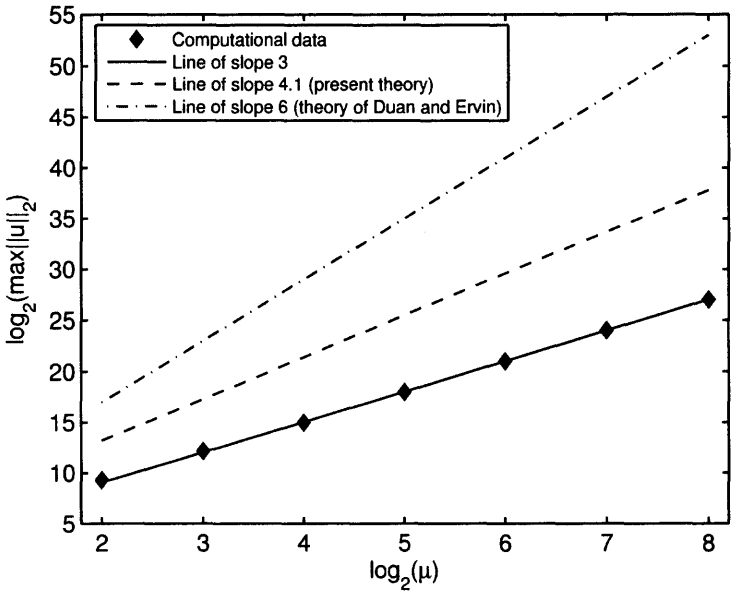

Figure 4.2 Variation of $\max \|u\|_2$ with increasing μ for fixed $\nu = 0.5$, $p = 3$. Diamonds – numerical computation (solid line is of slope 3); dashed line – current theoretical estimate (4.80); dashdot line – estimate of Duan & Ervin [34].

γ and large μ behaviors are identical due to the fact that ν is fixed. The computations are carried out to values of time beyond which transient behavior dies out and we can be confident that the computed trajectories lie close to the attractor. Given values of p, ν, and μ, the quantity $\max(\|u\|_2)(p, \nu; \mu)$ is found over a time interval beyond transients. This is repeated for a fixed $\nu = 0.5$ and a range of increasing values of $\mu = 2^2, 2^3, \ldots, 2^8$. The results are presented on logarithmic scales in Figures 4.2 and 4.3 for $p = 3$ and $p = 3.2$, respectively. As can be seen from the Figures, the behavior is linear and an estimate for the slope, providing a numerical best bound for the $\dot{L}^2_{\text{per}}$ norm as a power of μ (for large μ), is determined. The numerical results give the behavior

$$\max(\|u\|_2)(p = 3, \nu = 0.5; \mu) \sim \mu^3, \tag{4.116}$$

$$\max(\|u\|_2)(p = 3.2, \nu = 0.5; \mu) \sim \mu^{3.75} = \mu^{\frac{3}{(4-p)}}. \tag{4.117}$$

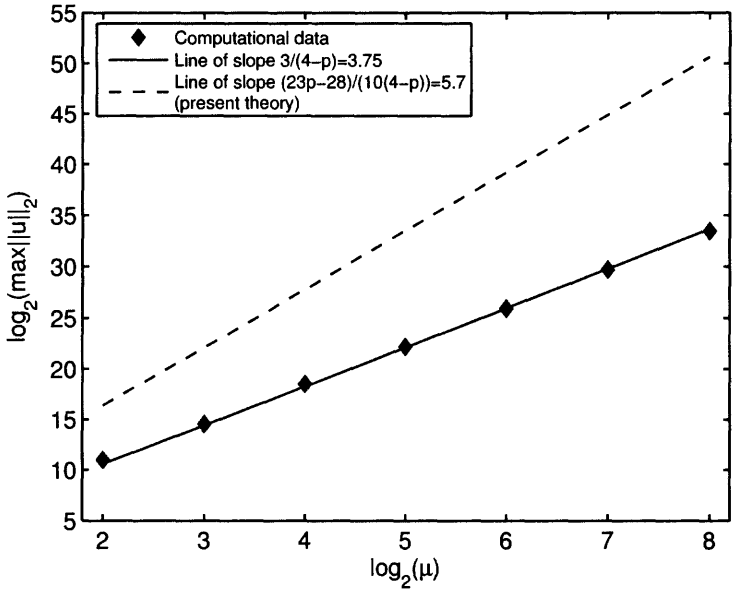

Figure 4.3 Variation of $\max \|u\|_2$ with increasing μ for fixed $\nu = 0.5, p = 3.2$. Diamonds – numerical computation (solid line is of slope $3/(4-p) = 3.75$); dashed line – current theoretical estimate (4.80).

Our corresponding analytical estimates (the values are 4.1 and 5.7, for $p = 3$, 3.2, respectively) are also given in the Figures along with the estimate of Duan & Ervin [34] when $p = 3$. The analytical results overestimate the numerically constructed bound, but the present estimates are better than those found in the literature.

As indicated in equations (4.116)-(4.117), the numerically computed large μ estimates are $\mathcal{O}\left(\mu^{\frac{3}{(4-p)}}\right)$. This can be understood by the following order-of-magnitude argument valid for large μ. Considering the equation

$$u_t + uu_x + u_{xx} + \nu u_{xxxx} - \mu(\mathcal{H} \circ \partial_x)^p[u] = 0, \tag{4.118}$$

a balance must take place between the nonlinearity, the fourth order diffusion and the nonlocal term (the unsteady term provides a time scale *a posteriori*). We have, then,

$$\frac{[u]}{[t]} \sim \frac{[u]^2}{[x]} \sim \frac{[u]}{[x]^4} \sim \mu \frac{[u]}{[x]^p}, \tag{4.119}$$

which in turn provides the scalings

$$[t] \sim \mu^{-\frac{4}{4-p}}, \quad [x] \sim \mu^{-\frac{1}{4-p}}, \quad [u] \sim \mu^{\frac{3}{4-p}}. \tag{4.120}$$

These scalings suggest that as μ increases typical amplitudes increase and at the same time the spatial scale over which the solution varies, decreases; in addition, the solution varies over typical time scales which are also decreasing asymptotically. This behavior places severe restrictions on the numerical parameters. Taking the case $p = 3$, for example, we observe that doubling the value of μ requires a decrease of the time-step by a factor of 2^4 and a doubling of the number of modes. In accordance with the scalings (4.120), in order to resolve the solution for the largest value $\mu = 256$, we used a time-step of 1.16×10^{-11} and 2^{14} Fourier modes. As p increases the situation worsens as evidenced by (4.120).

As shown in Figures 4.2 and 4.3, the values of $\|u\|_2$ follow the scaling for u shown in equation (4.120). This is consistent with the numerical solutions which exhibit pulses of width $\mathcal{O}(\mu^{-\frac{1}{4-p}})$ and height $\mathcal{O}(\mu^{\frac{3}{4-p}})$ whose net contribution over the interval $[-\pi, \pi]$ gives $\|u\|_2 \sim \mu^{\frac{3}{4-p}}$. This pulse behavior is indicated in Figures 4.4 and 4.5 for $p = 3$ and $\mu = 16$ and 32, respectively. There are approximately 28 pulses for $\mu = 16$ and 52 pulses for $\mu = 32$, while the pulse heights are approximately equal to 2×10^4 and 1.5×10^5; these numerical observations are in agreement with the scaling laws (4.120) and have been confirmed for all the computations presented here.

These findings enable us to formulate the following conjecture.

Conjecture 4.3.1 *Let $\nu \in (0, \nu_0(\mu))$ and $p \in [3, 4)$ be fixed. If $u(x, t)$ is a solution of equation (4.1) such that $u(x, 0) = u_0(x) \in \dot{H}^1_{\text{per}}$, then for μ sufficiently large*

$$\limsup_{t \to \infty} \|u\|_2 = \mathcal{O}(\mu^{\frac{3}{4-p}}). \tag{4.121}$$

Note that the values of μ need not be too large for (4.121) to hold. The numerical results give values of approximately 2.

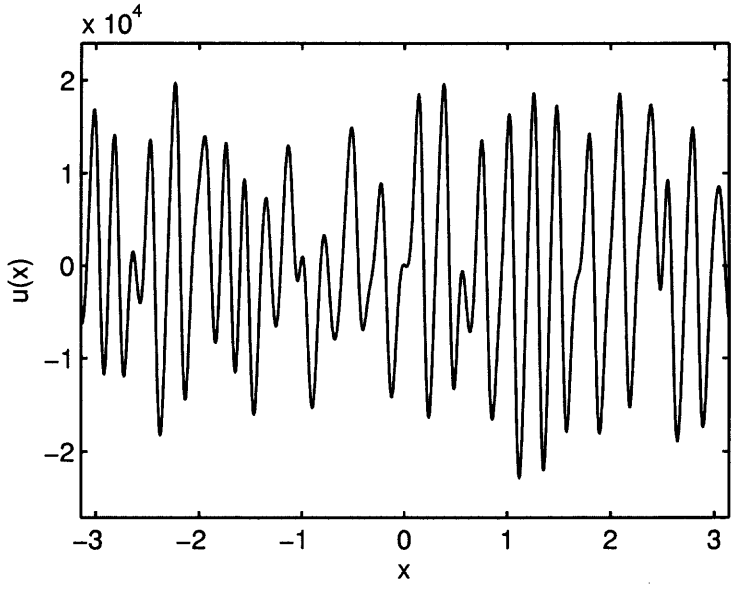

Figure 4.4 The solution $u(x,t)$ after 20000 time-steps; $\mu = 2^4$, $\nu = 0.5$, $p = 3$.

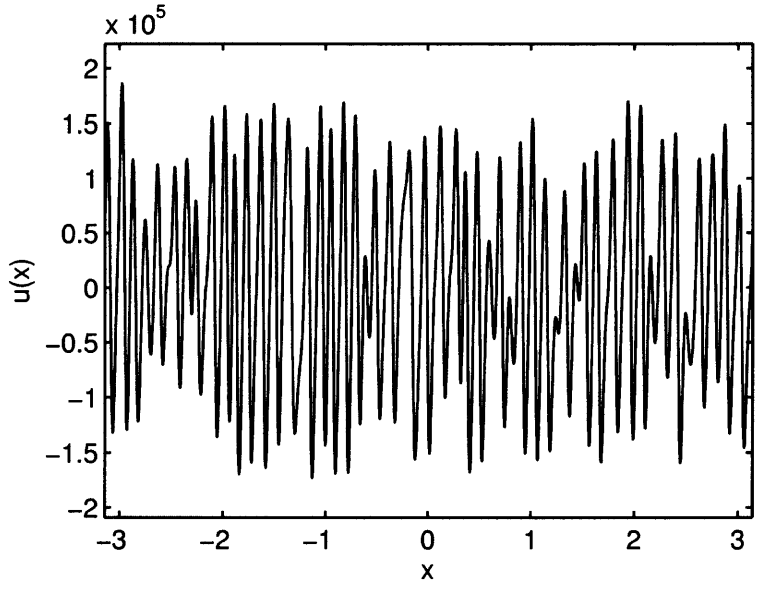

Figure 4.5 The solution $u(x,t)$ after 20000 time-steps; $\mu = 2^5$, $\nu = 0.5$, $p = 3$.

4.4 Analyticity of the Solutions of Nonlocal Kuramoto-Sivashinsky Equations

In this section we use the approach of Collet et al. [26] to prove that the solutions of the MKS equation are analytic in a strip around the real axis. The results for the DMKS equation are analogous and can be achieved by slight modifications of the analysis of this section.

Let us denote the righthand side of (4.122) by $R(\mu, \nu)$, i.e., let

$$R(\mu, \nu) = K\sqrt{\frac{\nu}{\eta(\gamma)}C(\gamma, \nu)} + \|\varphi\|_2, \tag{4.122}$$

where K, $C(\gamma, \nu)$, φ are the same as in Theorem 4.2.2.

So, for every $\beta > 1$ there exists $t' \geq 0$ (which depends on u_0, μ, ν, β), such that $\|u\|_2 = \sqrt{\int_{-\pi}^{\pi} u^2(x, t)dx} \leq \beta R(\mu, \nu)$ for all $t \geq t'$.

Theorem 4.4.1 *If the initial condition u_0 for equation (4.1) with 2π-periodic boundary conditions is in $\dot{H}^1_{\text{per}}$ then for large enough t the solution $u(x, t)$ satisfies the bound*

$$\left\|e^{\alpha^* t^* \boldsymbol{A}} u\right\|_2 \leq 2R(\mu, \nu), \tag{4.123}$$

where $\boldsymbol{A} = \mathcal{H} \circ \partial_x$, and α^*, t^* are functions of μ, ν, and p which will be determined later.

Proof: First, let $t' \geq 0$ be such that $\|u\|_2 \leq 1.5R(\mu, \nu)$ for all $t \geq t'$, and let us shift the origin to t'.

Let $\hat{u}_k(t)$ be the Fourier coefficients of $u(x, t)$, i.e.,

$$u(x, t) = \sum_{k \in \mathbb{Z}} e^{ikx}\hat{u}_k(t). \tag{4.124}$$

Since the function $u(x, t)$ is real we get $\hat{u}_{-k} = \hat{u}_k^*$, where $\hat{u}_k^*$ is a complex conjugate of $\hat{u}_k$. We can also easily get that if $\int_{-\pi}^{\pi} u_0(x)dx = 0$ then $\int_{-\pi}^{\pi} u(x, t)dx = 0$ for all t, i.e., $\hat{u}_0 \equiv 0$. Equation (4.1) takes the form

$$\frac{d\hat{u}_k(t)}{dt} = (-\nu k^4 + \mu|k|^p + k^2)\hat{u}_k(t) - \frac{i}{2}k \sum_{k_1 + k_2 = k} \hat{u}_{k_1}(t)\hat{u}_{k_2}(t). \tag{4.125}$$

Let $\boldsymbol{A} = \mathcal{H} \circ \partial_x$, i.e the operator $\boldsymbol{A}$ acts by multiplication on the Fourier coefficients as follows:

$$\widehat{(\boldsymbol{A}u)}_k = |k|\hat{u}_k, \quad k \in \mathbb{Z}. \tag{4.126}$$

(This operator can be also written as $\boldsymbol{A} = (-\partial_{xx})^{1/2}$.) Let also $v = e^{\alpha t \boldsymbol{A}}u$, i.e., the Fourier coefficients of v are

$$\hat{v}_k = e^{\alpha t|k|}\hat{u}_k, \quad k \in \mathbb{Z}. \tag{4.127}$$

Multiplying equation (4.125) by $e^{\alpha t|k|}\hat{v}_{-k}$ and summing over k we get

$$\frac{1}{2}\frac{d}{dt}\sum_{k\in\mathbb{Z}}|\hat{v}_k|^2 = \alpha\sum_{k\in\mathbb{Z}}|k||v_k|^2 + \sum_{k\in\mathbb{Z}}s_k|v_k|^2 - \frac{1}{2\pi}b(u,\, u,\, e^{\alpha t|k|\boldsymbol{A}}v), \tag{4.128}$$

where $s_k = -\nu k^4 + \mu|k|^p + k^2$ and

$$b(u,\, v,\, w) = \int_{-\pi}^{\pi} uv_x w dx. \tag{4.129}$$

The form b satisfies the following inequality:

$$|b(u,\, u,\, e^{\alpha t\boldsymbol{A}}v)| \leq C\sqrt{\alpha t}\|v\|_2\|\boldsymbol{A}v\|_2^2, \tag{4.130}$$

for some constant C, see Collet et al. [26] and Appendix D.

Applying (4.130) to (4.128) we obtain

$$\begin{aligned}\frac{1}{2}\frac{d}{dt}\|v\|_2^2 \leq& \alpha\|\boldsymbol{A}^{1/2}v\|_2^2 + \|\boldsymbol{A}v\|_2^2 + \mu\|\boldsymbol{A}^{p/2}v\|_2^2 \\ &- \nu\|\boldsymbol{A}^2v\|_2^2 + C\sqrt{\alpha t}\|v\|_2\|\boldsymbol{A}v\|_2^2.\end{aligned} \tag{4.131}$$

Next, we use the inequalities

$$\|\boldsymbol{A}^{1/2}v\|_2^2 \leq \|v\|_2^{3/2}\|\boldsymbol{A}^2v\|_2^{1/2}, \tag{4.132}$$

$$\|\boldsymbol{A}v\|_2^2 \leq \|v\|_2\|\boldsymbol{A}^2v\|_2, \tag{4.133}$$

$$\|\boldsymbol{A}^{p/2}v\|_2^2 \leq \|v\|_2^{2-p/2}\|\boldsymbol{A}^2v\|_2^{p/2}. \tag{4.134}$$

We get

$$\frac{1}{2}\frac{d}{dt}\|v\|_2^2 \leq \alpha\|v\|_2^{3/2}\|\boldsymbol{A}^2 v\|_2^{1/2} + \|v\|_2\|\boldsymbol{A}^2 v\|_2 + \mu\|v\|_2^{2-p/2}\|\boldsymbol{A}^2 v\|_2^{p/2} - \nu\|\boldsymbol{A}^2 v\|_2^2 + C\sqrt{\alpha t}\|v\|_2^2\|\boldsymbol{A}^2 v\|_2. \tag{4.135}$$

Applying Young's inequality (see Appendix C) we obtain

$$\frac{1}{2}\frac{d}{dt}\|v\|_2^2 \leq \frac{3\varepsilon_1}{4}\alpha^{4/3}\|v\|_2^2 + \frac{1}{4\varepsilon_1^3}\|\boldsymbol{A}^2 v\|_2^2 + \frac{\varepsilon_2}{2}\|v\|_2^2 + \frac{1}{2\varepsilon_2}\|\boldsymbol{A}^2 v\|_2^2 + \frac{\mu(4-p)\varepsilon_3}{4}\|v\|_2^2 + \frac{\mu p}{4\varepsilon_3^{(4-p)/p}}\|\boldsymbol{A}^2 v\|_2^2 - \nu\|\boldsymbol{A}^2 v\|_2^2 + \frac{C\epsilon_4}{2}\alpha t\|v\|_2^4 + \frac{C}{2\epsilon_4}\|\boldsymbol{A}^2 v\|_2^2, \tag{4.136}$$

where $\varepsilon_1, \varepsilon_2, \varepsilon_3, \varepsilon_4$ are some constants. Choosing these constants so that the coefficient of $\|\boldsymbol{A}^2 v\|_2^2$ becomes zero, i.e.,

$$\frac{1}{4\varepsilon_1^3} + \frac{1}{2\varepsilon_2} + \frac{\mu p}{4\varepsilon_3^{(4-p)/p}} - \nu + \frac{C}{2\varepsilon_4} = 0, \tag{4.137}$$

and denoting $\Phi(t) \equiv \|v\|_2^2$, we get

$$\frac{d}{dt}\Phi(t) \leq \left[\frac{3\varepsilon_1}{2}\alpha^{4/3} + \varepsilon_2 + \frac{\mu(4-p)\varepsilon_3}{2}\right]\Phi(t) + C\varepsilon_4\alpha t\Phi^2(t), \tag{4.138}$$

By the assumption $\Phi(0) \leq [1.5R(\mu, \nu)]^2$ (since the origin was shifted to t'). As long as $\Phi(t) \leq [2R(\mu, \nu)]^2$, equation (4.138) implies

$$\frac{d}{dt}\Phi(t) \leq \left[\frac{3\varepsilon_1}{2}\alpha^{4/3} + \varepsilon_2 + \frac{\mu(4-p)\varepsilon_3}{2} + 4R^2(\mu, \nu)C\varepsilon_4\alpha t\right]\Phi(t), \tag{4.139}$$

which leads to

$$\Phi(t) \leq [1.5R(\mu, \nu)]^2 \exp\left[\left(\frac{3\varepsilon_1}{2}\alpha^{4/3} + \varepsilon_2 + \frac{\mu(4-p)\varepsilon_3}{2}\right)t + 2R^2(\mu, \nu)C\varepsilon_4\alpha t^2\right]. \tag{4.140}$$

Therefore, $\Phi(t) \leq 4R^2(\mu, \nu)$ as long as

$$\left(\frac{3\varepsilon_1}{2}\alpha^{4/3} + \varepsilon_2 + \frac{\mu(4-p)\varepsilon_3}{2}\right)t + 2R^2(\mu, \nu)C\varepsilon_4\alpha t^2 \leq 2\ln\frac{4}{3}, \tag{4.141}$$

i.e., as long as $t \leq t^*$, where t^* is the positive solution of the quadratic equation

$$2R^2(\mu, \nu)C\varepsilon_4\alpha t^2 + \left(\frac{3\varepsilon_1}{2}\alpha^{4/3} + \varepsilon_2 + \frac{\mu(4-p)\varepsilon_3}{2}\right)t - 2\ln\frac{4}{3} = 0. \tag{4.142}$$

To get a wider estimate for the strip of analyticity we should choose ε_1, ε_2, ε_3, ε_4 and α so that αt^* is maximized while condition (4.137) is satisfied. Let the corresponding values be ε_1^*, ε_2^*, ε_3^*, ε_4^* and α^*. Then

$$\left\|e^{\alpha^* t\boldsymbol{A}}u\right\|_2 \leq 2R(\mu, \nu), \quad \text{for } t \leq t^*. \tag{4.143}$$

To finish the proof we note that $\|u\|_2 \leq 1.5R(\mu, \nu)$ for $t \geq t'$. Therefore we can shift the origin to any time $t \geq t'$ and the statement of the theorem follows. Condition (4.123) is satisfied for $t \geq t' + t^*$. ■

Remark 4.4.2 *Note that when μ, ν are fixed and $\nu < \mu$, condition (4.137) implies that $\varepsilon_3 \to \infty$ as $p \to 4^-$. Then it can be easily seen that $\alpha^* t^* \to 0$ as $p \to 4^-$. This suggests that analyticity breaks down in the limit $p \to 4^-$.*

Theorem 4.4.1 implies that for large enough t the Fourier coefficients of the solution of (4.1) satisfy

$$|\hat{u}_k| = \mathcal{O}(e^{-\alpha^* t^* |k|}). \tag{4.144}$$

Thus, the following result holds:

Theorem 4.4.3 *If the initial condition u_0 for equation (4.1) with 2π-periodic boundary conditions is in $\dot{H}^1_{\text{per}}$ then for large enough t the solution $u(x, t)$ is an analytic function of x in a strip around the real axis of width at least $\alpha^* t^*$.*

4.5 Summary and Further Discussion

We have studied a class of nonlocal Kuramoto-Sivashinsky (KS) equations arising in interfacial electrohydrodynamics. Two modifications of the well-known KS equation are afforded by the model: (i) the addition of a nonlocal Hilbert transform term that enhances the usual second derivative negative diffusion (equation (4.1) with the plus sign), and, (ii) the case when the nonlocal term is the only term providing instability (equation (4.1) with the minus sign), all other linear terms being diffusive. We have presented in detail rigorous results for case (i). In particular we proved global existence and uniqueness of the solutions in $\dot{H}^1_{\text{per}}$ by first proving local results and then establishing global results by proving uniform boundedness of the solutions in $\dot{H}^1_{\text{per}}$ on each time interval. We also established uniform boundedness of the solutions in $\dot{H}^1_{\text{per}}$ after proving uniform boundedness in $\dot{L}^2_{\text{per}}$, using a modification of the method of Collet et al. [27]. Along with global existence, this proves the existence of an absorbing ball in $\dot{L}^2_{\text{per}}$ and provides estimates for its radius. Our estimates improve those of Duan & Ervin [34], for $p = 3$, who used a different gauge function. Moreover, we have established that the solutions are analytic in a strip around the real axis.

An evaluation of the rigorous estimates valid at large values of the electrical parameter μ, as compared to numerical solutions of the equations is also carried out (see Figures 4.2, 4.3). The numerical work indicates that an optimal $\dot{L}^2_{\text{per}}$ solution bound arises; this is explained by a simple scaling argument. A conjecture valid for all p (and verified by extensive numerical simulations) is made regarding these findings.

In case (ii), results which parallel those above have been obtained when μ is larger than the threshold value $\mu_0(\nu;\, p)$ above which linearly unstable modes enter – for example when $p = 3$, we can take $\mu_0 = 2\sqrt{\nu}$. (When $\mu < \mu_0$ the value of $\|u\|_2$ decays to zero as $t \to \infty$.) The main differences are technical and result in other expressions for the quantities N, M, δ and $C(\gamma,\, \nu)$ and in turn result in different estimates for the radius of the absorbing ball. The large γ (note that $\gamma = \nu^{1-p/2}\mu$) behavior of this radius is identical to that given for case (i) – see estimate (4.80).

CHAPTER 5

INSTABILITIES AND SATURATION OF ELECTRIFIED THIN LIQUID FILMS

5.1 Physical Model

Consider a viscous liquid film wetting a solid horizontal substrate (we assume complete wetting and hence do not model the physics of contact line dynamics). Two related configurations are of interest: overlying two-dimensional films with the liquid layer resting on the substrate, and, overhanging two-dimensional films with the liquid layer wetting the underside of the horizontal substrate. A schematics is provided in Figure 5.1 for the overlying film and with a normal electric field present as analyzed later.

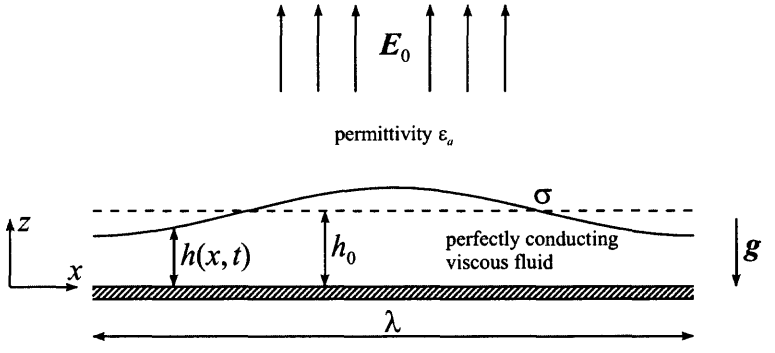

Figure 5.1 Schematics of the problem.

The essential physical difference between the two configurations is very intuitive: gravity is stabilizing for overlying films and destabilizing for overhanging ones. When surface tension is present, short waves are also linearly stable implying that overlying films will normally be stable and expected to return to their rest state of uniform thickness and zero flow. When the film wets the underside of the plate, gravity is destabilizing and the ensuing dynamics depend on several factors including the initial thickness of the layer (equivalently the mass), the size of the capillary forces, and the electric field if present.

If the mass is sufficiently large we expect to see two-dimensional lobes of fluid forming and falling vertically away from the plate. These may in turn break to leave disjoint threads of fluid which can in turn undergo secondary capillary instabilities in the transverse direction to form droplets. This breakaway scenario is very complicated and needs to be addressed by direct numerical simulations. Our interest in the present study is the modelling and analysis of interfacial flows which do not develop breakaway structures. It is reasonable to expect that sufficiently thin films (equivalently those having small mass) with sufficiently large surface tension, will evolve without breakaway structures. In the present chapter we derive model long wave equations which contain the competing physical mechanisms of gravitational stabilization or destabilization, surface tension, and electric field destabilization. The model equations are studied analytically and solved numerically to confirm the intuitive conjectures. Overlying films (with no field present) produce rather trivial and uninteresting dynamics with solutions approaching uniform states. Addition of a normal electric field introduces an instability that is not active in its absence – the instability has a high wavenumber cut-off which depends on surface tension. We find (through analysis and computations) that non-uniform large time structures emerge with positive solutions remaining smooth for all time – touchdowns occur locally but only after infinite time. According to our model equations, hanging films which are gravitationally unstable, do not form breakaway structures when surface tension is present. This result persists in the presence of the destabilizing electric field also. Evidence for the dynamical behavior of both configurations comes from a global boundedness of solutions theorem, as well as accurate numerical computations which indicate that the film thins locally to zero after infinite time (physically, when the film is thin enough, Van der Waals forces will enter to cause rupture and de-wetting in finite time).

The fluid is Newtonian of a constant density ρ and dynamic viscosity μ and is assumed to be a perfect conductor as in Chapter 3. The surface tension coefficient between the liquid and the surrounding medium is σ. We denote by $h(x,\, t)$ the local film thickness, which is

a function of space and time, and the unperturbed thickness of the liquid layer is h_0. The gravitational acceleration $\boldsymbol{g}$ acts in the vertical direction. By a small modification which switches the sign of $\boldsymbol{g}$, the equations that we will derive also describe hanging films below horizontal plates. The plate is considered to be an infinite electrode which is held at zero voltage potential, i.e., the electrode is grounded. Another flat electrode is parallel to the plate and is placed infinitely far from it, such that, in the limit, the resulting electric field is uniform and perpendicular to the plate, i.e., we assume that at infinity the electric field $\boldsymbol{E}$ approaches a constant value $\boldsymbol{E}_0$ which is normal to the plate. The surrounding medium is assumed to be a perfect dielectric with permittivity ε_a, and the corresponding voltage potential in it is denoted by V. Since the liquid is a perfect electric conductor, the potential is zero on the interface and there is no electric field inside the liquid layer (see Chapter 3 also).

5.2 Governing Equations

First, we introduce a rectangular coordinate system $(x,\, z)$ with the x-axis pointing along the plate and the z-axis pointing up and being perpendicular to the plate; the associated velocity field is denoted by $\boldsymbol{u} = (u,\, v)$. As in Chapter 3, we denote the liquid layer by Region I and the surrounding medium by Region II.

The governing equations in Region I are the mass conservation equation (2.23) and the momentum conservation equations (2.24), which for the present problem take the form:

$$u_t + uu_x + vu_z = -\frac{p_x}{\rho} + \nu(u_{xx} + u_{zz}), \tag{5.1}$$

$$v_t + uv_x + vv_z = -\frac{p_z}{\rho} + \nu(v_{xx} + v_{zz}) - g, \tag{5.2}$$

$$u_x + v_z = 0. \tag{5.3}$$

In Region II the electric field can be written as a gradient of a voltage potential V, $\boldsymbol{E} = -\nabla V$, and the potential V satisfies Laplace's equation:

$$V_{xx} + V_{zz} = 0. \tag{5.4}$$

The boundary conditions are the no-slip condition and the impermeability condition at the wall:

$$u|_{z=0} = 0, \quad v|_{z=0} = 0. \tag{5.5}$$

The condition that the electric field is constant and normal to the plate at infinity implies:

$$V_x \to 0,\ V_z \to -E_0 \text{ as } z \to \infty. \tag{5.6}$$

At the interface $z = h(x, t)$ the kinematic condition is satisfied:

$$v = h_t + uh_x. \tag{5.7}$$

Also, due to the assumed perfect conductivity of the fluid and continuity of the potential across the interface, the potential is zero at the interface:

$$V = 0 \quad \text{on } z = h(x, t), \tag{5.8}$$

which implies

$$V_x + h_x V_z = 0 \quad \text{on } z = h(x, t). \tag{5.9}$$

Finally, the tangential and normal stress balances at the interface become

$$(1 - h_x^2)(u_z + v_x) + 4h_x v_z = 0 \quad \text{on } z = h(x, t), \tag{5.10}$$

and

$$p_{\text{atm}} - p - \frac{\varepsilon_a}{2}(1 + h_x^2)V_z^2 + 2\mu\frac{1 + h_x^2}{1 - h_x^2}v_z = \frac{\sigma h_{xx}}{(1 + h_x^2)^{3/2}} \quad \text{on } z = h(x, t), \tag{5.11}$$

where p_{atm} is the constant (atmospheric) pressure in Region II.

This system of equations admits a zero flow basic solution which has $h(x, t) = h_0$, and $\boldsymbol{u} = 0$. This solution can be obtained assuming that all the dependent variables are functions of z only. The solution is

$$\bar{u} = 0, \tag{5.12}$$

$$\bar{v} = 0, \tag{5.13}$$

$$\bar{p} = p_{\text{atm}} - \frac{\varepsilon_a E_0^2}{2} - \rho g(z - h_0), \tag{5.14}$$

$$\overline{V} = E_0(h_0 - z). \tag{5.15}$$

5.3 Dimensionless Equations

Let the unperturbed depth h_0 be the scale for the lengths, U_0 be the velocity scale, the time scale be chosen to be $\frac{h_0}{U_0}$, the pressure scale be $\frac{\mu U_0}{h_0}$, and let the unit for the voltage potential be taken from the change in the basic potential, which is $E_0 h_0$. Hence, we introduce the following nondimensional variables:

$$x^* = \frac{1}{h_0}x, \quad z^* = \frac{1}{h_0}z, \quad t^* = \frac{U_0}{h_0}t, \tag{5.16}$$

$$u^* = \frac{1}{U_0}u, \quad v^* = \frac{1}{U_0}v, \quad p^* = \frac{h_0}{\mu U_0}p, \quad V^* = \frac{1}{E_0 h_0}V, \quad h^* = \frac{1}{h_0}h. \tag{5.17}$$

We substitute these variables into the system of governing equations and boundary conditions, and drop stars for convenience. The nondimensional equations in Region I are

$$u_t + uu_x + vu_z = \frac{1}{R}(-p_x + u_{xx} + u_{zz}), \tag{5.18}$$

$$v_t + uv_x + vv_z = \frac{1}{R}(-p_z + v_{xx} + v_{zz} - G), \tag{5.19}$$

$$u_x + v_z = 0, \tag{5.20}$$

and in Region II we obtain

$$V_{xx} + V_{zz} = 0. \tag{5.21}$$

The dimensionless boundary conditions become

$$u|_{z=0} = 0, \quad v|_{z=0} = 0, \tag{5.22}$$

$$V_x \to 0,\ V_z \to -1 \text{ as } z \to \infty, \tag{5.23}$$

and at the interface $z = h(x,\ t)$ we have

$$V = 0, \tag{5.24}$$

$$v = h_t + uh_x, \tag{5.25}$$

$$(1 - h_x^2)(u_z + v_x) + 4h_x v_z = 0, \tag{5.26}$$

$$-\frac{W_e}{2}(1 + h_x^2)V_z^2 + \frac{1 + h_x^2}{1 - h_x^2}v_z + \frac{1}{2}(\bar{p}_{\text{atm}} - p) = \frac{h_{xx}}{2C(1 + h_x^2)^{3/2}}, \tag{5.27}$$

where $\bar{p}_{\text{atm}} = (p_{\text{atm}}h_0)/(\mu U_0)$ is the nondimensional constant pressure in Region II. The other dimensionless parameters are a Reynolds number $R = \frac{U_0 h_0}{\nu}$, a Capillary number $C = \frac{U_0 \mu}{\sigma}$, an electric Weber number $W_e = \frac{\varepsilon_a E_0^2 h_0}{2\mu U_0}$, and a gravity number $G = \frac{\rho g h_0^2}{\mu U_0}$, measuring the ratio of gravitational and viscous forces.

Assuming that all dependent variables are independent of the longitudinal coordinate and time, yields the following basic solution of the dimensionless problem (5.18)-(5.27):

$$\bar{u} = 0, \tag{5.28}$$

$$\bar{v} = 0, \tag{5.29}$$

$$\bar{p} = \bar{p}_{\text{atm}} - W_e - G(z - 1), \tag{5.30}$$

$$\bar{V} = 1 - z, \tag{5.31}$$

and in the following we will consider arbitrary changes to these quantities. Thus, we introduce new unknowns $\tilde{u}$, $\tilde{v}$, $\tilde{p}$, $\widetilde{V}$:

$$u = \bar{u} + \tilde{u}, \quad v = \bar{v} + \tilde{v}, \quad p = \bar{p} + \tilde{p}, \quad V = \overline{V} + \widetilde{V}. \tag{5.32}$$

The equations take the following form (dropping the tildes):

In Region I:

$$u_t + uu_x + vu_z = \frac{1}{R}(-p_x + u_{xx} + u_{zz}), \tag{5.33}$$

$$v_t + uv_x + vv_z = \frac{1}{R}(-p_z + v_{xx} + v_{zz}), \tag{5.34}$$

$$u_x + v_z = 0. \tag{5.35}$$

In Region II:

$$V_{xx} + V_{zz} = 0. \tag{5.36}$$

Boundary conditions at the wall:

$$u|_{z=0} = 0, \quad v|_{z=0} = 0. \tag{5.37}$$

Boundary conditions at infinity:

$$V_x \to 0,\ V_z \to 0 \text{ as } z \to \infty. \tag{5.38}$$

Boundary conditions at the interface $z = h(x, t)$:

$$V = h - 1, \tag{5.39}$$

$$v = h_t + uh_x, \tag{5.40}$$

$$(1 - h_x^2)(u_z + v_x) + 4h_x v_z = 0, \tag{5.41}$$

$$-\frac{W_e}{2}\left[(V_z - 1)^2(1 + h_x^2) - 1\right] + \frac{1 + h_x^2}{1 - h_x^2}v_z$$
$$-\frac{G}{2}(1 - h) - \frac{p}{2} = \frac{h_{xx}}{2C(1 + h_x^2)^{3/2}}. \tag{5.42}$$

The above dimensionless system is fully nonlinear and presents a formidable computational and analytical task. In what follows we make analytical progress by studying the physically relevant case of thin films using a long wave nonlinear theory. The main difference between

this analysis and that of Chapter 3, is the absence of a shear flow due to the zero inclination of the plate. This in turn produces a fully nonlinear model for the evolution that is not amenable to a weakly nonlinear analysis and Kuramoto-Sivashinsky type dynamics.

5.4 Long Wave Asymptotics

In the analysis presented next we assume that the typical length λ of the interface deformation is long compared to the undisturbed thickness h_0, i.e., we assume that $\delta = \frac{h_0}{\lambda}$ is a small parameter. The separation of scales provides for the following rescalings in Region I:

$$x = \frac{1}{\delta}\xi, \quad t = \frac{1}{\delta}\tau, \quad v = \delta w, \quad p = \frac{1}{\delta}P. \tag{5.43}$$

The scaling for v follows from the continuity equation (5.35) noting that $u = \mathcal{O}(1)$, while the size of the pressure is picked to enable capillary forces to enter. Using the transformations

$$\partial_x = \delta\partial_\xi, \quad \partial_t = \delta\partial_\tau, \tag{5.44}$$

casts the problem in Region I into

$$u_\tau + uu_\xi + wu_z = \frac{1}{R}\left(-\frac{1}{\delta}P_\xi + \delta u_{\xi\xi} + \frac{1}{\delta}u_{zz}\right), \tag{5.45}$$

$$w_\tau + uw_\xi + ww_z = \frac{1}{R}\left(-\frac{1}{\delta^3}P_z + \delta w_{\xi\xi} + \frac{1}{\delta}w_{zz}\right), \tag{5.46}$$

$$u_\xi + w_z = 0, \tag{5.47}$$

for the hydrodynamics. The wall conditions become

$$u|_{z=0} = 0, \quad w|_{z=0} = 0, \tag{5.48}$$

while the boundary conditions at the interface $z = h(\xi, t)$ read

$$w = h_\tau + uh_\xi, \tag{5.49}$$

$$(1 - \delta^2 h_\xi^2)(u_z + \delta^2 w_\xi) + 4\delta^2 h_\xi w_z = 0, \tag{5.50}$$

$$-\frac{W_e}{2}\left[(V_z-1)^2(1+\delta^2 h_\xi^2)-1\right]+\delta\frac{1+\delta^2 h_x^2}{1-\delta^2 h_x^2}w_z$$
$$-\frac{G}{2}(1-h)-\frac{P}{2\delta}=\frac{\delta^2 h_{\xi\xi}}{2C(1+\delta^2 h_\xi^2)^{3/2}}. \tag{5.51}$$

The last boundary condition contains a nonlocal contribution since V satisfies Laplace's equation in the potential region above the fluid layer. Equations (5.45)-(5.47) and boundary conditions (5.48)-(5.51) are exact and amenable to an asymptotic analysis for small δ. Before developing such expansions we consider the problem in the potential region above the liquid layer.

Considering the problem in Region II, we will calculate the nonlocal contribution in (5.51) in terms of the interface position. We introduce the scalings

$$x=\frac{1}{\delta}\xi, \quad z=\frac{1}{\delta}\zeta, \quad t=\frac{1}{\delta}\tau, \tag{5.52}$$

i.e., we also introduce a large vertical coordinate in order to facilitate the application of the voltage condition (5.38) at infinity. Noting that $\partial_x = \delta\partial_\xi$, $\partial_z = \delta\partial_\zeta$ yields the following harmonic problem for V:

$$V_{\xi\xi}+V_{\zeta\zeta}=0. \tag{5.53}$$

The corresponding boundary conditions at infinity are

$$V_\xi \to 0,\ V_\zeta \to 0 \text{ as } \zeta \to \infty. \tag{5.54}$$

and the boundary condition (5.39) at the interface becomes

$$V|_{\zeta=\delta h} = h(\xi,\tau)-1. \tag{5.55}$$

For small δ, condition (5.55) becomes, to leading order,

$$V|_{\zeta\approx 0} = h(\xi,\tau)-1. \tag{5.56}$$

This voltage potential problem is solved in the same way that the problem (3.45)-(3.46) was solved in Chapter 3. Using those results, we obtain

$$V_\zeta(\xi, 0) = -\mathcal{H}[h_\xi], \tag{5.57}$$

where we recall that $\mathcal{H}$ is the Hilbert transform operator defined by

$$\mathcal{H}[g](\xi) = \frac{1}{\pi} PV \int_{-\infty}^{\infty} \frac{g(\xi')}{\xi - \xi'} d\xi'. \tag{5.58}$$

(See Appendix A for definitions and properties of the Hilbert transform.)

Knowing the nonlocal contribution due to the electric field in Region II, we can reconsider the normal stress boundary condition (5.51), noting that V_z transforms to δV_ζ when the Region II change of variables (5.52) is applied. We obtain

$$-\delta W_e \mathcal{H}[h_\xi] + \delta w_z - \frac{G}{2}(1 - h) - \frac{P}{2\delta} = \frac{\delta^2 h_{\xi\xi}}{2C} + \mathcal{O}(\delta^2). \tag{5.59}$$

In order to arrive at a system whose dynamics retains the effects of the electric field, gravity and surface tension, we are led to the following canonical scalings:

$$C = \delta^3 \overline{C}, \quad W_e = \frac{\overline{W}_e}{\delta^2}, \quad G = \frac{1}{\delta} \overline{G}. \tag{5.60}$$

where $\overline{C}$, $\overline{W}_e$, $\overline{G}$ are order one quantities. The Reynolds number R is assumed to be of order one throughout.

The derivation of the nonlinear evolution equation of the interface is accomplished by introducing the following asymptotic expansions

$$u = u_0 + \delta u_1 + \cdots, \quad w = w_0 + \delta w_1 + \cdots, \tag{5.61}$$

$$P = P_0 + \delta P_1 + \cdots, \quad h = H_0 + \delta H_1 + \cdots, \tag{5.62}$$

along with the scaled dimensionless groups (5.60). Substituting these expansions into the equations in Region I yields the following leading order solutions:

$$u_0 = \frac{P_{0\xi}}{2}z^2 - P_{0\xi}H_0 z, \tag{5.63}$$

$$w_0 = -\frac{P_{0\xi\xi}z^3}{6} + \frac{P_{0\xi\xi}H_0 z^2}{2} + \frac{P_{0\xi}H_{0\xi}z^2}{2}, \tag{5.64}$$

$$P_0 = -2\overline{W}_e\mathcal{H}[H_{0\xi}] - \overline{G}(1 - H_0) - \frac{1}{\overline{C}}H_{0\xi\xi}. \tag{5.65}$$

Using the solution for the velocities (5.63) and (5.64) in the kinematic condition (5.49) gives, to leading order,

$$H_{0\tau} = \frac{1}{3}[H_0^3 P_{0\xi}]_\xi. \tag{5.66}$$

Written in full, by use of expression (5.65) for P_0, the evolution equation is

$$H_{0\tau} + \frac{1}{3}\left[H_0^3\left(\frac{1}{\overline{C}}H_{0\xi\xi\xi} - \overline{G}H_{0\xi} + 2\overline{W}_e\mathcal{H}[H_{0\xi\xi}]\right)\right]_\xi = 0. \tag{5.67}$$

There are several noteworthy features of this equation. First, the electric field enters through a nonlocal term and has a destabilizing effect in much the same way as described for electrified falling films in Chapter 3. Gravity is also present, and if we allow the sign of $\overline{G}$ to become negative then the equation describes the long wave thin film dynamics of hanging films. In the absence of an electric field ($\overline{W}_e = 0$) and if $\overline{G} > 0$, the flow is stable to small disturbances – gravity and surface tension act to damp out perturbations. Instability is possible (with $\overline{W}_e = 0$ still) if $\overline{G} < 0$ as is intuitive for hanging films (this case has been considered by previous investigators, see Bertozzi & Pugh [14], Ehrhard [37], Ehrhard & Davis [38], Yiantsios & Higgins [124], Yiantsios & Higgins [125]). The electric field, however, can be utilized to destabilize liquid films lying on top of a substrate electrode ($\overline{G} > 0$), and the novel equation (5.67) enables a quantitative study of such phenomena.

In order to quantify some of the physically intuitive observations outlined above, we carry out a linear stability analysis which is helpful in identifying stable and unstable

regimes when the electric field is present. The fully nonlinear evolution is considered in later sections.

5.5 Linear Stability Analysis

For simplicity we write t and x for τ and ξ, and H for H_0. We also drop the bars above the nondimensional parameters $\overline{C}$, $\overline{G}$, $\overline{W}_e$ to get

$$H_t + \frac{1}{3}\left[H^3\left(\frac{1}{C}H_{xxx} - GH_x + 2W_e\mathcal{H}[H_{xx}]\right)\right]_x = 0. \tag{5.68}$$

We write $H = 1 + \epsilon\eta$, and substitute into the equation. This gives the following linearized equation at $\mathcal{O}(\epsilon)$:

$$\eta_t + \frac{1}{3C}\eta_{xxxx} - \frac{G}{3}\eta_{xx} + \frac{2W_e}{3}\mathcal{H}[\eta_{xxx}] = 0. \tag{5.69}$$

Looking for normal mode solutions $\eta = \hat{\eta}\exp(st + ikx)$, where $\hat{\eta}$ is in general a complex constant, leads to the following linear dispersion relation

$$s(k) = -\frac{1}{3C}k^4 + \frac{2W_e}{3}|k|^3 - \frac{G}{3}k^2. \tag{5.70}$$

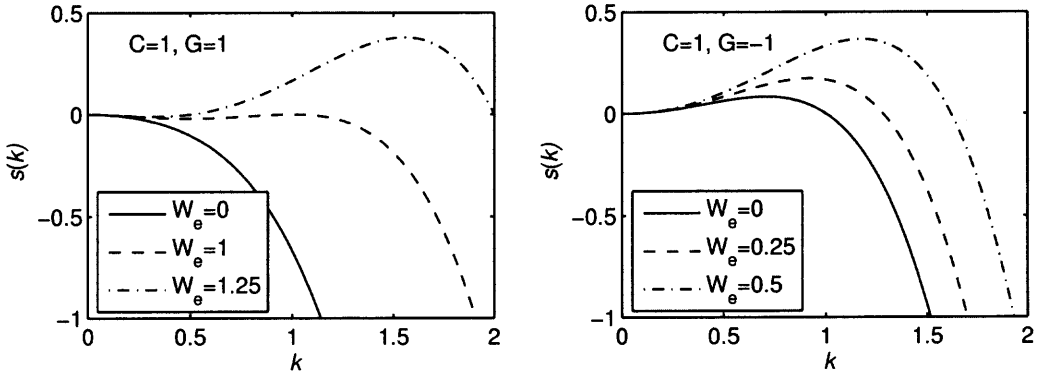

Figure 5.2 Changes in the dispersion relation due to the electric field. The left panel corresponds the positive sign of G, the right panel corresponds to the negative sign of G.

When $G > 0$, we get that for $W_e < (G/C)^{1/2}$ all modes are stable, i.e., $s(k) < 0$ for all k, and for $W_e > (G/C)^{1/2}$ there is a band of unstable waves extending from $k = CW_e - \sqrt{(CW_e)^2 - CG}$ to $k = CW_e + \sqrt{(CW_e)^2 - CG}$, and the electric field is destabilizing. The most unstable mode has the wavenumber $k = \frac{3CW_e + \sqrt{9(CW_e)^2 - 8CG}}{4}$. Typical results are shown in Figure 5.2 (left panel).

When $G < 0$, there is always a band of unstable waves extending from $k = 0$ to $k = CW_e + \sqrt{(CW_e)^2 - CG}$, see Figure 5.2 (right panel). The size of the band scales with W_e when this is large and hence increasingly shorter wavelengths become linearly unstable as W_e increases. Damping of sufficiently high wavenumber modes (and hence well-posedness) is provided by the presence of surface tension which is extremely important in this case.

5.6 Numerical Methods

We have used two methods to solve the initial boundary value problem corresponding to equation (5.68). In both cases the solution is assumed to be periodic of period $2L$ (the equation is solved on the periodic interval $[-L, L]$), and H is taken to be an even function of x (it can be seen from (5.68) that if H is an even function of x initially, then it will remain so for all t). The complicating feature for numerical methods is the nonlinearity in the coefficient of the highest derivative (the H_{xxxx} term here). Both methods are implicit, but the first uses a linearization of the nonlinear "diffusion" coefficient while the second method is fully implicit. In the former case linear pentadiagonal systems need to be solved at each time step while in the second case an iterative Newton method is used to solve the nonlinear systems. We find that the linear solver method behaves diffusively in the sense that mass is lost over large computational times. We note that the evolution develops to slow draining dynamics where the film appears to touch down at infinite times (we do not have a proof of this, but we prove rigorously that the solution does not blow up in finite time). The importance of accurate large time computations, therefore, leads us to choose

the fully implicit scheme as the more appropriate for the problem at hand. In what follows we describe both methods in detail.

5.6.1 Numerical Method 1: Linearized Implicit Scheme

We consider equation (5.68) on a finite interval $[-L,\ L]$ with periodic boundary conditions; L measures the size of the system and controls the number of linearly unstable modes present (when the electric field is large enough to produce instabilities). As noted earlier, we will compute even solutions H, so it is enough to consider the equation on the half interval $[0,\ L]$ with the corresponding boundary conditions $H_x(0,\ t) = H_{xxx}(0,\ t) = 0$, $H_x(L,\ t) = H_{xxx}(L,\ t) = 0$.

First, we rewrite the equation as follows:

$$H_t + \frac{1}{3C}\left[H^3 H_{xxx}\right]_x = \frac{1}{3}\left[GH^3 H_x - 2W_e H^3 \mathcal{H}[H_{xx}]\right]_x. \tag{5.71}$$

Noting that

$$\left[H^3 H_{xxx}\right]_x = \frac{1}{4}\left[H^4\right]_{xxxx} - 36HH_x^2 H_{xx} - 9H^2 H_x H_{xxx} - 9H^2 H_{xx}^2 - 6H_x^4, \tag{5.72}$$

recasts the equation into

$$\begin{aligned} H_t + \frac{1}{12C}\left[H^4\right]_{xxxx} &= \frac{1}{3}\left[GH^3 H_x - 2W_e H^3 \mathcal{H}[H_{xx}]\right]_x \\ &+ \frac{1}{C}\left[12HH_x^2 H_{xx} + 3H^2 H_x H_{xxx} + 3H^2 H_{xx}^2 + 2H_x^4\right]. \end{aligned} \tag{5.73}$$

We use a semi-implicit scheme to solve equation (5.73) numerically. Let H_m^n denote the numerical approximation for H at $x = x_m = m\Delta x$, $t = t_n = n\Delta t$, $m = 0,\ 1,\ \ldots,\ M$, $n = 0,\ 1,\ \ldots$; here $\Delta x = \frac{L}{M}$. Define $\delta_m^{n+1} = H_m^{n+1} - H_m^n$. On the left side of the equation the terms are treated implicitly, where for the second term $\left[H^4\right]_{xxxx}$ we expand the function $\alpha(H) = H^4$ into Taylor series at $H = H_m^n$ and keep only the first two terms of this expansion, namely,

$$(H_m^{n+1})^4 \approx (H_m^n)^4 + 4(H_m^n)^3 \delta_m^{n+1}. \tag{5.74}$$

The terms on the right side are treated explicitly. Denoting $H^n = \left[H_0^n \; H_1^n \; \cdots \; H_M^n\right]^T$, etc., our scheme can be written as

$$\frac{\delta^{n+1}}{\Delta t} + \frac{1}{12C}\left[D_4(H^n)^4 + 4[D_4 \mathrm{diag}(H^n)^3]\delta^{n+1}\right] = \mathrm{RHS}(H^n), \tag{5.75}$$

where $(H^n)^4 = \left[(H_0^n)^4 \; (H_1^n)^4 \; \cdots \; (H_M^n)^4\right]^T$ etc., and D_4 is the following 4th order differentiation matrix:

$$D_4 = \frac{1}{\Delta x^4}\begin{bmatrix} 6 & -8 & 2 & 0 & 0 & \cdots & 0 & 0 & 0 \\ -4 & 7 & -4 & 1 & 0 & \cdots & 0 & 0 & 0 \\ 1 & -4 & 6 & -4 & 1 & \cdots & 0 & 0 & 0 \\ 0 & 1 & -4 & 6 & -4 & \cdots & 0 & 0 & 0 \\ 0 & 0 & 1 & -4 & 6 & \cdots & 0 & 0 & 0 \\ \vdots & \vdots & \vdots & \vdots & \vdots & \ddots & \vdots & \vdots & \vdots \\ 0 & 0 & 0 & 0 & 0 & \cdots & 6 & -4 & 1 \\ 0 & 0 & 0 & 0 & 0 & \cdots & -4 & 7 & -4 \\ 0 & 0 & 0 & 0 & 0 & \cdots & 2 & -8 & 6 \end{bmatrix}. \tag{5.76}$$

In addition, $\mathrm{RHS}(H^n)$ is the approximation for the right hand side of equation (5.73) at $H = H^n$. (Derivatives can be approximated using central differences and the Hilbert transforms can be found with spectral accuracy using the trapezoidal rule for the integral formula evaluated at midpoints to avoid the singularity of the kernel. Alternatively, we can approximate the derivatives and the Hilbert transforms spectrally using FFTs).

Finally, we get the following system of linear equations for $\delta_0^{n+1}, \delta_1^{n+1}, \ldots, \delta_M^{n+1}$:

$$\left[I + \frac{\Delta t}{3C} D_4 \mathrm{diag}(H^n)^3\right]\delta^{n+1} = \Delta t \mathrm{RHS}(H^n) - \frac{\Delta t}{12C} D_4 (H^n)^4. \tag{5.77}$$

At each time step we solve the above pentadiagonal system for δ^{n+1} and set $H^{n+1} = H^n + \delta^{n+1}$. The accuracy of the scheme is monitored by using the fact that the spatial integral of the solution is conserved.

5.6.2 Numerical Method 2: Fully Nonlinear Scheme with Newton Iterations

We consider equation (5.68) on a finite interval $[-L,\ L]$ with periodic boundary conditions. The numerical method was developed for the following more general equation (this also includes the fully nonlinear falling film equation derived in Chapter 3 – see below):

$$H_t + \left[f_1(H)H_{xxx}\right]_x + \left[f_2(H)\right]_{xx} + \left[f_3(H)\mathcal{H}[H_{xx}]\right]_x + \left[f_4(H)\right]_x = 0, \tag{5.78}$$

with $f_1, \ldots, f_4$ polynomials in H. When $f_1(\phi) = \frac{1}{3C}\phi^3$, $f_2(\phi) = -\frac{G}{12}\phi^4$, $f_3(\phi) = \frac{2W_e}{3}\phi^3$, $f_4(\phi) = 0$, we get equation (5.68) for a horizontal perfectly conducting thin liquid film under the action of an electric field. When $f_1(\phi) = \frac{\delta}{3C}\phi^3$, $f_2(\phi) = \delta\left(\frac{8R}{105}\phi^7 - \frac{\cot\beta}{6}\phi^4\right)$, $f_3(\phi) = \frac{2\delta W_e}{3}\phi^3$, $f_4(\phi) = \frac{2}{3}\phi^3$ we get the equation which corresponds to the case of a thin perfectly conducting liquid film flowing down an inclined plate under the action of an electric field (see Chapter 3). (Recall that δ is the ratio of undisturbed film thickness and the typical interfacial deformation wavelengths, which is assumed to be small, β is the angle of inclination, R is the Reynolds number, and C and W_e are the rescaled Capillary number and the electric Weber number, respectively.)

The numerical method for equation (5.78) is a fully implicit two level scheme. We use the ideas introduced in Bertozzi & Pugh [13], Diez et al. [32], to extend the methods to nonlinear, nonlocal problems. The equation is solved on a uniform spatial grid, and the spatial derivatives are discretized using central differences. More precisely, we consider the following $2M$ mesh points: $x_m = (m - M)\Delta x$, $m = 1,\ 2,\ \ldots,\ 2M$, where $\Delta x = L/M$. Let H_m be the values of a $2L$-periodic function H at the mesh points $x = x_m$. We also set $H_0 = H_{2M}$, $H_{-1} = H_{2M-1}$, etc., and $H_{2M+1} = H_1$, $H_{2M+2} = H_2$, etc., which follow by the periodicity of H. For simplicity we also introduce the points

$$x_{1/2} = \frac{1}{2}(-L + x_1), \tag{5.79}$$

$$x_{m+1/2} = \frac{1}{2}(x_m + x_{m+1}), \quad m = 1,\ 2\ \ldots,\ 2M - 1, \tag{5.80}$$

and set $H_{m+1/2} = \frac{1}{2}(H_m + H_{m+1})$. Then, the following approximations for the spatial derivatives are used:

$$H_x(x_{m+1/2}) \approx \partial_1(H)_{m+1/2} \equiv \frac{H_{m+1} - H_m}{\Delta x}, \tag{5.81}$$

$$H_{xx}(x_m) \approx \partial_2(H)_m \equiv \frac{\partial_1(H)_{m+1/2} - \partial_1(H)_{m-1/2}}{\Delta x}, \tag{5.82}$$

$$H_{xxx}(x_{m+1/2}) \approx \partial_3(H)_{m+1/2} \equiv \frac{\partial_2(H)_{m+1} - \partial_2(H)_m}{\Delta x}. \tag{5.83}$$

To approximate the Hilbert transform of H_{xx} at $x = x_{m+1/2}$ we use the trapezoidal rule for the integral in formula (A.7):

$$\mathcal{H}[H_{xx}](x_{m+1/2}) \approx \widetilde{\mathcal{H}}[\partial_2(H)]_{m+1/2} \equiv \frac{\Delta x}{2L} \sum_{k=1}^{2M} \partial_2(H)_k \cot\left(\frac{\pi(x_{m+1/2} - x_k)}{2L}\right). \tag{5.84}$$

After discretizing the spatial derivatives and the Hilbert transform, we get the following system of ODEs for $H_1, H_2, \ldots, H_{2M}$:

$$\begin{aligned} \frac{dH_m}{dt} = & - \frac{f_1(H_{m+1/2})\partial_3(H)_{m+1/2} - f_1(H_{m-1/2})\partial_3(H)_{m-1/2}}{\Delta x} - \partial_2(f_2(H))_m \\ & - \frac{f_3(H_{m+1/2})\widetilde{\mathcal{H}}[\partial_2(H)]_{m+1/2} - f_3(H_{m-1/2})\widetilde{\mathcal{H}}[\partial_2(H)]_{m-1/2}}{\Delta x} \\ & - \frac{f_4(H_{m+1/2}) - f_4(H_{m-1/2})}{\Delta x}, \end{aligned} \tag{5.85}$$

which can be written in the following compact form:

$$\frac{d\boldsymbol{H}}{dt} = \boldsymbol{F}(\boldsymbol{H}), \tag{5.86}$$

where $\boldsymbol{H} = (H_1, H_2, \ldots, H_{2M})^T$, $\boldsymbol{F}(\boldsymbol{H}) = (F_1(\boldsymbol{H}), F_2(\boldsymbol{H}), \ldots, F_{2M}(\boldsymbol{H}))^T$, and each $F_m(\boldsymbol{H})$, $m = 1, 2, \ldots, 2M$, is given by the expression on the righthand side of (5.85). (Note that unlike similar thin film problems that have been studied previously, $F_m(\boldsymbol{H})$ depends on all the components of $\boldsymbol{H}$ due to the presence of the Hilbert transform, which is nonlocal.)

It is important to emphasize that this semi-discrete scheme preserves the discrete form of the volume. We show this by multiplying (5.85) by Δx and summing over $m =$

$1, 2, \ldots, 2M$ to obtain

$$\sum_{m=1}^{2M} \frac{dH_m}{dt} \Delta x = 0. \tag{5.87}$$

It follows from a time integration of the last equation that

$$\sum_{m=1}^{2M} H_m(t) \Delta x = \sum_{m=1}^{2M} H_m(0) \Delta x. \tag{5.88}$$

For time discretization we use the following implicit two level scheme:

$$\frac{\boldsymbol{H}^{n+1} - \boldsymbol{H}^n}{\Delta t_n} = \boldsymbol{F}(\theta \boldsymbol{H}^{n+1} + (1-\theta)\boldsymbol{H}^n), \tag{5.89}$$

where $\boldsymbol{H}^n = (H_1^n, H_2^n, \ldots, H_{2M}^n)$ is the numerical solution for $\boldsymbol{H}$ at $t = t_n$, $\Delta t_n = t_{n+1} - t_n$, and θ is some real number between 0 and 1.

To advance from the time level n to the time level $n+1$, the algebraic system of nonlinear equations (5.89) for $\boldsymbol{H}^{n+1}$ is solved iteratively using Newton's method. The time step is chosen dynamically for each time level by requiring several constraints to be satisfied as described below (see also Bertozzi & Pugh [13], Diez et al. [32]). If the numerical solution violates one of the constraints, then the time step is reduced and the calculation is repeated. This is done until all the constraints are met. On the other hand, if all the constraints are met after the first application of the Newton's method, the time step is increased at the next time level (this is done to prevent using unnecessarily small time steps). The constrains are the following: (a) the minimum of the solution should change by no more than 10%, (b) the local relative error should be small (10^{-3} say). The local relative error e_m is computed as follows (see Bertozzi & Pugh [13], Diez et al. [32]):

$$e_m = \frac{(\Delta t_{n-1})^2}{H_m^n} \frac{d^2 H_m^n}{dt^2} \approx \frac{2\Delta t_{n-1}}{\Delta t_{n-2}} \frac{\Delta t_{n-2} H_m^{n+1} + \Delta t_{n-1} H_m^{n-1} - (\Delta t_{n-2} + \Delta t_{n-1}) H_m^n}{(\Delta t_{n-2} + \Delta t_{n-1}) H_m^n}. \tag{5.90}$$

In addition, the spatial grid is refined during the calculation to get better resolution of the solution. This is done by doubling the number of mesh points when the number of the significant Fourier modes becomes bigger that some critical value. Typically we double the

number of mesh points when more than $2/3$ Fourier modes are larger than a set tolerance of 10^{-13}. Note that the Fast Fourier Transform is merely used as an accuracy diagnostic rather than being part of the method.

The numerical method has been described and implemented for the non-parity general case. If $f_4 \equiv 0$, however, and the initial condition is an even function, then the solution H will remain even for all time. In this case we can consider $2L$-periodic even solutions and discretize the equation on the interval $[0, L]$ alone. The appropriate boundary conditions are (see earlier also):

$$H_x(0, t) = H_{xxx}(0, t) = 0, \tag{5.91}$$

$$H_x(L, t) = H_{xxx}(L, t) = 0, \tag{5.92}$$

with periodicity used as needed in calculating difference formulas.

5.6.3 Numerical Results

Before proceeding with numerical results of the electrified problem, we briefly describe two code validation runs that can be compared with the literature.

We consider first the problem studied by Yiantsios & Higgins [124]. They considered the behavior of a viscous fluid film bounded below by a wall and above by a second heavier immiscible fluid. For the case when the ratio of the viscosities $m = \mu_1/\mu_2$ is $\mathcal{O}(1)$ they obtained the following evolution equation for the interface

$$H_t + \frac{1}{3}\left[H^3(H_{xxx} + H_x)\right]_x = 0. \tag{5.93}$$

This is a special case of equation (5.68) when $C = 1$, $G = -1$, $W_e = 0$. (In our case it corresponds to a film hanging down from the ceiling without presence of an electric field.) They solved this equation on the periodic intervals of lengths $2\sqrt{2}\pi$, $4\sqrt{2}\pi$, $6\sqrt{2}\pi$, 5π. We have confirmed that our results reproduce those of [124]. More detailed features of the numerical solutions are shown in Figure 5.3 and are described later.

A second validation check is the reproduction of the results of Bertozzi & Pugh [14]. Part of their work involved the numerical solution of equation (5.68) on the interval $[-1, 1]$, with $C = 1$, $G = -80$, $W_e = 0$. Our code has reproduced these results with indistinguishable differences at $t = 100$, which is the largest time that Bertozzi & Pugh integrated to.

For the results presented here we take fixed representative values $C = 1$, and $G = -1$ or $G = 1$ and vary W_e. We solve equation (5.68) on the periodic interval $[-10, 10]$ ($L = 10$) for different values of W_e. The initial condition is taken to be the following small amplitude disturbance

$$u_0(x) = 1 + 0.1\cos(\pi x/L). \tag{5.94}$$

The results are shown in Figures 5.3-5.9 for $W_e = 0, 0.5, 1, 1.02, 1.1, 1.5$ and 2, respectively. Each Figure contains eight panels. The top two panels show the evolution of the interfacial shape $H(x, t)$ (left) and its first spatial derivative $H_x(x, t)$ (right). The second row shows the time evolution of the norms $\|H\|_2^2$ (left) and $\|H_x\|_2^2$ (right), while the third row of panels shows the evolution of the $\|H_{xx}\|_2^2$ (left) along with the evolution of $\int(1/H(x,t))dx$ (right). Finally, the last row of panels shows the evolution of the maximum value of the interfacial shape, $\max(H)$ (left), and its minimum value, $\min(H)$ (right).

We see that initially the evolution follows the predictions of the linear theory – the solution grows exponentially. As time increases, higher harmonics are generated due to the nonlinearities, and the most dominant mode appears to be the most unstable mode predicted by linear theory; note that this mode corresponds to the number of the drops which appear during the course of evolution. This can be seen, for example, for the case when $G = -1$ and the linear result. It was shown earlier that the wavenumber of the maximally unstable linear wave is $k = \frac{3CW_e+\sqrt{9(CW_e)^2-8CG}}{4}$. This calculation is based on 2π-periodic waves, and modifying the result to $2L$ periodic waves we obtain

$$k = \frac{L}{\pi}\frac{3CW_e + \sqrt{9(CW_e)^2 - 8CG}}{4}. \tag{5.95}$$

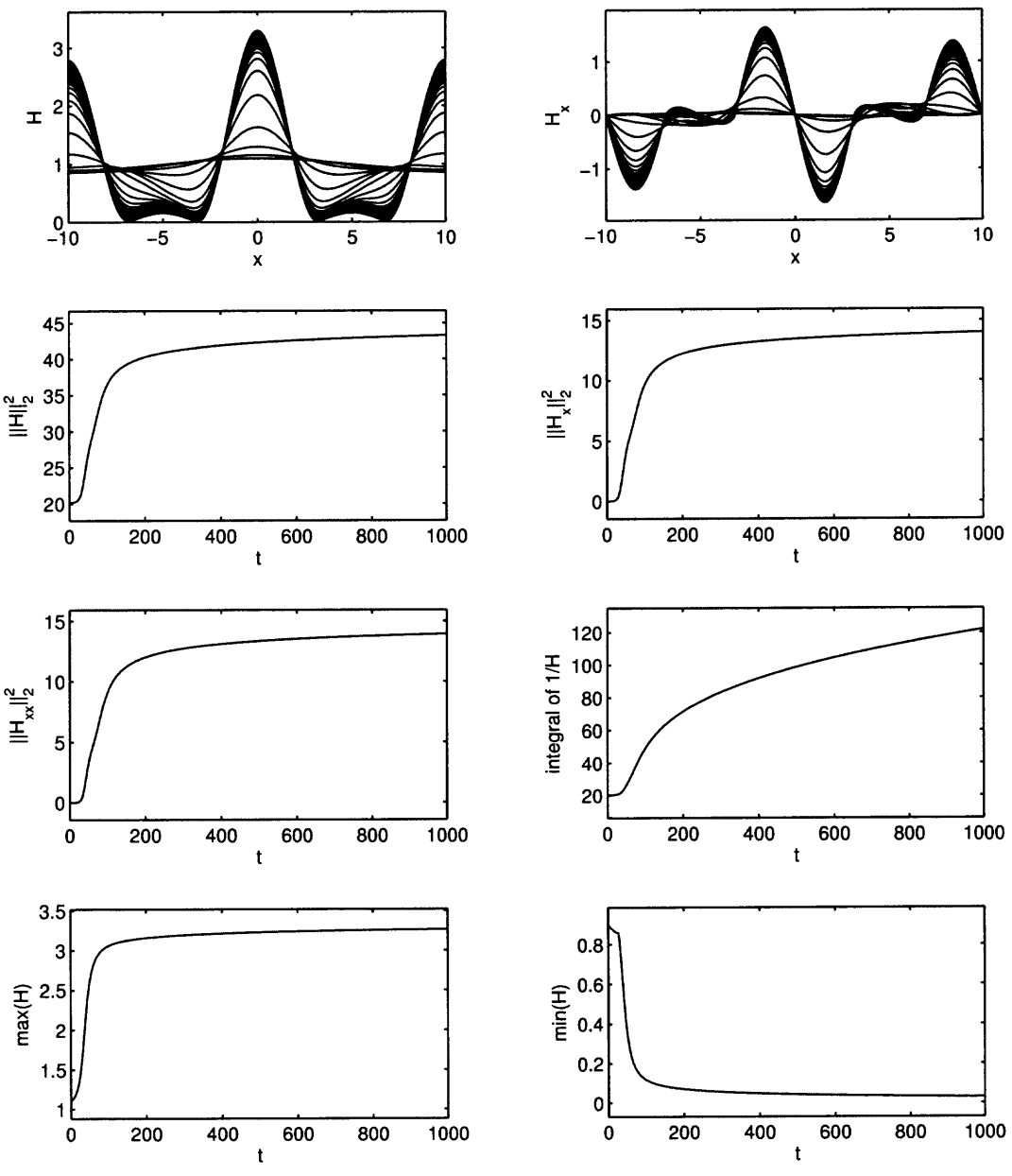

Figure 5.3 Evolution of the spatially periodic interface for $C = 1$, $G = -1$, $W_e = 0$. The equation was integrated for $0 \leq t \leq 1000$. The upper left and right panels show the evolution of the profile H and H_x, respectively (the time interval between the plots is 10). Also, the evolution of $\|H\|_2^2$, $\|H_x\|_2^2$, $\|H_{xx}\|_2^2$, as well as the evolution of $\int_{-10}^{10}(1/H)dx$ and the maximum and minimum of H are shown.

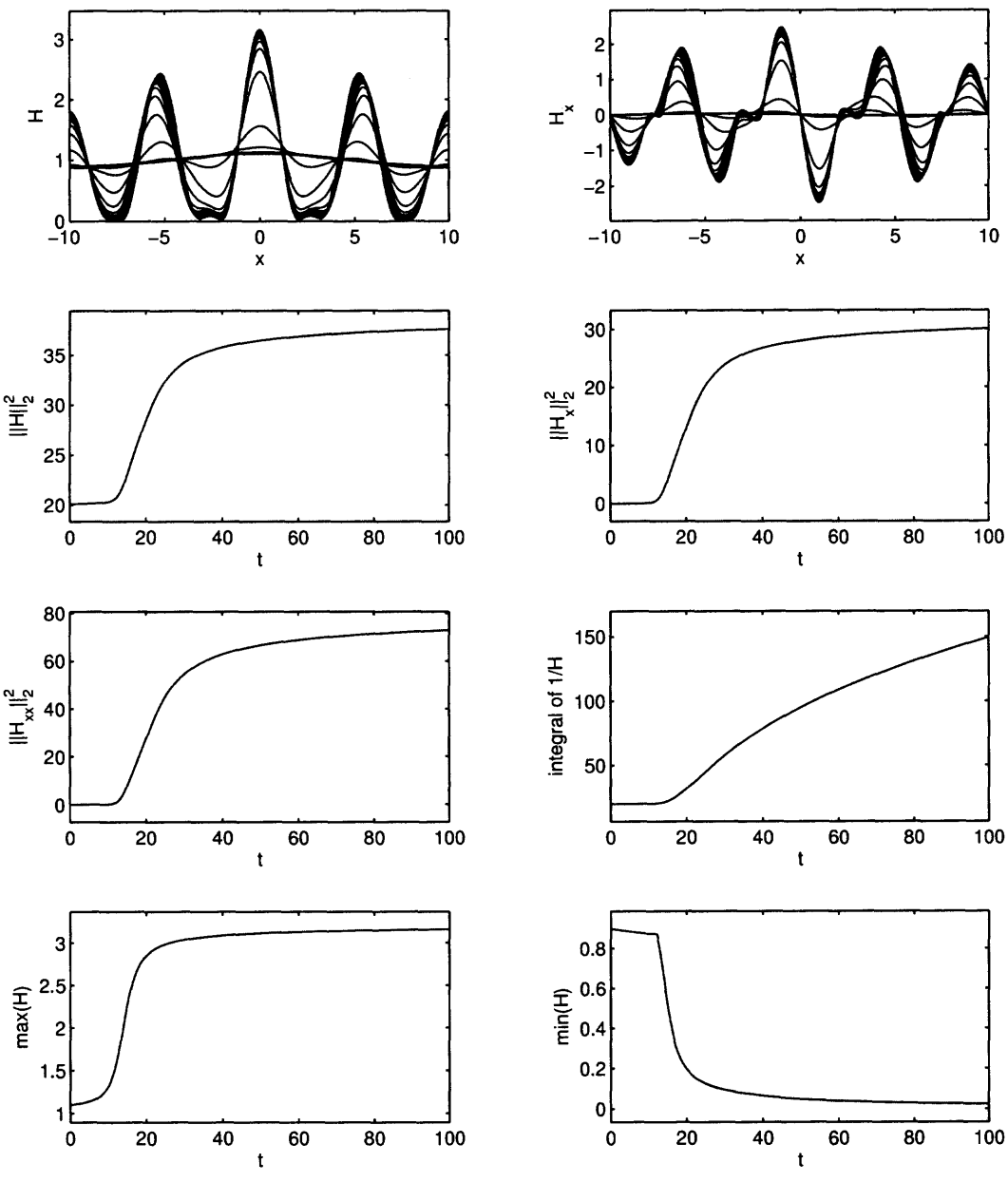

Figure 5.4 Evolution of the spatially periodic interface for $C = 1$, $G = -1$, $W_e = 0.5$. The equation was integrated for $0 \leq t \leq 100$. The upper left and right panels show the evolution of the profile H and H_x, respectively (the time interval between the plots is 4). Also, the evolution of $||H||_2^2$, $||H_x||_2^2$, $||H_{xx}||_2^2$, as well as the evolution of $\int_{-10}^{10}(1/H)dx$ and the maximum and minimum of H are shown.

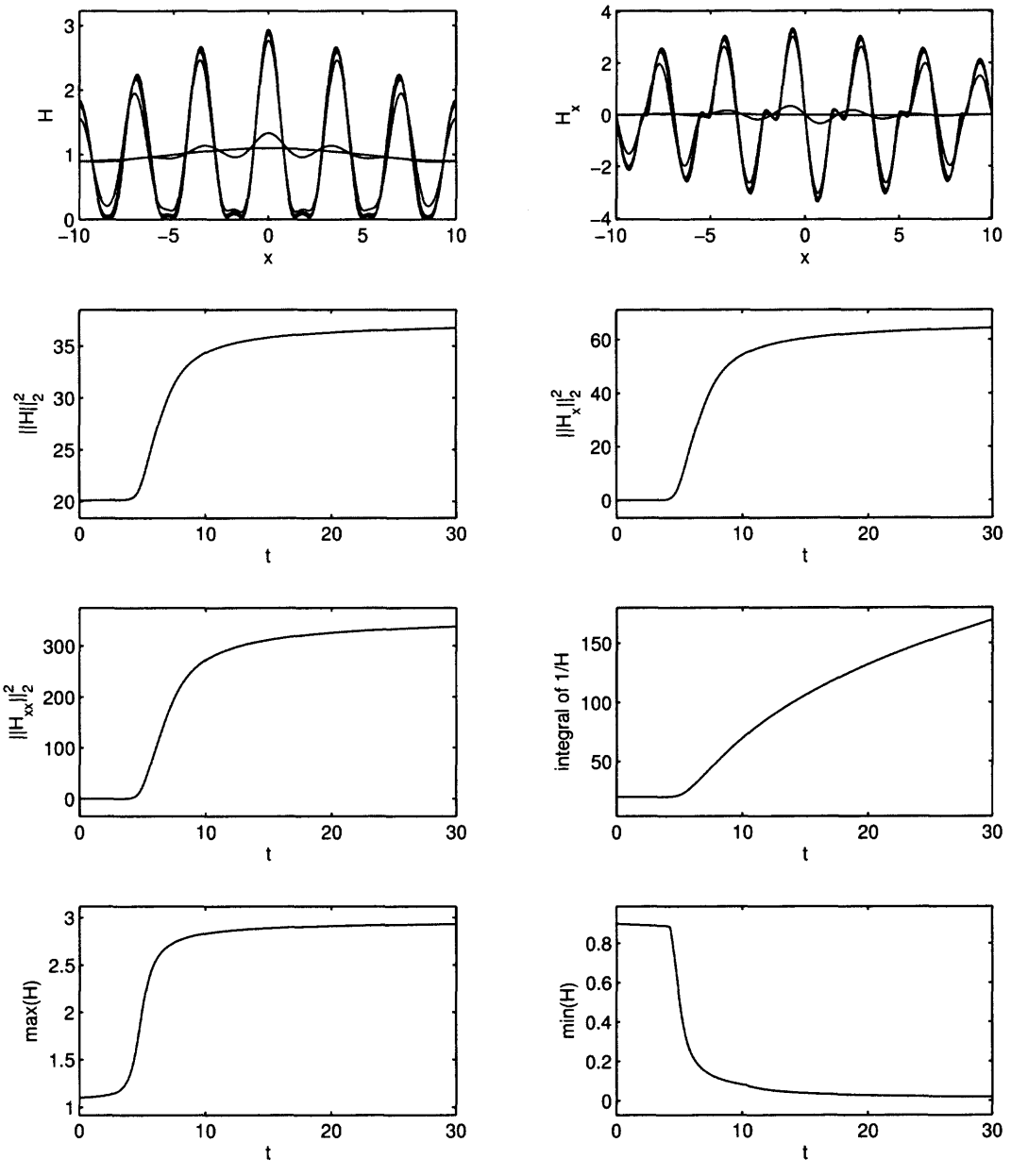

Figure 5.5 Evolution of the spatially periodic interface for $C = 1$, $G = -1$, $W_e = 1$. The equation was integrated for $0 \leq t \leq 30$. The upper left and right panels show the evolution of the profile H and H_x, respectively (the time interval between the plots is 4). Also, the evolution of $||H||_2^2$, $||H_x||_2^2$, $||H_{xx}||_2^2$, as well as the evolution of $\int_{-10}^{10}(1/H)dx$ and the maximum and minimum of H are shown.

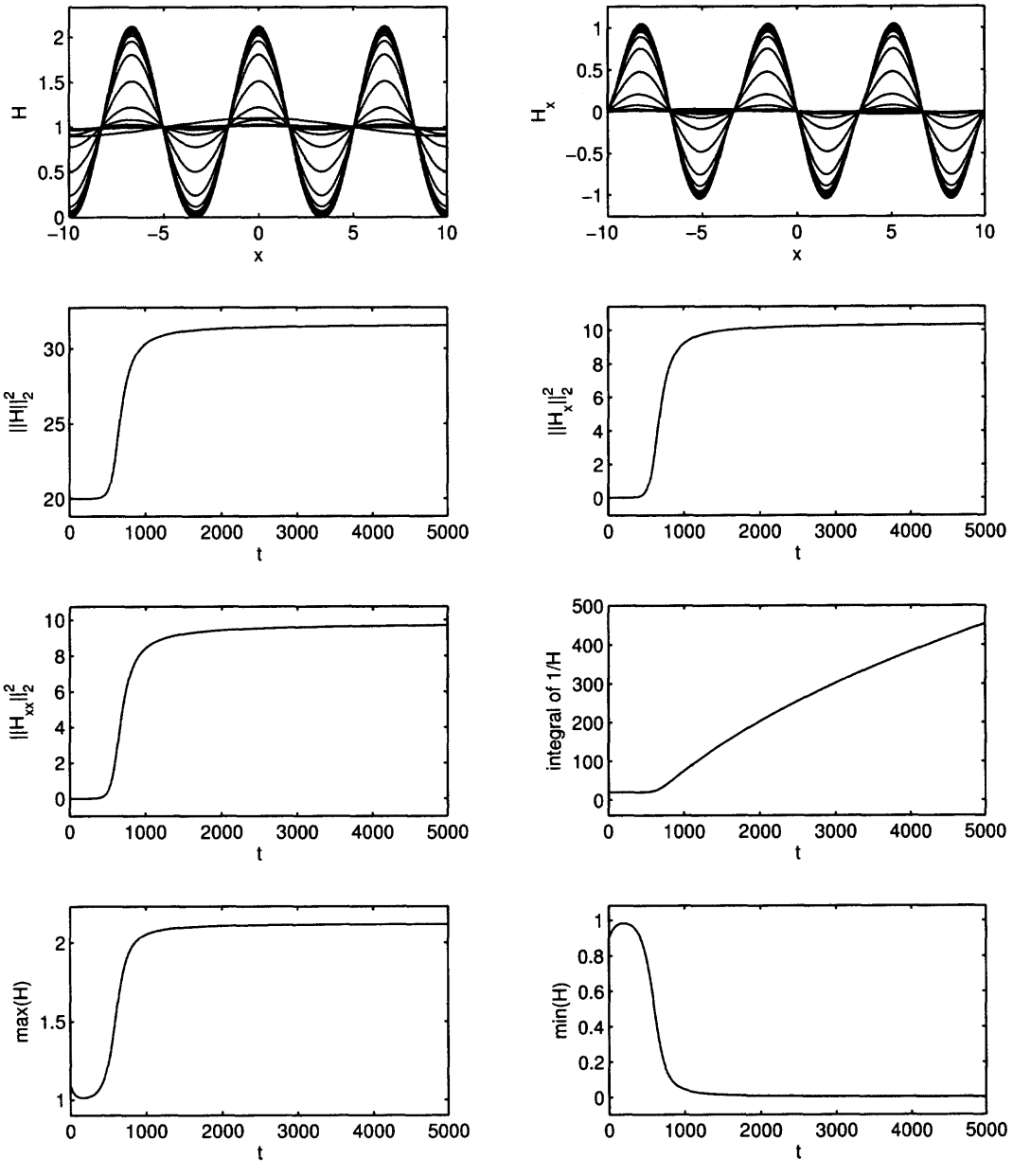

Figure 5.6 Evolution of the spatially periodic interface for $C = 1$, $G = 1$, $W_e = 1.02$. The equation was integrated for $0 \leq t \leq 5000$. The upper left and right panels show the evolution of the profile H and H_x, respectively (the time interval between the plots is 100). Also, the evolution of $||H||_2^2$, $||H_x||_2^2$, $||H_{xx}||_2^2$, as well as the evolution of $\int_{-10}^{10}(1/H)dx$ and the maximum and minimum of H are shown.

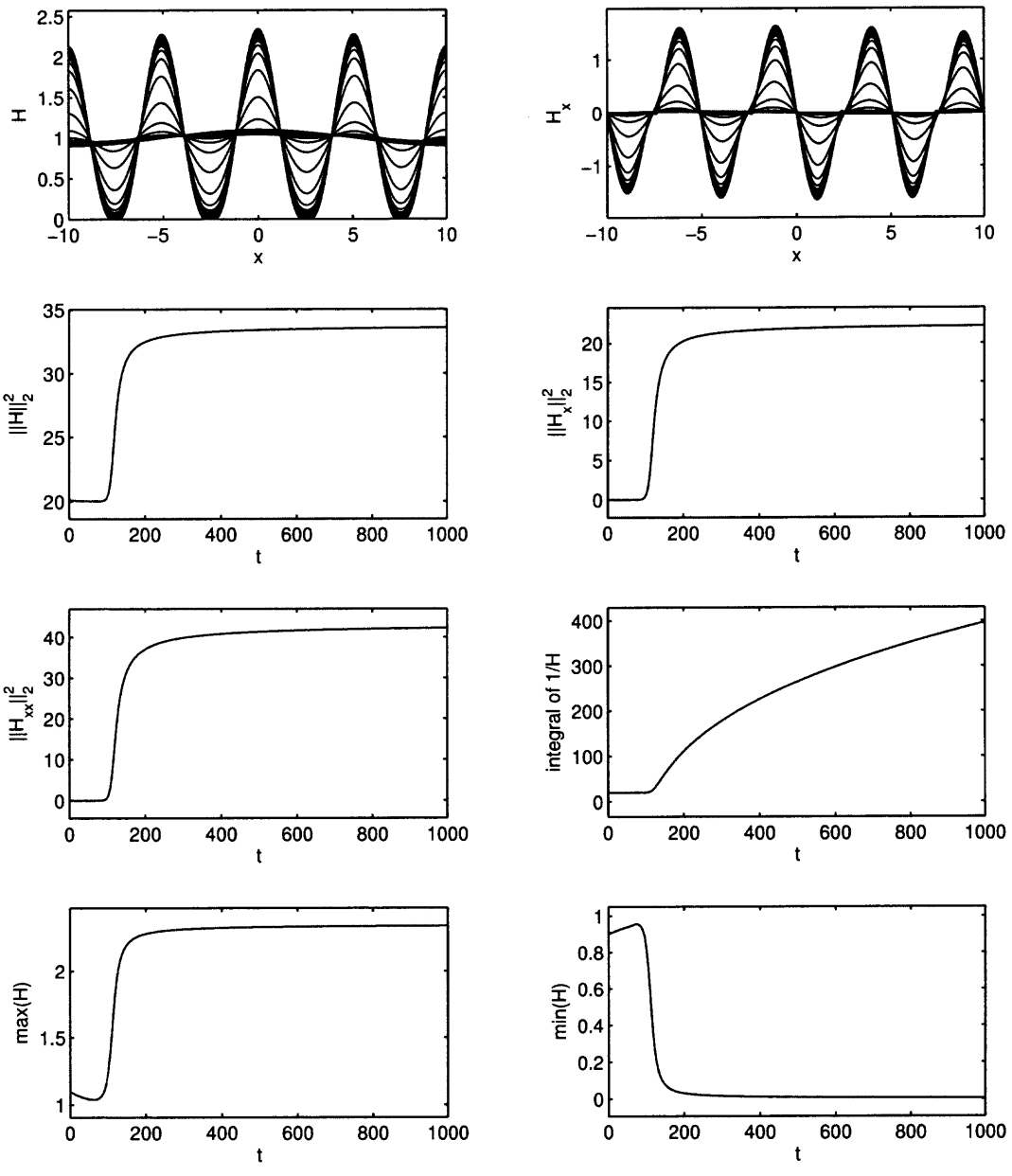

Figure 5.7 Evolution of the spatially periodic interface for $C = 1$, $G = 1$, $W_e = 1.1$. The equation was integrated for $0 \leq t \leq 1000$. The upper left and right panels show the evolution of the profile H and H_x, respectively (the time interval between the plots is 10). Also, the evolution of $||H||_2^2$, $||H_x||_2^2$, $||H_{xx}||_2^2$, as well as the evolution of $\int_{-10}^{10}(1/H)dx$ and the maximum and minimum of H are shown.

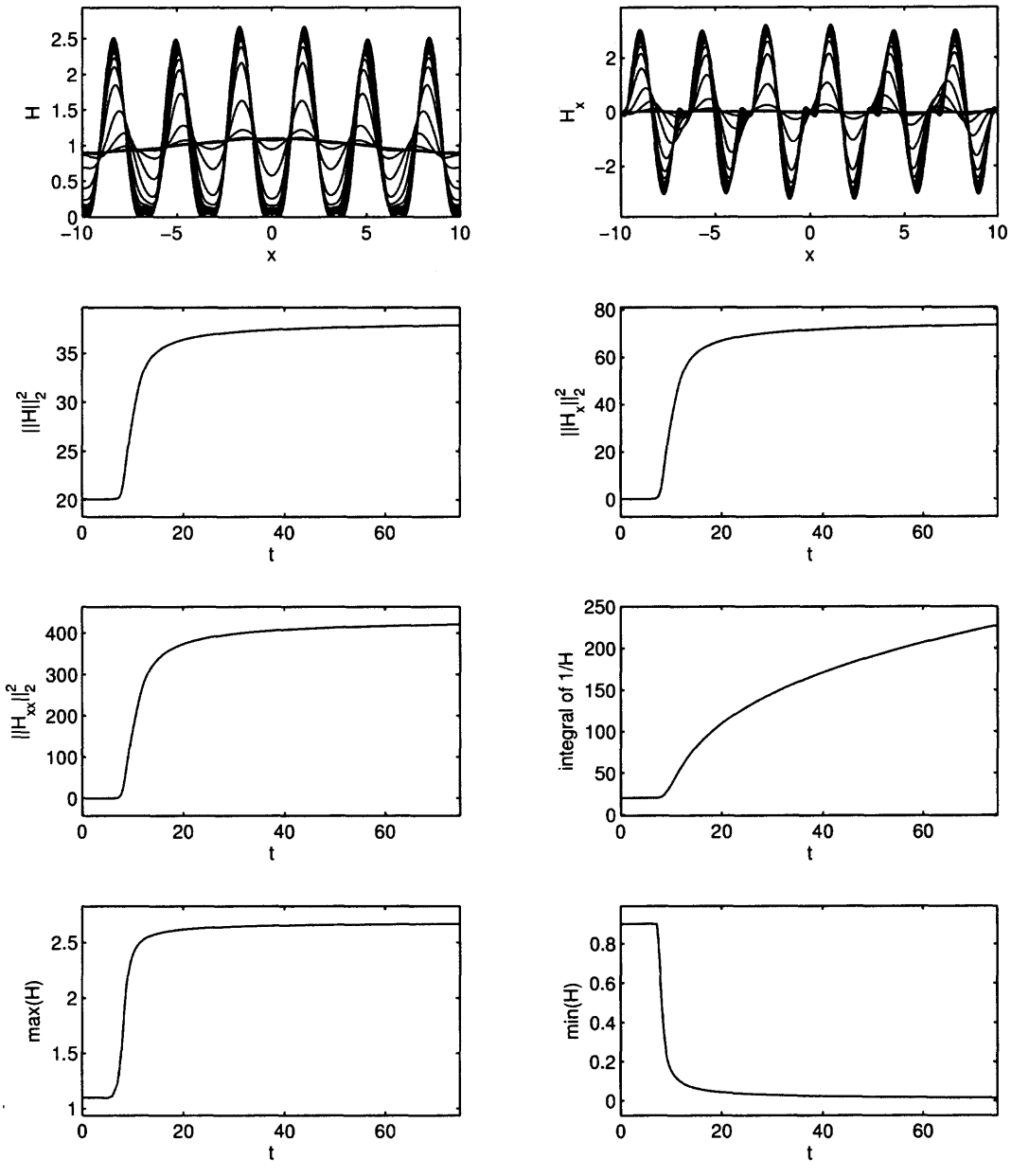

Figure 5.8 Evolution of the spatially periodic interface for $C = 1$, $G = 1$, $W_e = 1.5$. The equation was integrated for $0 \leq t \leq 75$. The upper left and right panels show the evolution of the profile H and H_x, respectively (the time interval between the plots is 1). Also, the evolution of $||H||_2^2$, $||H_x||_2^2$, $||H_{xx}||_2^2$, as well as the evolution of $\int_{-10}^{10}(1/H)dx$ and the maximum and minimum of H are shown.

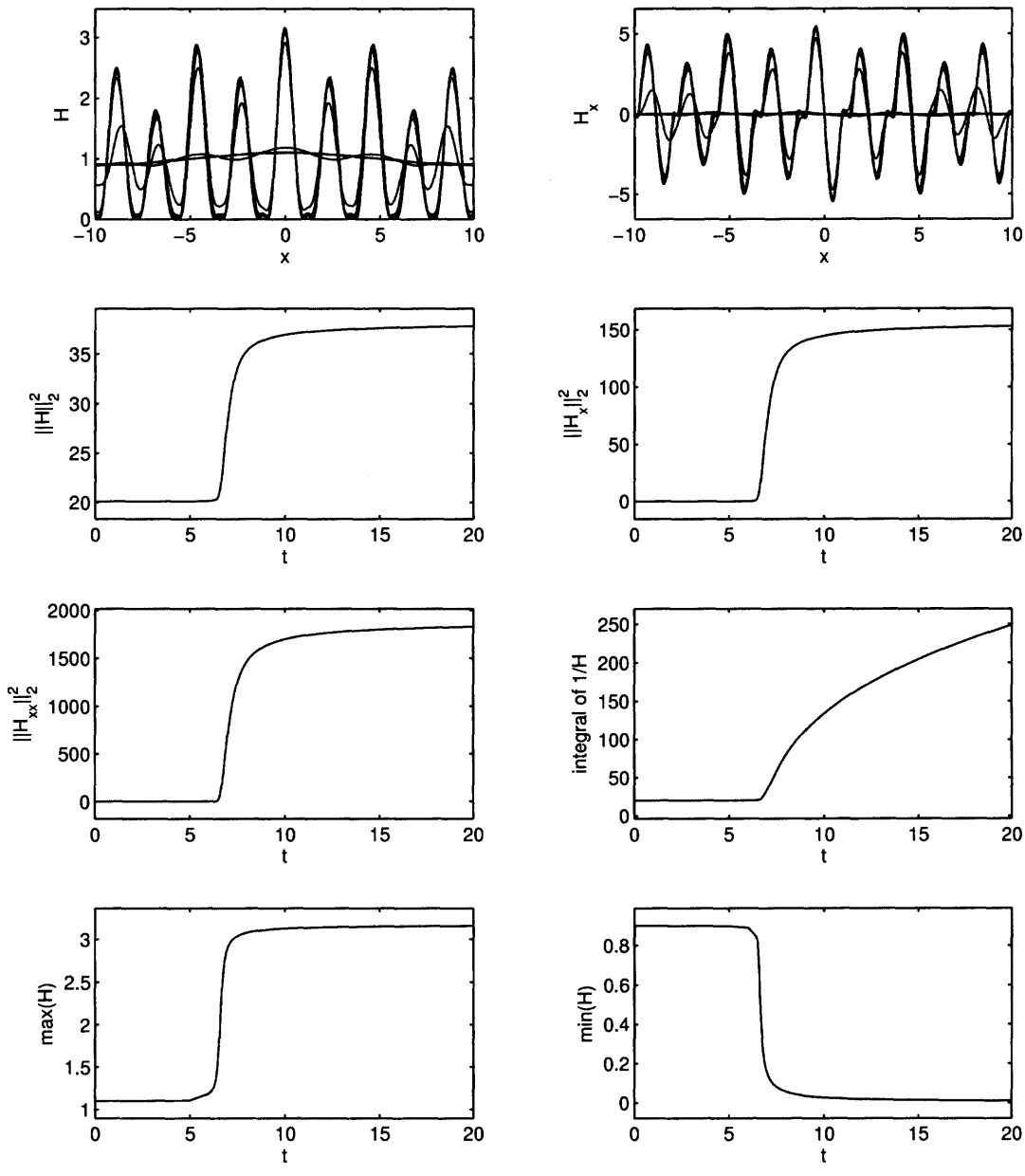

Figure 5.9 Evolution of the spatially periodic interface for $C = 1$, $G = 1$, $W_e = 2$. The equation was integrated for $0 \leq t \leq 20$. The upper left and right panels show the evolution of the profile H and H_x, respectively (the time interval between the plots is 1). Also, the evolution of $||H||_2^2$, $||H_x||_2^2$, $||H_{xx}||_2^2$, as well as the evolution of $\int_{-10}^{10}(1/H)dx$ and the maximum and minimum of H are shown.

This can be used, with $L = 10$, $C = -G = 1$, to estimate the most unstable wavenumber to be approximately 2.25, 3.74 and 5.67 for $W_e = 0$, $W_e = 0.5$ and $W_e = 1$, respectively. This in turn provides an estimate for the most unstable Fourier wavenumbers to be 2, 4 and 6, respectively, and these correspond to the number of drops which appear in the large time evolution of the system at the corresponding values of W_e – see the top left panels of Figures 5.3-5.5. The linear theory, therefore, provides an excellent prediction of the qualitative behavior of the solution at large times by predicting the number of large scale structures. Nonlinearity, of course, is responsible for this evolution and the finer details of the solution, such as touchdown.

Similar findings are established for the case when $G = 1$ (i.e., when the film rests above the plate). Again using the linear prediction (5.95), we predict the most unstable Fourier modes to be 3, 4, 6 and 9 for $W_e = 1.02$, $W_e = 1.1$, $W_e = 1.5$ and $W_e = 2$, respectively. These again correspond to the number of drops which emerge at large times as is evidenced in the interfacial evolution results in the top left panels of Figures 5.6-5.9.

It can be seen from the numerical results that the qualitative features of the solutions for $G < 0$ and W_e zero or non-zero, are similar to those with $G > 0$ and $W_e > 0$ (in the latter case a non-zero electric field is required to destabilize the flow and to produce non-trivial dynamics). The amplitude of the interfacial shape remains bounded throughout the evolution, and an increase in W_e (or equivalently a decrease of a negative G), produces increasingly more drops at large times, their number is governed by linear theory. This coarsening behavior is one of the main features of the dynamics as additional unstable modes enter. In all computed cases, as the time increases the evolution slows down (this can be seen in any of the different computational panels in the Figures, but is most clearly evidenced by the evolution of $\min(H)$). The spatial features at large times are also quite intricate: First, as the interface reaches the vicinity of the wall it tends to flatten and after that the solution tends to bulge near the ends of the flat regions forming a secondary hump in between – see Figure 5.3, for example, for the graphically most clear manifestation

of this phenomenon. All the results indicate that the solution remains positive – the film does not touch down within finite time. Also, the solution is bounded for all time, despite the fact that the electric field increases the instability and promotes the process of the formation of increasingly larger numbers of drops – i.e., coarsening. Numerical evidence of the boundedness of solutions is seen from the evolution of $\max(H)$, for example, in all the results presented. This is proved rigorously in the following section. The numerical results also indicate that the L^2 norms of H, H_x and H_{xx} also remain bounded, thus providing numerical evidence about the smoothness of the solutions. Finally, we consider the evolution of $\int(1/H(x,t))dx$ included in each of Figures 5.3-5.9. The results indicate that this quantity grows without bound as t increases which is consistent with the fact that H is tending to zero as t becomes large. In the next section we prove that the rate of growth is at most linear with t, which in combination with the evolution of the derivative norms shown in the Figures, implies an algebraic decay rate for the minimum film thickness.

Remark. It is shown analytically in Section 5.7 that the H^1-norm of positive solutions is bounded for all time. Due to Agmon's inequality (see equation (C.7) in Appendix C, for instance) this also implies boundedness of the maximum of the solution. Hence, if the solution is positive for all time it should be also uniformly bounded above, i.e., it does not blow up in finite or infinite time. Let us also note that it is shown analytically in Section 5.7 that the spatial integral of a positive solution is bounded on each finite time interval, i.e., it does not blow up in finite time (though it can happen in infinite time). Together with the fact that the H^2-norm of positive solutions is bounded it would imply that if a solution is initially positive, it will be positive for all time. Despite the fact that all our numerical results indicate the uniform boundedness of the H^2-norm of positive solutions, we have not shown this analytically yet.

5.7 Analytical Results

5.7.1 The Energy Functional

Let us first consider the following generalized equation:

$$H_t + \left[f(H)\mathcal{A}[H]_x\right]_x = 0, \tag{5.96}$$

where f is a function which takes positive values for positive arguments and is zero only at zero, and $\mathcal{A}[H]$ is some integro-differential operator, which involves the function H, its first and second order derivatives with respect to x, and the Hilbert transform operator. The additional condition that is satisfied by this operator will be given below. We will consider this equation on a periodic interval $[-L,\ L]$ with positive initial data $H_0(x) = H(x,\ 0)$.

Steady state solutions of equation (5.96) are found by integrating once to obtain

$$f(H)\mathcal{A}[H]_x = C_1, \tag{5.97}$$

where C_1 is some constant. If H vanishes at some point, then $C_1 = 0$. Otherwise $\mathcal{A}[H]_x = \frac{C_1}{f(H)}$, and integration gives $C_1 \int_{-L}^{L} \frac{dx}{f(H)} = 0$, which in turn implies that $C_1 = 0$. So, for steady state solutions $\mathcal{A}[H]_x = 0$, i.e.,

$$\mathcal{A}[H] = C_2, \tag{5.98}$$

where C_2 is some constant.

Let $\mathcal{E}[H]$ be the energy functional having the following form

$$\mathcal{E}[H] = \int_{-L}^{L} \mathcal{L}\big(H,\ H_x,\ \mathcal{H}[H]\big)dx, \tag{5.99}$$

for which the steady state solutions of equation (5.96) are extrema. More precisely, we assume that the following generalized Euler-Lagrange equation,

$$\frac{\partial \mathcal{L}}{\partial H} - \frac{d}{dx}\left[\frac{\partial \mathcal{L}}{\partial H_x}\right] - \mathcal{H}\left[\frac{\partial \mathcal{L}}{\partial \mathcal{H}[H]}\right] = 0, \tag{5.100}$$

coincides with the equation $C_2 - \mathcal{A}[H]$=0. Then

$$\frac{d\mathcal{E}[H]}{dt} = \int_{-L}^{L} \left(\frac{\partial \mathcal{L}}{\partial H} H_t + \frac{\partial \mathcal{L}}{\partial H_x} H_{xt} + \frac{\partial \mathcal{L}}{\partial \mathcal{H}[H]} \mathcal{H}[H_t] \right) dx. \tag{5.101}$$

Integrating the second term by parts and applying property (A.4) from Appendix A to the third term gives

$$\frac{d\mathcal{E}[H]}{dt} = \int_{-L}^{L} \left(\frac{\partial \mathcal{L}}{\partial H} - \frac{d}{dx}\left[\frac{\partial \mathcal{L}}{\partial H_x}\right] - \mathcal{H}\left[\frac{\partial \mathcal{L}}{\partial \mathcal{H}[H]}\right] \right) H_t dx \tag{5.102}$$

$$= -\int_{-L}^{L} (C_2 - \mathcal{A}[H]) \left[f(H) \mathcal{A}[H]_x \right]_x dx = -\int_{-L}^{L} f(H) \mathcal{A}[H]_x^2 dx \tag{5.103}$$

Therefore $\frac{d\mathcal{E}[H]}{dt} \leq 0$ for nonnegative H, i.e., $\mathcal{E}[H]$ is bounded above.

Let us now consider equation (5.68) corresponding to the physical problem at hand. For this equation $f(H) = H^3/3$ and

$$\mathcal{A}[H] = \frac{1}{C} H_{xx} - GH + 2W_e \mathcal{H}[H_x]. \tag{5.104}$$

The steady state solutions are determined by the equation

$$\frac{1}{C} H_{xx} - GH + 2W_e \mathcal{H}[H_x] = C_2. \tag{5.105}$$

Integrating this equation gives the following expression for C_2 in terms of the integral of a steady state solution

$$C_2 = -\frac{G}{2L} \int_{-L}^{L} H dx. \tag{5.106}$$

The functional $\mathcal{L}\big(H,\, H_x,\, \mathcal{H}[H]\big)$ can be chosen in the following form:

$$\mathcal{L}\big(H,\, H_x,\, \mathcal{H}[H]\big) = \frac{1}{2C} H_x^2 + \frac{G}{2} H^2 + W_e H_x \mathcal{H}[H] + C_2 H. \tag{5.107}$$

Thus, the following energy functional

$$\mathcal{E}[H] = \int_{-L}^{L} \left(\frac{1}{2C} H_x^2 + \frac{G}{2} H^2 + W_e H_x \mathcal{H}[H] + C_2 H \right) dx \tag{5.108}$$

is a nonincreasing function of time for a nonnegative solution H.

5.7.2 Uniform Boundedness of Positive Smooth Solutions

In the previous section we have shown that the energy functional $\mathcal{E}[H]$ is bounded above by its initial value for a nonnegative solution H of equation (5.68). In this section we will show uniform boundedness of solutions. It will be assumed that solutions are smooth. We will restrict our consideration to positive solutions, since given upper and lower bounds for positive solutions the equation is uniformly parabolic, which implies small time smoothness of the solutions (see Eidelman [39] and Friedman [40]).

We begin with the following lemma:

Lemma 5.7.1 *Let $\mathcal{E}[H]$ be the functional defined on $H^1(-L, L)$ by formula (5.108). Then there exist constants $\alpha > 0$, $\beta > 0$, and γ such that*

$$\|H\|_{H^1}^2 \leq \alpha \mathcal{E}[H] + \beta \|H\|_1^2 + \gamma \|H\|_1 \tag{5.109}$$

for all nonnegative $H \in H^1_{\text{per}}$. (Here and everywhere else we denote by L^2_{per}, H^k_{per}, $k = 1, 2, \ldots$, the subspaces of the Sobolev spaces $L^2(-L, L)$, $H^k(-L, L)$ consisting of periodic functions with period $2L$.)

Proof: First, using the Cauchy-Schwartz and Young's inequalities and property (A.5) of the Hilbert transform from Appendix A gives

$$\begin{aligned} \int_{-L}^{L} H_x \mathcal{H}[H] dx &\geq -\|H_x\|_2 \|\mathcal{H}[H]\|_2 = -\|H_x\|_2 \|H\|_2 \\ &\geq -\frac{\varepsilon_1}{2}\|H_x\|_2^2 - \frac{1}{2\varepsilon_1}\|H\|_2^2, \end{aligned} \tag{5.110}$$

where ε_1 is some positive number. Hence,

$$\begin{aligned} \mathcal{E}[H] &\geq \int_{-L}^{L} \left(\frac{1}{2C} H_x^2 + \frac{G}{2} H^2 + C_2 H \right) dx - \frac{\varepsilon_1 W_e}{2}\|H_x\|_2^2 - \frac{W_e}{2\varepsilon_1}\|H\|_2^2 \\ &= \left(\frac{1}{2C} - \frac{\varepsilon_1 W_e}{2} \right) \|H_x\|_2^2 + \left(\frac{G}{2} - \frac{W_e}{2\varepsilon_1} \right) \|H\|_2^2 + C_2 \int_{-L}^{L} H dx \end{aligned}$$

$$= \left(\frac{1}{2C} - \frac{\varepsilon_1 W_e}{2}\right)\|H\|_{H^1}^2 + \left(\frac{G}{2} - \frac{W_e}{2\varepsilon_1} - \frac{1}{2C} + \frac{\varepsilon_1 W_e}{2}\right)\|H\|_2^2 + C_2\int_{-L}^{L} H dx. \tag{5.111}$$

Note that $\int_{-L}^{L} H dx = \|H\|_1$ for a nonnegative H. We denote $A = \frac{1}{2C} - \frac{\varepsilon_1 W_e}{2}$ and $B = -\frac{G}{2} + \frac{W_e}{2\varepsilon_1} + \frac{1}{2C} - \frac{\varepsilon_1 W_e}{2}$. Choosing ε_1 sufficiently small gives $A > 0$, $B > 0$. Also, using the following interpolation inequality

$$\|H\|_2 \leq C_3 \|H\|_{H^1}^{1/3} \|H\|_1^{2/3} \tag{5.112}$$

and applying Young's inequality for the righthand side of the expression above gives

$$\|H\|_2 \leq C_3\left(\frac{\varepsilon_2}{3}\|H\|_{H^1} + \frac{2}{3\varepsilon_2^{1/2}}\|H\|_1\right), \tag{5.113}$$

where ε_2 is some positive number. Therefore

$$\|H\|_2^2 \leq \frac{2\varepsilon_2^2 C_3^2}{9}\|H\|_{H^1}^2 + \frac{8C_3^2}{9\varepsilon_2}\|H\|_1^2, \tag{5.114}$$

and we get

$$\begin{aligned}
\mathcal{E}[H] &\geq A\|H\|_{H^1}^2 - B\|H\|_2^2 + C_2\|H\|_1 && (5.115)\\
&\geq A\|H\|_{H^1}^2 - B\left(\frac{2\varepsilon_2^2 C_3^2}{9}\|H\|_{H^1}^2 + \frac{8C_3^2}{9\varepsilon_2}\|H\|_1^2\right) + C_2\|H\|_1 && (5.116)\\
&= \left(A - \frac{2\varepsilon_2^2 B C_3^2}{9}\right)\|H\|_{H^1}^2 - \frac{2BC_3^2}{9\varepsilon_2}\|H\|_1^2 + C_2\|H\|_1. && (5.117)
\end{aligned}$$

We denote $\tilde{A} = A - \frac{2\varepsilon_2^2 B C_3^2}{9}$ and $\tilde{B} = \frac{8BC_3^2}{9\varepsilon_2}$. Note that $\tilde{B} > 0$ and choosing ε_2 small enough gives $\tilde{A} > 0$. Thus

$$\mathcal{E}[H] \geq \tilde{A}\|H\|_{H^1}^2 - \tilde{B}\|H\|_1^2 + C_2\|H\|_1, \tag{5.118}$$

i.e.,

$$\|H\|_{H^1}^2 \leq \alpha\mathcal{E}[H] + \beta\|H\|_1^2 + \gamma\|H\|_1, \tag{5.119}$$

where $\alpha = 1/\tilde{A}$, $\beta = \tilde{B}/\tilde{A}$, $\gamma = -C_2/\tilde{A}$, as required. ■

We can prove the uniform boundedness of positive smooth solutions to (5.68):

Proposition 5.7.2 *Let $H(x, t)$ be a positive smooth solution of (5.68) with periodic boundary conditions on some time interval $[0, T]$. If $H(x, 0) = H_0(x) \in H^1_{\text{per}}$ then $\|H\|_{H^1}$ is uniformly bounded.*

Proof: First, note that equation (5.68) is a conservation law. The spatial integral of the solution is conserved. Indeed, integrating over $[-L, L]$ gives

$$\frac{d}{dt}\int_{-L}^{L} H dx = -\frac{1}{3}\int_{-L}^{L}\left[H^3\left(\frac{1}{C}H_{xxx} - GH_x + 2W_e\mathcal{H}[H_{xx}]\right)\right]_x dx \quad (5.120)$$

$$= -\frac{1}{3}\left[H^3\left(\frac{1}{C}H_{xxx} - GH_x + 2W_e\mathcal{H}[H_{xx}]\right)\right]_{-L}^{L} = 0. \quad (5.121)$$

Therefore $\|H\|_1 = \|H_0\|_1$. Also, since $\mathcal{E}[H]$ is a nonincreasing function of time, equation (5.109) implies

$$\|H\|^2_{H^1} \leq \alpha\mathcal{E}[H] + \beta\|H\|_1^2 + \gamma\|H\|_1 \quad (5.122)$$

$$= \alpha\mathcal{E}[H] + \beta\|H_0\|_1^2 + \gamma\|H_0\|_1 \quad (5.123)$$

$$\leq \alpha\mathcal{E}[H_0] + \beta\|H_0\|_1^2 + \gamma\|H_0\|_1. \quad (5.124)$$

■

Remark. Proposition 5.7.2 is essentially a no blow-up theorem for the solution H. The result does not prevent a touchdown (as predicted by the numerics). Furthermore, the boundedness of $\|H\|_{H^1}$ does not exclude touchdowns with cusp-like behavior having $H\,|x|^p$, $p \in [1/2, 1]$. Such singular solutions have not been observed numerically, however.

5.7.3 Evolution of $\int_{-L}^{L} H^{-1}dx$

In this section we show that the spatial integral of H^{-1} is bounded on each finite time interval. Indeed,

$$\frac{d}{dt}\int_{-L}^{L}\frac{dx}{H} = -\int_{-L}^{L}\frac{H_t}{H^2}dx. \quad (5.125)$$

Substituting the expression for H_t from (5.68) into (5.125) gives

$$\begin{aligned}\frac{d}{dt}\int_{-L}^{L}\frac{dx}{H} =&\frac{1}{3}\int_{-L}^{L}\frac{1}{H^2}\left[H^3\left(\frac{1}{C}H_{xxx}-GH_x+2W_e\mathcal{H}[H_{xx}]\right)\right]_x dx\\ =&\frac{1}{3}\int_{-L}^{L}\frac{1}{H^2}(3H^2H_x)\left(\frac{1}{C}H_{xxx}-GH_x+2W_e\mathcal{H}[H_{xx}]\right)dx\\ &+\frac{1}{3}\int_{-L}^{L}\frac{1}{H^2}H^3\left(\frac{1}{C}H_{xxx}-GH_x+2W_e\mathcal{H}[H_{xx}]\right)_x dx\\ =&\frac{1}{C}\int_{-L}^{L}H_xH_{xxx}dx-G\int_{-L}^{L}H_x^2dx+2W_e\int_{-L}^{L}H_x\mathcal{H}[H_{xx}]dx\\ &+\frac{1}{3C}\int_{-L}^{L}HH_{xxxx}dx-\frac{G}{3}\int_{-L}^{L}HH_{xx}dx+\frac{2W_e}{3}\int_{-L}^{L}H\mathcal{H}[H_{xxx}]dx.\end{aligned} \tag{5.126}$$

Integration by parts then gives

$$\begin{aligned}\frac{d}{dt}\int_{-L}^{L}\frac{dx}{H} =&-\frac{1}{C}\int_{-L}^{L}H_{xx}^2dx-G\int_{-L}^{L}H_x^2dx+2W_e\int_{-L}^{L}H_x\mathcal{H}[H_{xx}]dx\\ &+\frac{1}{3C}\int_{-L}^{L}H_{xx}^2dx+\frac{G}{3}\int_{-L}^{L}H_x^2dx-\frac{2W_e}{3}\int_{-L}^{L}H_x\mathcal{H}[H_{xx}]dx.\end{aligned} \tag{5.127}$$

Therefore,

$$\frac{d}{dt}\int_{-L}^{L}\frac{dx}{H}=-\frac{2}{3C}\int_{-L}^{L}H_{xx}^2dx-\frac{2G}{3}\int_{-L}^{L}H_x^2dx+\frac{4W_e}{3}\int_{-L}^{L}H_x\mathcal{H}[H_{xx}]dx. \tag{5.128}$$

Using the Cauchy-Schwartz and Young's inequalities and property (A.5) of the Hilbert transform from Appendix A gives

$$\begin{aligned}\int_{-L}^{L}H_x\mathcal{H}[H_{xx}]dx &\le \|H_x\|_2\|\mathcal{H}[H_{xx}]\|_2=\|H_x\|_2\|H_{xx}]\|_2\\ &\le\frac{1}{2\varepsilon}\|H_x\|_2^2+\frac{\varepsilon}{2}\|H_{xx}\|_2^2,\end{aligned} \tag{5.129}$$

where ε is some positive number. Hence,

$$\begin{aligned}\frac{d}{dt}\int_{-L}^{L}\frac{dx}{H}&\le-\frac{2}{3C}\|H_{xx}\|_2^2-\frac{2G}{3}\|H_x\|_2^2+\frac{4W_e}{3}\left(\frac{1}{2\varepsilon}\|H_x\|_2^2+\frac{\varepsilon}{2}\|H_{xx}\|_2^2\right)\\ &=A\|H_{xx}\|_2^2+B\|H_x\|_2^2,\end{aligned} \tag{5.130}$$

where $A = -\frac{2}{3C} + \frac{2W_e\varepsilon}{3}$, $B = -\frac{2G}{3} + \frac{2W_e}{3\varepsilon}$. Choosing ε small enough (s.t. $A < 0$) implies

$$\frac{d}{dt}\int_{-L}^{L}\frac{dx}{H} \leq B\|H_x\|_2^2. \tag{5.131}$$

Since the H^1-norm of the positive solution H is uniformly bounded, we get that there exists a constant D, s.t.

$$\frac{d}{dt}\int_{-L}^{L}\frac{dx}{H} \leq C, \tag{5.132}$$

which also implies boundedness of $\frac{d}{dt}\int_{-L}^{L}\frac{dx}{H}$

APPENDIX A

PROPERTIES OF THE HILBERT TRANSFORM

In this appendix we list some important properties of the Hilbert transform, see also [1]. The Hilbert transform operator $\mathcal{H}$ is defined as follows:

$$\mathcal{H}[f](x) = \frac{1}{\pi} PV \int_{-\infty}^{\infty} \frac{f(\xi)}{x-\xi} d\xi, \tag{A.1}$$

where the integral is understood in the sense of Cauchy principal value.

The Hilbert transform $\mathcal{H} : L^2(I) \to L^2(I)$ (or $\mathcal{H} : H^k(I) \to H^k(I)$) is a linear, invertible, bounded operator from L^2 to L^2 (and from Sobolev space H^k to H^k).

$$\partial_x \circ \mathcal{H} = \mathcal{H} \circ \partial_x, \tag{A.2}$$

$$\mathcal{H}^{-1} = -\mathcal{H}, \tag{A.3}$$

$$\int_I u(x)\mathcal{H}[v](x)dx = -\int_I v(x)\mathcal{H}[u](x)dx, \tag{A.4}$$

$$\|\mathcal{H}[u]\| = \|u\|, \tag{A.5}$$

$$\mathcal{F}\big[\mathcal{H}[u]\big](k) = -i\text{sign}(\text{Re}k)\hat{u}(k). \tag{A.6}$$

Here $\mathcal{F}$ is the Fourier transform operator and I is either $\mathbb{R}$ or a periodic interval.

For periodic functions on $[-\pi, \pi]$ we have

$$\mathcal{H}[f](x) = \frac{1}{2\pi} PV \int_{-\pi}^{\pi} f(\xi) \cot\Big(\frac{x-\xi}{2}\Big) d\xi. \tag{A.7}$$

APPENDIX B

DETAILS OF THE DERIVATION OF EQUATION (3.65)

The evolution equations for the two leading terms H_0 and H_1 are given by equations (3.59) and (3.64). Defining $H = H_0 + \delta H_1$, we can eliminate H_1 in favor of H and H_0 in (3.59) and (3.64), noting that we keep terms up to and including $\mathcal{O}(\delta^2)$ for (3.59) and $\mathcal{O}(\delta)$ for (3.64), so that the combined equation for H is correct to $\mathcal{O}(\delta^2)$ and with the functional form of the error known. The equations become:

$$H_\tau + 2H^2 H_\xi - \delta\left[H_{1\tau} + 2H^2 H_{1\xi} + 4HH_\xi H_1\right] + 2\delta^2\left[HH_1^2\right]_\xi + \mathcal{O}(\delta^3) = 0, \tag{B.1}$$

$$H_{1\tau} + \left[2H^2 H_1 - \frac{R}{3}H^3 p_{0\xi}^{(1)} + \frac{8}{15}RH^6 H_\xi\right]_\xi + \delta\left[-4HH_1{}^2 + RH^2 H_1 p_{0\xi}^{(1)} - \frac{R}{3}H^3 p_{0\xi}^{(2)} - \frac{8}{15}R(H^6 H_1)_\xi\right]_\xi + \mathcal{O}(\delta^2) = 0, \tag{B.2}$$

where

$$p_{0\xi}^{(1)} = -\frac{2}{R}\left[\overline{W}_e\mathcal{H}[H_\xi] - H\cot\beta + \frac{1}{2\overline{C}}H_{\xi\xi}\right]_\xi, \tag{B.3}$$

$$p_{0\xi}^{(2)} = \frac{2}{R}\left[\overline{W}_e\mathcal{H}[H_{1\xi}] - H_1\cot\beta + \frac{1}{2\overline{C}}H_{1\xi\xi}\right]_\xi. \tag{B.4}$$

Next, adding δ times equation (B.2) to equation (B.1) we find that $\mathcal{O}(\delta)$ terms of (B.1) proportional to H_1 cancel exactly the same order terms containing H_1 in (B.2), so that a single equation for H is found consistently at $\mathcal{O}(\delta)$. The final equation with $\mathcal{O}(\delta^2)$ terms included is

$$H_\tau + \left[\frac{2}{3}H^3 + \delta\left(\frac{8}{15}RH^6 - \frac{2}{3}\cot\beta H^3\right)H_\xi + \frac{\delta}{3\overline{C}}H^3 H_{\xi\xi\xi} + \frac{2\delta}{3}\overline{W}_e H^3\mathcal{H}[H_{\xi\xi}]\right]_\xi + \delta^2\left[-2HH_1^2 + RH^2 H_1 p_{0x}^{(1)} - \frac{R}{3}H^3 p_{0x}^{(2)} - \frac{8}{15}R(H^6 H_1)_\xi\right]_\xi + \mathcal{O}(\delta^3) = 0. \tag{B.5}$$

Dropping $\mathcal{O}(\delta^2)$ terms gives a closed system. We note, however, that the correction contains H_1 and its spatial derivatives and cannot be expressed in terms of H alone without going to higher order and obtaining regularized equations for $H_0 + \delta H_1 + \delta^2 H_2$ for example. It is not clear that this will work and we have not attempted this calculation yet.

APPENDIX C

SOME USEFUL INEQUALITIES

Young's inequality:

$$ab \leq \frac{|a|^p}{p} + \frac{|a|^q}{q}, \tag{C.1}$$

for $a,\ b \in \mathbb{R}$, $1/p + 1/q = 1$. In particular, for $\varepsilon > 0$,

$$ab \leq \frac{\varepsilon}{2}a^2 + \frac{1}{2\varepsilon}b^2. \tag{C.2}$$

Uniform Gronwall's inequality. Assume that positive locally integrable functions $y(t)$, $g(t)$, $h(t)$ satisfy

$$\frac{dy}{dt} \leq gy + h, \quad t \geq 0, \tag{C.3}$$

and moreover

$$\int_t^{t+r} g(s)ds \leq a_1, \quad \int_t^{t+r} h(s)ds \leq a_2, \quad \int_t^{t+r} y(s)ds \leq a_3, \tag{C.4}$$

where r, a_1, a_2, a_3 are positive constants. Then

$$y(t+r) \leq \left(\frac{a_3}{r} + a_2\right)e^{a_1}, \quad t \geq 0. \tag{C.5}$$

Nirenberg-Gagliardo inequality:

$$\|g^{(j)}\|_2 \leq C\|g^{(m)}\|_2^{j/m}\|g\|_2^{(m-j)/m}, \quad 0 \leq j \leq m, \tag{C.6}$$

for $g \in \dot{H}^m_{\text{per}}$. The positive constant C depends on m only.

Agmon's inequality:

$$\|g\|_\infty^2 \leq 2\|g\|_2\|g_x\|_2 \tag{C.7}$$

for $g \in \dot{H}^1_{\text{per}}$.

APPENDIX D

USEFUL LEMMA

Lemma D.0.3 *There is a constant C such that*

$$|b(u,\, u,\, e^{\alpha t \boldsymbol{A}} v)| \leq C\sqrt{\alpha t}\|v\|_2 \|\boldsymbol{A}v\|_2^2, \tag{D.1}$$

where the form b is defined as follows:

$$b(u,\, v,\, w) = \int_{-\pi}^{\pi} u v_x w dx, \tag{D.2}$$

and $\boldsymbol{A} = \mathcal{H} \circ \partial_x$, i.e., the operator $\boldsymbol{A}$ acts by multiplication on the Fourier coefficients as follows:

$$\widehat{(\boldsymbol{A}u)}_k = |k|\hat{u}_k, \quad k \in \mathbb{Z}, \tag{D.3}$$

and $v = e^{\alpha t \boldsymbol{A}} u$.

Proof: Using $b(u,\, u,\, w) = -\frac{1}{2} b(u,\, w,\, u)$, and in particular, $b(u,\, u,\, u) = 0$, we obtain

$$\begin{aligned} b(u,\, u,\, e^{\alpha t \boldsymbol{A}} v) &= -\frac{1}{2} b(u,\, e^{\alpha t \boldsymbol{A}} v,\, u) \\ &= -\frac{1}{2}\left[b(e^{-\alpha t \boldsymbol{A}} v,\, e^{\alpha t \boldsymbol{A}} v,\, e^{-\alpha t \boldsymbol{A}} v) - b(v,\, v\, v)\right] \\ &= i\pi \sum_{n \in \mathbb{Z}} \sum_{m \in \mathbb{Z}} n \hat{v}_m \hat{v}_{n-m} \hat{v}_{-n} \left[e^{\alpha t (|n|-|m|-|n-m|)} - 1\right]. \end{aligned} \tag{D.4}$$

Note that

$$|n| - |m| - |n-m| = \begin{cases} 0, & \text{if } n \geq m > 0 \text{ or } n \leq m < 0, \\ -2|m|, & \text{if } n > 0 > m > \text{ or } n < 0 < m, \\ -2|n-m|, & \text{if } m > n > 0 \text{ or } m < n < 0. \end{cases} \tag{D.5}$$

After rearranging summation indices, we find

$$b(u,\, u,\, e^{\alpha t \boldsymbol{A}} v) = 4\pi \mathrm{Im} \sum_{k>m>0} (k-m)\hat{v}_{-m}\hat{v}_k\hat{v}_{m-k}\big(1 - e^{-2\alpha t|m|}\big). \tag{D.6}$$

We apply the Cauchy-Schwarz and the Minkowski inequalities and get the following estimates:

$$\begin{aligned} b(u,\, u,\, e^{\alpha t \boldsymbol{A}} v) \leq & 4\pi \Big(\sum_{k>0} |\hat{v}_k|^2\Big)^{1/2} \Big(\sum_{m>0} m^2 |\hat{v}_m|^2\Big)^{1/2} \\ & \times \Big(\sum_{k>m>0} (k-m)^2 |\hat{v}_{k-m}|^2 \Big(\frac{1-e^{-2\alpha t m}}{m}\Big)^2\Big)^{1/2} \\ \leq & 4\pi \Big(\sum_{k>0} |\hat{v}_k|^2\Big)^{1/2} \sum_{m>0} m^2 |\hat{v}_m|^2 \\ & \times \Big(2\alpha t \int_0^\infty \Big(\frac{1-e^{-x}}{x}\Big)^2 dx\Big)^{1/2}. \end{aligned} \tag{D.7}$$

Reexpressing the sums in terms of the norms $\|\cdot\|_2$ in x-space, the Lemma follows with

$$C^2 = \frac{1}{2\pi} \int_0^\infty \Big(\frac{1-e^{-x}}{x}\Big)^2 dx. \tag{D.8}$$

■

REFERENCES

[1] A. Abdelouhab, J. L. Bona, M. Felland, and J.-C. Saut. Nonlocal models for nonlinear dispersive waves. *Phys. D*, 40:360–392, 1989.

[2] M. J. Ablowitz and A. S. Fokas. *Complex Variables: Introduction and Applications.* Cambridge University Press, Cambridge; New York, 1997.

[3] D. J. Acheson. *Elementary Fluid Dynamics.* Clarendon Press, Oxford, 1990.

[4] S. V. Alekseenko, V. E. Nakoryakov, and B. G. Pokusaev. Wave formation on a vertical falling liquid film. *AIChE J.*, 31:1446–1460, 1985.

[5] R. S. Allan and S. G. Mason. Particle behavior in shear and electric fields. I. deformation and burst of fluid drops. *Proc. Roy. Soc. London Ser. A*, 267:45–61, 1962.

[6] K. Argyriadi, K. Serifi, and V. Bontozoglou. Nonlinear dynamics of inclined films under low-frequency forcing. *Phys. Fluids*, 16(7):2457–2468, 2004.

[7] S. G. Bankoff, E. M. Griffing, and R. A. Schluter. Use of an electric field in an electrostatic liquid film radiator. *Ann. N.Y. Acad. Sci.*, 974:1–9, 2002.

[8] S. G. Bankoff, M. J. Miksis, and H. Kim R. Gwinner. Design considerations for the rotating electrostatic liquid-film radiator. *Nucl. Eng. Des.*, 149:441–447, 1994.

[9] G. K. Batchelor. *An Introduction to Fluid Dynamics.* Cambridge University Press, Cambridge, 1967.

[10] T. B. Benjamin. Wave formation in laminar flow down an inclined plane. *J. Fluid Mech.*, 2(6):554–574, 1957.

[11] D. J. Benney. Long waves on liquid films. *J. Math. Phys.*, 45:150–155, 1966.

[12] A. L. Bertozzi. The mathematics of moving contact lines in thin liquid films. *Notices Amer. Math. Soc.*, 45:689–697, 1998.

[13] A. L. Bertozzi and M. C. Pugh. The lubrication approximation for thin viscous films: the moving contact line with 'porous media' cutt off of Van der Waals interactions. *Nonlinearity*, 7:1535–1564, 1994.

[14] A. L. Bertozzi and M. C. Pugh. Long-wave instabilities and saturation in thin film equations. *Commun. Pure Appl. Math.*, 51:625–661, 1998.

[15] A. L. Bertozzi and M. C. Pugh. Finite-time blow-up of solutions of some long-wave unstable thin film equations. *Indiana Univ. Math. J.*, 49(4):1323–1366, 2000.

[16] A. M. Binny. Experiments on the onset of wave formation on a film of water flowing down a vertical plane. *J. Fluid Mech.*, 2:551–555, 1957.

[17] M. G. Blyth, P. Hall, and D. T. Papageorgiou. Chaotic flows in pulsating cylindrical tubes: a class of exact navier-stokes solutions. *J. Fluid. Mech.*, 481:187–213, 2003.

[18] V. Bontozoglou. A numerical study of interfacial transport to a gas-sheared wavy liquid. *Int. J. Heat Mass Tran.*, 41(15):2297–2305, 1998.

[19] C. L. Burcham and D. A. Saville. The electrohydrodynamic stability of a liquid bridge: microgravity experiments on a bridge suspended in a dielectric gas. *J. Fluid Mech.*, 405:37–56, 2000.

[20] A. Castellanos. *Electrohydrodynamics*. Springer, Wien; New York, 1998.

[21] A. Castellanos and A. Gonzalez. Nonlinear electrohydrodynamics of free surfaces. *IEEE Transactions on Dielectrics and Electrical Insulation*, 5(4).

[22] H.-C. Chang. Wave evolution on a falling film. *Annu. Rev. Fluid Mech.*, 26:103–136, 1994.

[23] H.-C. Chang, M. Cheng, E. A. Demekhin, and D. I. Kopelevich. Secondary and tertiary excitation of three-dimensional patterns on a falling film. *J. Fluid. Mech.*, 270:251–275, 1994.

[24] H.-C. Chang and E. A. Demekhin. *Complex Wave Dynamics on Thin Films*. Elsevier, Amsterdam; The Netherlands, 2002.

[25] B. I. Cohen, J. A. Krommes, W. M. Tang, and M. N. Rosenbluth. Non-linear saturation of the dissipative trapped ion mode by mode coupling. *Nucl. Fusion*, 16:971–992, 1976.

[26] P. Collet, J.-P. Eckmann, H. Epstein, and J. Stubbe. Analyticity for the Kuramoto-Sivashinsky equation. *Phys. D*, 67:321–326, 1993.

[27] P. Collet, J.-P. Eckmann, H. Epstein, and J. Stubbe. A global attracting set for the Kuramoto-Sivashinsky equation. *Commun. Math. Phys.*, 152:203–214, 1993.

[28] A. V. Coward, D. T. Papageorgiou, and Y. S. Smyrlis. Nonlinear stability of oscillatory core-annular flow: A generalized Kuramoto-Sivashinsky equation with time periodic coefficients. *Zeit. Angew. Math. Phys. (ZAMP)*, 46:1–39, 1995.

[29] R. V. Craster and O. K. Matar. Electrically induced pattern formation in thin leaky dielectric films. *Phys. Fluids*, 17:032104, 2005.

[30] J. A. Diez and L. Kondic. Contact line instabilities of thin liquid films. *Phys. Rev. Lett.*, 86(4):632–635, 2001.

[31] J. A. Diez and L. Kondic. Computing three-dimensional thin film flows including contact lines. *J. Comput. Phys.*, 183(1):274–306, 2002.

[32] J. A. Diez, L. Kondic, and A. L. Bertozzi. Global models for moving contact lines. *Phys. Rev. E*, 63:011208, 2000.

[33] J. Dong, V. F. de Almeida, and C. Tsouris. Formation of liquid columns on liquid-liquid interfaces under applied electric fields. *J. Colloid Interface Sci.*, 242:327–336, 2001.

[34] J. Duan and V. J. Ervin. Dynamics of a nonlocal Kuramoto-Sivashinsky equation. *J. Diff. Eq.*, 143:243–266, 1998.

[35] A. E. Dukler. The role of waves in two phase flow: some new understanding. *Chem. Eng. Educ.*, Summer 1976:108–138, 1976.

[36] E. B. Dussan V. On the spreading of liquids on solid surfaces, static and dynamic contact angles. *Ann. Rev. Fluid Mech.*, 11:371–400, 1979.

[37] P. Ehrhard. The spreading of hanging drops. *J. Colloid Interface Sci.*, 168:242–246, 1994.

[38] P. Ehrhard and S. H. Davis. Non-isothermal spreading of liquid drops on horizontal plates. *J. Fluid. Mech.*, 229:365–388, 1991.

[39] E. D. Eidelman. *Parabolic Systems*. North-Holland, Amsterdam, 1969.

[40] A. Friedman. Interior estimates for parabolic systems of partial differential equations. *J. Math. Mech.*, 7:393–418, 1958.

[41] U. Frisch, Zhen Su She, and O. Thual. Viscoelastic behaviour of cellular solutions to the Kuramoto-Sivashinsky model. *J. Fluid Mech.*, 186:221–240, 1986.

[42] D. Gao, N. B. Morley, and V. Dhir. Numerical simulation of wavy falling film flow using VOF method. *J. Comput. Phys.*, 192:624–642, 2003.

[43] B. Gjevik. Occurrence of finite-amplitude surface waves on falling liquid films. *Phys. Fluids*, 13(8):1918–1925, 1970.

[44] A. Gonzalez and A. Castellanos. Nonlinear electrohydrodynamic waves on films falling down an inclined plane. *Phys. Rev. E*, 53(4).

[45] J. Goodman. Stability of the Kuramoto-Sivashinsky and related systems. *Commun. Pure Appl. Math.*, 47:293–306, 1994.

[46] J. M. Greene and J.-S. Kim. The steady states of the Kuramoto-Sivashinsky equation. *Phys. D*, 33:99–120, 1988.

[47] H. P. Greenspan. On the motion of a small viscous droplet that wets a surface. *J. Fluid Mech.*, 84:125–143, 1978.

[48] E. M. Griffing, S. G. Bankoff, M. J. Miksis, and R. A. Schluter. Electrohydrodynamics of thin flowing films. *Preprint*, 2004.

[49] F. Gu, C. J. Liu, X. G. Yuan, and G. C. Yu. Cfd simulation of liquid film flow on inclined plates. *Chem. Eng. Technol.*, 27(10):1099–1104, 2004.

[50] P. J. Haley and M. J. Miksis. The effect of the contact line on droplet spreading. *J. Fluid Mech.*, 223:57–81, 1991.

[51] P. Hall and D. T. Papageorgiou. The onset of chaos in a class of exact navier-stokes solutions. *J. Fluid. Mech.*, 393:59–87, 1999.

[52] D. Henry. *Geometric Theory of Semilinear Parabolic Equations*, volume 840 of *Lecture notes in mathematics*. Springer-Verlag, Berlin; New York, 1981.

[53] T. Hocherman and P. Rosenau. On KS-type equations describing the evolution and rupture of a liquid interface. *Physica D*, 67:113–125, 1993.

[54] L. M. Hocking. Rival contact-angle models and the spreading of drops. *J. Fluid Mech.*, 239:671–681, 1992.

[55] A. P. Hooper and R. Grimshaw. Nonlinear instability at the interface between two fluids. *Phys. Fluids*, 28:37–45, 1985.

[56] J. M. Hyman and B. Nikolaenko. The Kuramoto-Sivashinsky equations, a bridge between PDEs and dynamical systems. *Phys. D*, 18:113–126, 1986.

[57] J. M. Hyman, B. Nikolaenko, and S. Zaleski. Order and complexity in the Kuramoto-Sivashinsky model of turbulent interfaces. *Phys. D*, 23:265–292, 1986.

[58] J. S. Il'yashenko. Global analysis of the phase portrait for the Kuramoto-Sivashinsky equation. *J. Dyn. Diff. Equations*, 4(4):585–615, 1992.

[59] J. D. Jackson. *Classical Electrodynamics*. Wiley, New York, 1963.

[60] M. F. G. Johnson, R. A. Schluter, S. G. Bankoff, and M. J. Miksis. Experimental study of rivulet formation on an inclined plate by fluorescent imaging. *J. Fluid Mech.*, 394:339–354, 1999.

[61] M. S. Jolly, R. Rosa, and R. Temam. Evaluating the dimension of an inertial manifold for the Kuramoto-Sivashinsky equation. *Adv. Differ. Equ.*, 5:31–66, 2000.

[62] S. W. Joo and S. H. Davis. Instabilities of three-dimensional viscous falling films. *J. Fluid Mech.*, 242:529–547, 1992.

[63] S. W. Joo, S. H. Davis, and S. G. Bankhoff. Long-wave instabilities of heated falling films: two-dimensional theory of uniform layers. *J. Fluid Mech.*, 230:117, 1991.

[64] P. L. Kapitza and S. P. Kapitza. Wave flow of thin fluid layers of liquids. *Zh. Eksp. Teor. Fiz.*, 19:105–120, 1949.

[65] I. G. Kevrekidis, B. Nicolaenko, and C. Scovel. Back in the saddle again: a computer assisted study of the Kuramoto-Sivashinsky equation. *SIAM J. Appl. Math.*, 50(3):760–790, 1990.

[66] H. Kim, S. G. Bankoff, and M. J. Miksis. The effect of an electrostatic field on film flow down an inclined plane. *Phys. Fluids A*, 4:2117–2130, 1992.

[67] H. Kim, S. G. Bankoff, and M. J. Miksis. The cylindrical electrostatic liquid-film radiator for heat rejection in space. *J. Heat Trans. – T. ASME*, 116:986–992, 1994.

[68] L. Kondic and J. A. Diez. Pattern formation in the flow of thin films down an incline: Constant flux configuration. *Phys. Fluids*, 13(11):3168–3184, 2001.

[69] T. Kunugi and C. Kino. DNS of falling film structure and heat transfer via mars method. *Comput. Struct.*, 83(6-7):455–462, 2005.

[70] Y. Kuramoto. Diffusion-induced chaos in reaction systems. *Prog. Theoret. Phys. Suppl.*, 64:346–367, 1978.

[71] Y. Kuramoto and T. Tsuzuki. On the formation of dissipative structures in reaction diffusion systems. *Prog. Theoret. Phys.*, 54:687–699, 1975.

[72] Y. Kuramoto and T. Tsuzuki. Persistent propogation of concentration waves in dissipative media far from thermal equilibrium. *Prog. Theoret. Phys.*, 55:356–369, 1976.

[73] L. D. Landau and E. M. Lifshitz. *Fluid Mechanics (trans. from the Russian)*. Pergamon Press, Oxford; New York, 1989.

[74] L. D. Landau and E. M. Lifshitz. *The Classical Theory of Fields (trans. from the Russian)*. Butterworth Heinemann, Oxford; Boston, 2000.

[75] S. P. Lin. Finite amplitude sideband stability of a viscous film. *J. Fluid Mech.*, 63:417–429, 1974.

[76] J. Liu and J. P. Gollub. Onset of spatially chaotic waves on flowing films. *Phys. Rev. Lett.*, 70:2289–2292, 1993.

[77] J. Liu and J. P. Gollub. Solitary wave dynamics of film flows. *Phys. Fluids*, 6(5):1702–1712, 1994.

[78] J. Liu, J. D. Paul, and J. P. Gollub. Measurements of the primary instabilities of film flows. *J. Fluid Mech.*, 250:69–101, 1993.

[79] N. A. Malamataris and V. Bontozoglou. Computer aided analysis of viscous film flow along an inclined wavy wall. *J. Comput. Phys.*, 154(2):372–392, 1999.

[80] N. A. Malamataris, M. Vlachogiannis, and V. Bontozoglou. Solitary waves on inclined films: Flow structure and binary interactions. *Phys. Fluids*, 14(3):1082–1094, 2002.

[81] A. I. Markushevich. *Theory of Functions of a Complex Variable (trans. from the Russian)*. Prentice-Hall, Englewood Cliffs, 1965.

[82] T. G. Myers. Thin films with high surface tension. *SIAM Rev.*, 40(3):441–462, 1998.

[83] T. Nagasaki, H. Akiyama, and H. Nakagawa. Numerical analysis of flow and mass transfer in a falling liquid film with interfacial waves. *Thermal Sci. Eng.*, 10:1231–1240, 2002.

[84] C. Nakaya. Long waves on a thin fluid layer flowing down an inclined plane. *Phys. Fluids*, 18(11).

[85] B. Nicolaenko and B. Scheurer. Remarks on the Kuramoto-Sivashinsky equation. *Proc. Conference on Fronts, Interfaces and Patterns, Physica D*, 12:391–395, 1984.

[86] B. Nicolaenko, B. Scheurer, and R. Temam. Some global dynamical properties of the Kuramoto-Sivashinsky equation: Nonlinear stability and attractors. *Phys. D*, 16(2):155–183, 1985.

[87] W. Nusselt. Die oberflachenkondesation des wasserdampfes. *Z. Ver. Deut. Indr.*, 60(27):541–546, 1916.

[88] A. Oron, S. H. Davis, and S. G. Bankhoff. Long-scale evolution of thin liquid films. *Rev. Mod. Phys.*, 69:931–980, 1997.

[89] W. K. H. Panofsky and M. Phillips. *Classical Electricity and Magnetism.* Addison-Wesley Publishing Company, Inc., Reading, MA, 1963.

[90] D. T. Papageorgiou, C. Maldarelli, and D. S. Rumschitzki. Nonlinear interfacial stability of core-annular film flow. *Phys. Fluids A*, 2(3):340–352, 1990.

[91] D. T. Papageorgiou and P. G. Petropoulos. Generation of interfacial instabilities in charged electrified viscous liquid films. *J. Eng. Math*, 50(2-3):223–240, 2004.

[92] D. T. Papageorgiou and Y. S. Smyrlis. The route to chaos for the Kuramoto-Sivashinsky equation. *Theoret. Comput. Fluid Dynamics*, 3:15–42, 1991.

[93] D. T. Papageorgiou and J.-M. Vanden-Broeck. Antisymmetric capillary waves in electrified fluid sheets. *European J. Appl. Math.*, 15:609–623, 2004.

[94] D. T. Papageorgiou and J.-M. Vanden-Broeck. Large amplitude capillary waves in electrified fluid sheets. *J. Fluid. Mech.*, 508:71–88, 2004.

[95] L. F. Pease and W. B. Russel. Linear stability analysis of thin leaky dielectric films subjected to electric fields. *J. Non-Newtonian Fluid Mech.*, 102:233–250, 2002.

[96] R. Plonsey. *Bioelectric phenomena.* McGraw-Hill, New York, 1969.

[97] A. Pumir, P. Manneville, and Y. Pomeau. On solitary waves running down an inclined plane. *J. Fluid Mech.*, 135:27–50, 1983.

[98] P. Rosenau and A. Oron. Bounded and unbounded patterns of the benney equation. *Phys. Fluids A*, 4:117, 1992.

[99] W. B. Russel, D. A. Saville, and W. R. Schowalter. *Colloidal Dispersions.* Cambridge University Press, Cambridge; New York, 1989.

[100] T. R. Salamon, R. C. Armstrong, and R. A. Brown. Traveling waves on vertical films: Numerical analysis using the finite element method. *Phys. Fluids*, 6(6), 1994.

[101] K. Savettaseranee, P. G. Petropoulos D. T. Papageorgiou, and B. S. Tilley. The effect of electric fields on the rupture of thin viscous films by van der waals forces. *Phys. Fluids*, 15(3):641–652, 2003.

[102] D. A. Saville. Electrokinetic effects with small particles. *Annu. Rev. Fluid Mech.*, 9:321–337, 1977.

[103] D. A. Saville. Electrohydrodynamics: The Taylor-Melcher leaky dielectric model. *Annu. Rev. Fluid Mech.*, 29:27–64, 1997.

[104] G. R. Sell and Y. You. *Dynamics of Evolutionary Equations*, volume 143 of *Applied Mathematical Sciences*. Springer, New York, 2002.

[105] K. Serifi, N. A. Malamataris, and V. Bontozoglou. Transient flow and heat transfer phenomena in inclined wavy films. *Int. J. Therm. Sci.*, 43(8):761–767, 2004.

[106] T. Shlang and G. I. Sivashinsky. Irregular flow of a liquid film down a vertical column. *J. Phys.*, 43:459–466, 1982.

[107] G. A. Sisoev, O. K. Matar, and C. J. Lawrence. Absortption of gas into a wavy falling film. *Chem. Eng. Sci.*, 60(3):827–838, 2005.

[108] G. I. Sivashinsky. Nonlinear analysis of hydrodynamic instability in laminar flames, part 1. *Acta Astronautica*, 4:1176–1206, 1977.

[109] G. I. Sivashinsky. Instabilities, pattern formation, and turbulence in flames. *Ann. Rev. Fluid Mech.*, 15:179–199, 1983.

[110] G. I. Sivashinsky and D. M. Michelson. On irregular wavy flow on liquid film down a vertical plane. *Prog. Theor. Phys.*, 63(6), 1980.

[111] G. I. Sivashinsky and T. Shlang. Irregular flow of a liquid down a vertical column. *J. de Phys.*, 43:459–466, 1982.

[112] Y. S. Smyrlis and D. T. Papageorgiou. Predicting chaos for the infinite dimensional dynamical systems: The Kuramoto-Sivashinsky equation, a case study. *Proc. Natl. Acad. Sci. USA*, 88(24):11129–11132, 1991.

[113] Y. S. Smyrlis and D. T. Papageorgiou. Computational study of chaotic and ordered solutions of the Kuramoto-Sivashinsky equation. *ICASE Report No. 96-12*, pages 1–32, 1996.

[114] E. Tadmor. The well-posedness of the Kuramoto-Sivashinsky equation. *SIAM J. Math. Anal.*, 17(4):884–893, 1986.

[115] G. I. Taylor. Electrically driven jets. *Proc. Roy. Soc. London Ser. A*, 313:453–475, 1969.

[116] R. Temam. *Infinite-dimensional Dynamical Systems in Mechanics and Physics*. Springer-Verlag, New York, 1988.

[117] B. S. Tilley, P. G. Petropoulos, and D. T. Papageorgiou. Dynamics and rupture of planar electrified liquid sheets. *Phys. Fluids*, 13(12):3547–3563, 2001.

[118] L. N. Trefethen. *Spectral methods in Matlab.* Society for Industrial and Applied Mathematics, Philadelphia, PA, 2000.

[119] D. Tseluiko and D. T. Papageorgiou. Wave evolution on electrified falling films. *accepted for publication in J. Fluid Mech.*, 2006.

[120] D. Tseluiko and D.T. Papageorgiou. A global attracting set for a nonlocal Kuramoto-Sivashinsky equation arising in interfacial electrohydrodynamics. *submitted to European J. Appl. Math.*, 2006.

[121] M. Vlachogiannis and V. Bontozoglou. Observations of solitary wave dynamics of film flows. *J. Fluid Mech.*, 435:191–215, 2001.

[122] M. Vlachogiannis and V. Bontozoglou. Experiments on laminar film flow along a periodic wall. *J. Fluid Mech.*, 457:133–156, 2002.

[123] T. P. Witelski, A. J. Bernoff, and A. L. Bertozzi. Blowup and dissipation in a critical-case unstable thin film equation. *European J. Appl. Math.*, 15(2):223–256, 2004.

[124] S. G. Yiantsios and B. G. Higgins. Rayleigh-Taylor instability in thin viscous films. *Phis. Fluids A*, 1(6):1484–1501, 1989.

[125] S. G. Yiantsios and B. G. Higgins. Rupture of thin films: nonlinear stability analysis. *J. Colloid Interface Sci.*, 147:341–350, 1991.

[126] C.-H. Yih. Stability of liquid flow down an inclined plane. *Phis. Fluids*, 6:321–334, 1963.

[127] P. N. Yoshimura, T. Nosoko, and T. Nagata. Enhancement of mass transfer into a falling laminar liquid film by two-dimensional surface waves – some experimental observations and modeling. *Chem. Eng. Science*, 51:1231–1240, 1996.